INVESTIGATION OF CRYSTAL GROWTH IN ZERO GRAVITY ENVIRONMENT

AND

INVESTIGATION OF METALLIC WHISKERS

by

J. H. Davis

R. B. Lal

H. U. Walter

J. G. Castle, Jr.

Final Technical Report

School of Graduate Programs and Research
The University of Alabama in Huntsville
Huntsville, Alabama

December 1972

INVESTIGATION OF CRYSTAL GROWTH IN ZERO GRAVITY ENVIRONMENT

AND

INVESTIGATION OF METALLIC WHISKERS

by

J. H. Davis

R. B. Lal

H. U. Walter

J. G. Castle, Jr.

Final Technical Report

School of Graduate Programs and Research
The University of Alabama in Huntsville
Huntsville, Alabama

December 1972

TABLE OF CONTENTS

(Responsible Investigator listed by initials after each section)

APPENDIX

FOREWORD

The present report is a final technical report for two contracts:

(1) NAS8-24612 for the period April 17, 1970, through June 30, 1972.

(2) NAS8-26793 for the period March 15, 1971, through September 30, 1972.

Since the two efforts were complementary, the report has been unified under one
cover as recommended by the COR, Mr. T. C. Bannister. These studies were
sponsored through these contracts by the George C. Marshall Space Flight Center,
National Aeronautics and Space Administration, Huntsville, Alabama 35812. The
Contract Officer Representatives have been T. C. Bannister, L. L. Lacy, and R.L. Kroes.

The effort dealt with a variety of proposed and approved flight experiments and the
associated materials growth and characterization. During the last year, emphasis
shifted from support of proposed Apollo flyback experiments to support of the approved
Skylab experiments, M555 (Solution growth of GaAs) and M560 (Containerless solidi-
fication of InSb(Se)).

The UAH technical staff and its responsibilities were as follows:

J. H. Davis, Associate Professor of Physics and Principal Investigator

R. B. Lal, Senior Research Associate in Physics and Co-Principal Investigator
since February 1, 1971. Area of responsibility: Electrical characterization.

H. U. Walter, Senior Research Associate in Physics and Co-Principal Investigator
since May 1971. Area of responsibility: Crystal growth and characterization
of structural perfection.

For the high frequency characterization (HFC) of GaAs, described in IV of this report, the following UAH staff was added March 1972:

J. G. Castle, Jr., Professor of Physics and Principal Investigator

R. R. Lattanzi, Research Engineer

P. T. Huang, Graduate Student in Physics.

The following undergraduate research assistants were involved in this study:

Mr. Howard Camp, Mr. Mike Guillebeau, Mr. Len Gibbs, Mr. James Levie III,

Mr. James Gordon, Mr. Don Owen, Mr. James Robinson and Mr. Robert Fatheree.

OBJECTIVES

The specific objectives of this contract were (1) to identify and perform both experiments and calculations to isolate the beneficial effects of near-zero gravity on crystal growth and (2) to develop a crystal chracterization program capable of detecting the expected effects of zero gravity on the growth of specific crystals. The above objectives are part of the broad objectives of utilizing the near-zero gravity environment of space to produce higher quality single crystalline materials.

SUMMARY OF ACCOMPLISHMENTS

FLIGHT EXPERIMENT DEVELOPMENT

- Spherical Crystal Growth Proposal Accepted for Skylab

- Proposals Submitted for Skylab on Whisker Growth

- Proposals Submitted for Apollo 15, 16 and 17 Flight Experiment

- Observed Direct Adverse Effects of Increased Acceleration on Cd Whisker Growth

- Zero Gravity Brownian Motion Vacuum Gauge Invented

CRYSTAL CHARACTERIZATION

- Five Open Literature Publications - See Appendices III through VII

- Two Papers Delivered to American Physical Society on Characterization Results

- Implementation of a Contactless Microwave Surface Resistance Measuring Technique for GaAs Epitaxial Films Grown in Skylab M-555

- Correction Made to an Erroneous Journal Article on InBi Characterization - See Appendix IV

- Discovery of Self-Rupturing in Polycrystalline InBi under Changing Temperature - See Appendix VI

- Development of Etchant for Revealing Dislocations in InBi

ACKNOWLEDGEMENTS

I. DEVELOPMENTS FOR FLIGHT EXPERIMENTS ON CRYSTAL GROWTH: STUDIES ON GROWTH AND CHARACTERIZATION OF CANDIDATE MATERIALS

A STUDIES ON INDIUM-BISMUTH COMPOUNDS

1. APOLLO FLYBACK EXPERIMENTS, GROWTH, AND CHARACTERIZATION OF STRUCTURAL PERFECTION OF InBi SINGLE CRYSTALS*

a. Apollo Flyback Experiments on Solidification of InBi

The major goals of the work performed under Contract NAS8-24612 were

    (1) to develop flight experiments on crystal growth

    (2) to support existing flight experiments on crystal growth.

Our efforts in developing flight experiments were mainly concerned with crystal growth from the melt. Due to the technical and scientific importance of elemental and compound semiconductors, we were aiming towards experimentation on growth of semiconductors. Since the overwhelming majority of semiconductor devices (above 90%) is based on crystals grown from the melt, solidification from the melt was given first priority. Material of superior quality is being produced rather exclusively by melt growth techniques that avoid or minimize crucible contact,

---

*Responsible Investigator - H. U. Walter

such as Czochralski, floating zone and horizontal boat technique. Even though these techniques have been optimized, progress in solid state device technology is unquestionably limited by chemical and crystalline imperfections of the materials produced. The parameters affecting the quality of melt-grown crystals are as follows:

1. Variations in microscopic growth rates

2. Radial thermal gradients in the growing crystal

3. Thermal convection in the melt

4. Thermal convection in the gas phase

5. Variations in boundary layer thickness and composition

6. Constitutional and kinetic supercooling

7. Surface tension gradients

8. Heterogeneous nucleation and contamination by crucible material

The conditions summarized above are the major causes of lattice imperfections and chemical inhomogeneity. The parameters directly affected by gravity are (3), (4) and as a result (1), (2), (5). Parameter (7) is not gravity sensitive, there are possibilities to avoid (8) in near zero gravity by applying proper growth techniques that are adapted to space environment. Development of growth techniques by which crucible contact is avoided and no fluid motions are induced by the growth technique itself (a condition that exists both with Czochralski and floating zone technique) was, therefore, of major concern. Based on an essentially containerless technique [1,2]

that was developed by us earlier, where melt is suspended by wetting and hemispherical crystals are produced by solidification of this pendant drop from the inside out (Fig. 1), growth of spherical crystals was proposed. The experimental approach pursued for Apollo flyback experiments (Apollo 14 and 15) was as follows:

A cylindrical cast was placed in a cylindrical cavity of the experiment cartridge. After melting, the material was extruded by means of a spring-loaded piston through a 1 mm orifice into a spherical furnace cavity. Wetting conditions were chosen such that the melt would be positioned and suspended at the end of the capillary. Solidification would be initiated in the melt that remained in the cylinder; growth would proceed through the capillary and thereby provide a single crystalline seed. Solidification would proceed into the containerless melt which would solidify according to the shape of the isotherm in the spherical furnace cavity from the inside out. A schematic of the experimental arrangement plus furnace is shown in Fig. 2(a) and 2(b).

A second experiment applying soft mold Bridgman growth was conceived in cooperation with the S&E-PT-PE and S&E-SSL-T staff. This experiment was intended to be a simple demonstration on melt growth that would provide first information on improvement of crystal quality due to absence of gravitational forces. The arrangement is shown in Fig. 2(c).

A third experiment that was proposed and carried on by Mr. B. Aldrich (S&E-PT-MXX) concerned eutectic solidification. Our involvement in this experiment was restricted to support in characterization.

Fig. 1. Hemispherical Crystal of Nickel. Melt was suspended by wetting; controlled solidification by linearly reducing the power input into the heating (RF) cavity surrounding the melt.
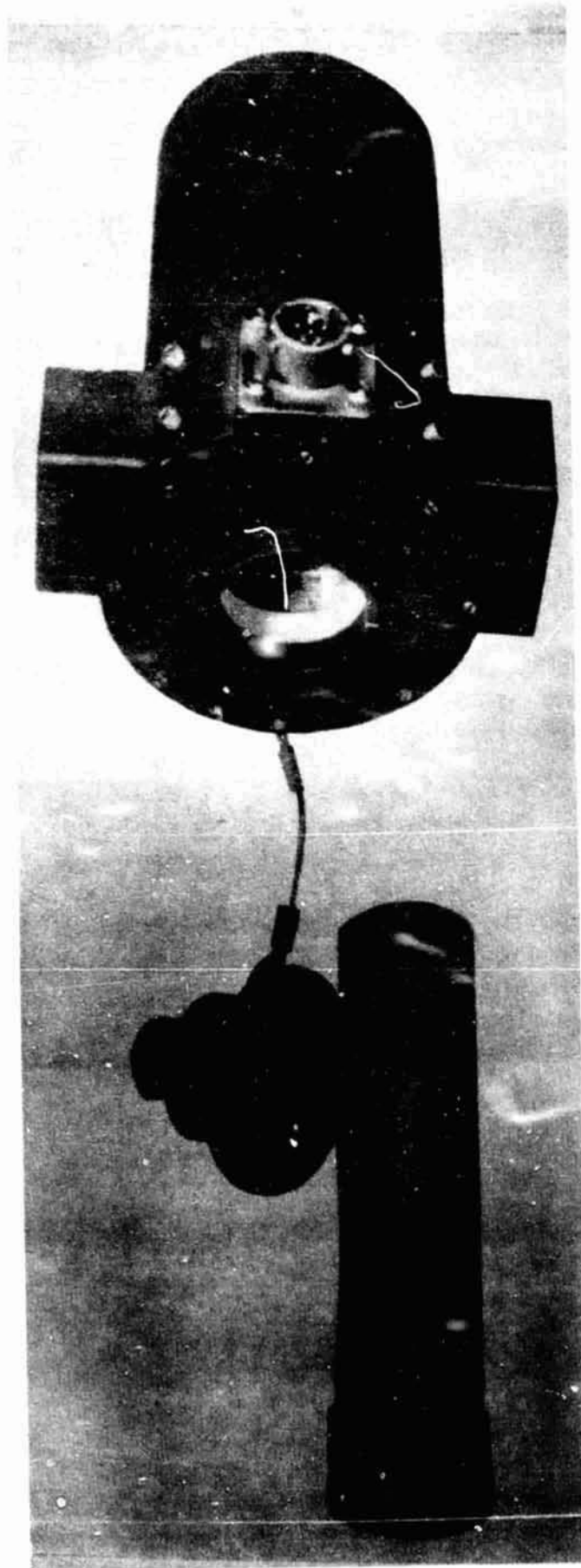
Fig. 2(a) Apollo 14, 15 Cartridge Plus Furnace for "Growth of Spherical Crystals of InBi."

RE CASTING
DEMONSTRATION

SPECIMEN I

In Bi METAL

CAST SPHERE
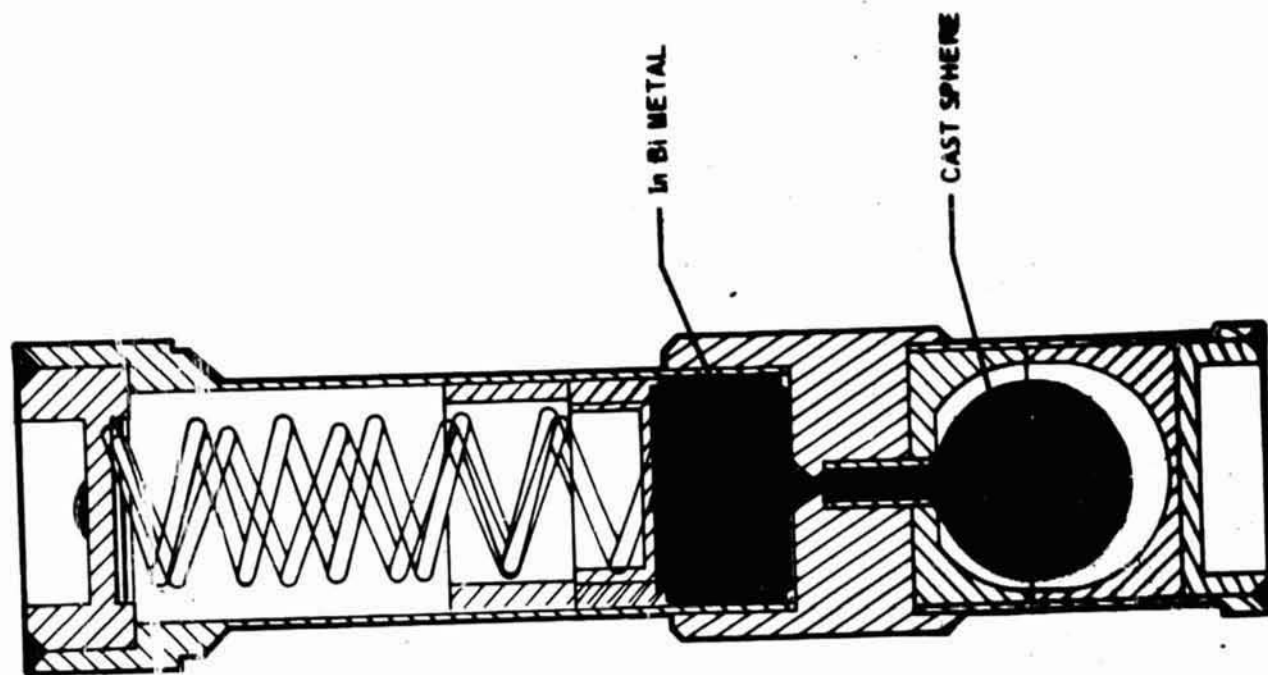
Fig. 2(b) Cartridge for Spherical Crystal Growth of InBi

SELF-NUCLEATED CRYSTAL DEMONSTRATION

SPECIMEN 1

In Bi METAL
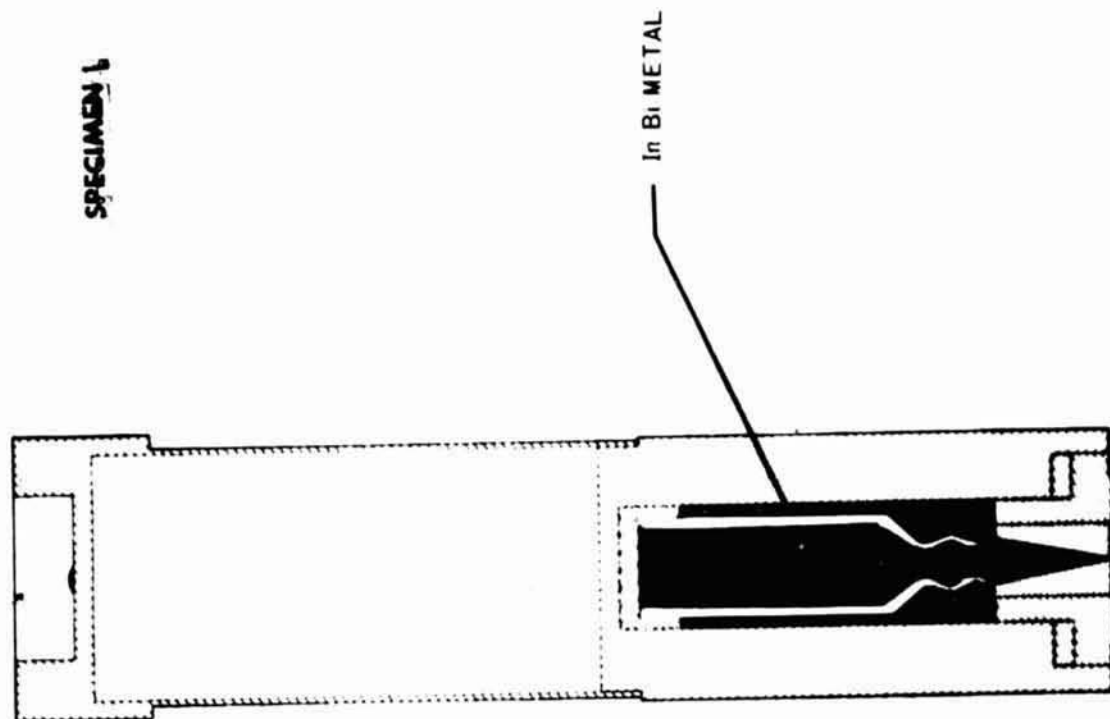
Fig. 2(c) Cartridge for Soft Mold Bridgman Growth of InBi.

Since dopant distribution in melt grown crystals is expected to be more homogeneous in crystals grown in space environment as compared to crystals grown on earth, an experiment that would elucidate the doping process was proposed. A Bridgman growth tube with alternating slabs of doped and undoped slabs was to be processed; the initial square function dopant distribution would be altered after melting and unidirectional solidification according to diffusion and segregation coefficients, residual convection, temperature, temperature gradients and soak time.

Materials selection was very much subject to the parameters of the gradient furnace that was designed and constructed at S&E-PT-PE. The maximum temperature that could be reached due to available power, allowed skin temperature of only $120^{\circ}F$, and restriction in size and weight was $130^{\circ}C$ at the hot end of the heating cavity. For experimentation during Apollo 14 and 15 flights, InBi, a III-V compound with metallic properties and a melting point of $110 \pm 0.5^{\circ}C$, was chosen.

For Apollo 16 and 17 a more sophisticated furnace that was capable of reaching about $600^{\circ}C$ at the hot zone was constructed at S&E-PT, permitting the use of higher melting materials. We were in charge of an experiment on containerless solidification; doped and undoped samples of Indium Antimonide ($T_M = 525^{\circ}C$) were to be processed. The experiment arrangement was different from the one used for Apollo 14 and 15; a schematic of furnace plus cartridges is shown in Fig. 3.

For Apollo 14, 15 and 16, cartridges for the spherical crystal experiments were designed and fabricated at The University of Alabama in Huntsville (UAH).* The outer

---

* This effort was also supported by NASA Contract NAS8-28112.

14
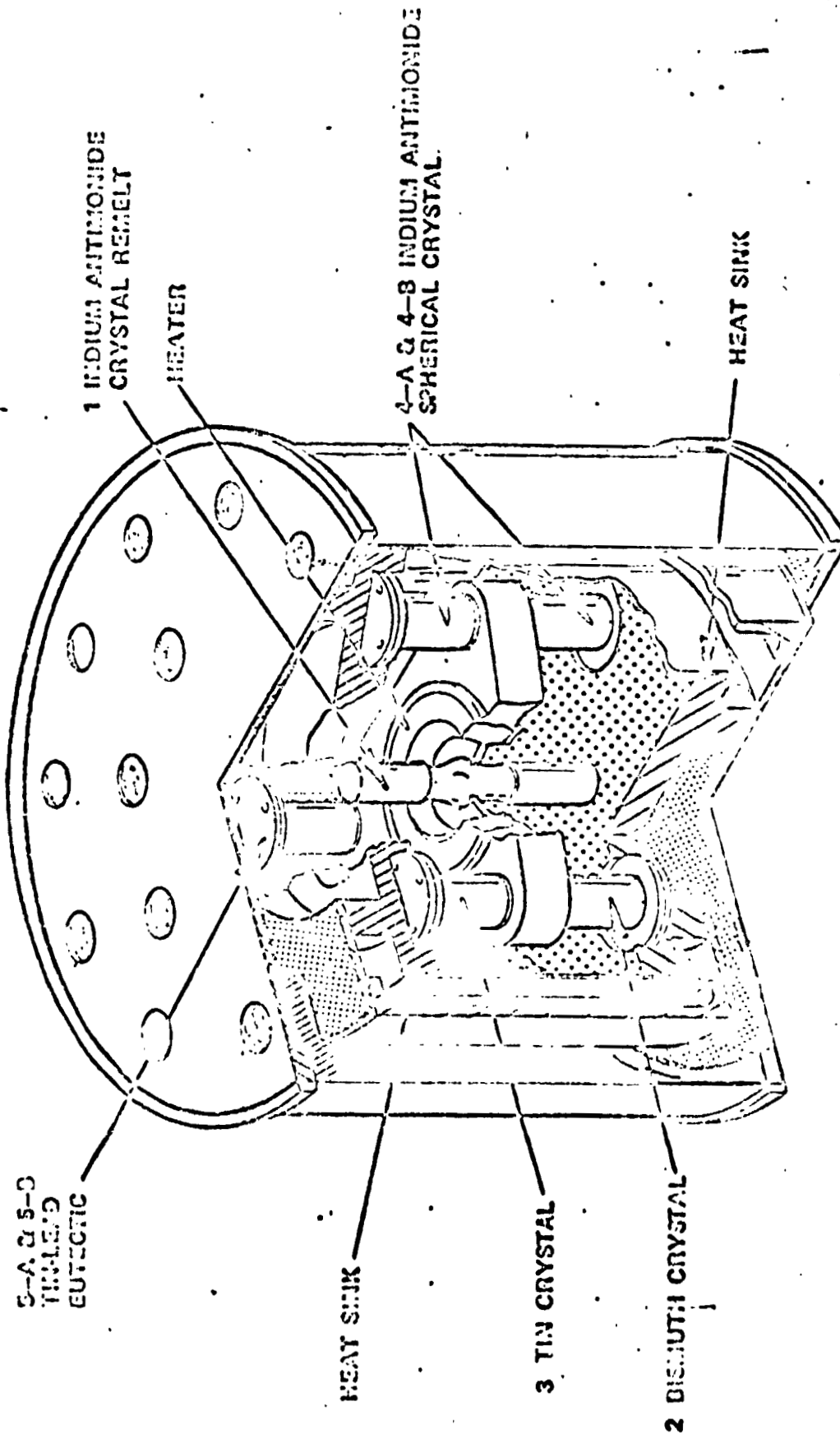
Fig. 3. Apollo 16 Furnace.

stainless steel envelopes were designed and fabricated at S&E-PT-PE. Support was given

to PT-PE on thermal analysis of flight prototype furnace and samples.* A step-by-step

characterization plan on each of the experiments mentioned above was written together with

T. C. Bannister (S&E-SSL-T) and R. B. Lal (UAH)*; see Appendix I.

The experiments mentioned for the Apollo 14 flight were approved for flight by

NASA as part of an experiment package that also contained a series of experiments on

solidification of multicomponent systems. Most of the experiments in this package were

carried out during flight; all of the experiments on crystal growth and eutectic solidification

were not processed due to time losses because of docking problems during flight. The

omitted experiments were then again scheduled for the Apollo 15 flight; however, due to

a short circuit in the furnace manufactured by PT-PE, which was discovered only a few days

prior to launch, the package did not go on board.

A more sophisticated package of experiments with a more versatile furnace was

then prepared, fabricated and tested for Apollo 16 and 17; however, it was not approved

for flight.

Since InBi was a compound that had then been investigated very little, consider-

able time was spent in establishing optimal growth parameters for InBi and methods for analysis

and characterization. An outline on properties of InBi with emphasis on our findings on phase

width, growth and structural perfection of InBi is given in the following paragraphs.

---

*This effort was also supported by NASA Contract NAS8-28112.

b. Structure, Phase Width and Physical Properties of InBi

According to X-ray structure analysis reported by Binnie,[3] InBi crystallizes in the ditetragonal-bypyramidal point symmetry group (4/mmm); the space group is P4/nmm, $c/a = 0.9555$. The structure consists of alternating layers of indium and bismuth atoms normal to the c-axis. (Fig. 4).

	In ---- Bi	3·13 Å
In	Bi	Bi	3·68 Å
Bi	In	In	3·54 Å

Tetrahedral angles: 106° (2) and 111° (4)

Pyramidal angles: 106° (2) and 67° (4)
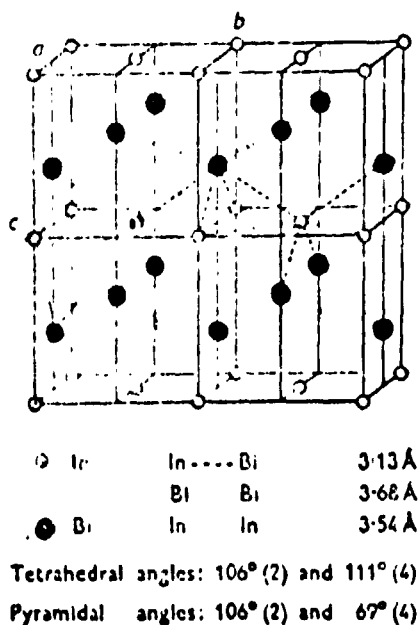
Fig. 4. Atomic Arrangement in Four
Unit Cells of InBi.

Since the positions of the bismuth atoms with respect to the c-axis are ± 1.876 and −1.876 Å, two sublayers of bismuth exist. Each indium layer is in first coordination with the bismuth sublayer on either side of it and the closest spacing of atoms in

neighboring bismuth layers is 3.68 Å. This is larger than the spacing of atoms in adjacent layers of metallic bismuth (3.47 Å) and InBi, therefore, cleaves readily between neighboring bismuth layers along (001).

The phase diagram of Bi-In shown in Fig. 5 was investigated by Henry and Badwick[4], by Peretti and Corapella,[5] and more recently by Giessen.[6]
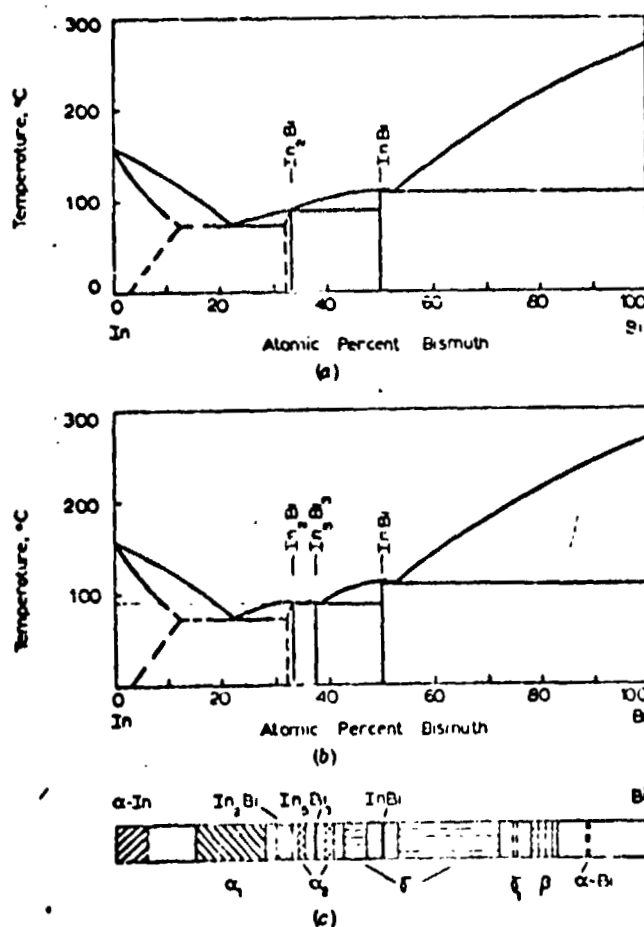
Fig. 5. (a) The equilibrium phase diagram In-Bi. (b) Tentative revised equilibrium phase diagram In-Bi containing the new phase In_5Bi_3. (c) The nonequilibrium phase diagram In-Bi at $-190^\circ C$, as obtained by splat cooling. Retained equilibrium phases marked above the diagram, retained nonequilibrium phases below the diagram.

Fig. 6. Characteristic X-ray spectra of InBi (a clean surface, (001), (b) flaw) obtained with nondispersive X-ray probe (GEOL, SEMU-3).

18

75
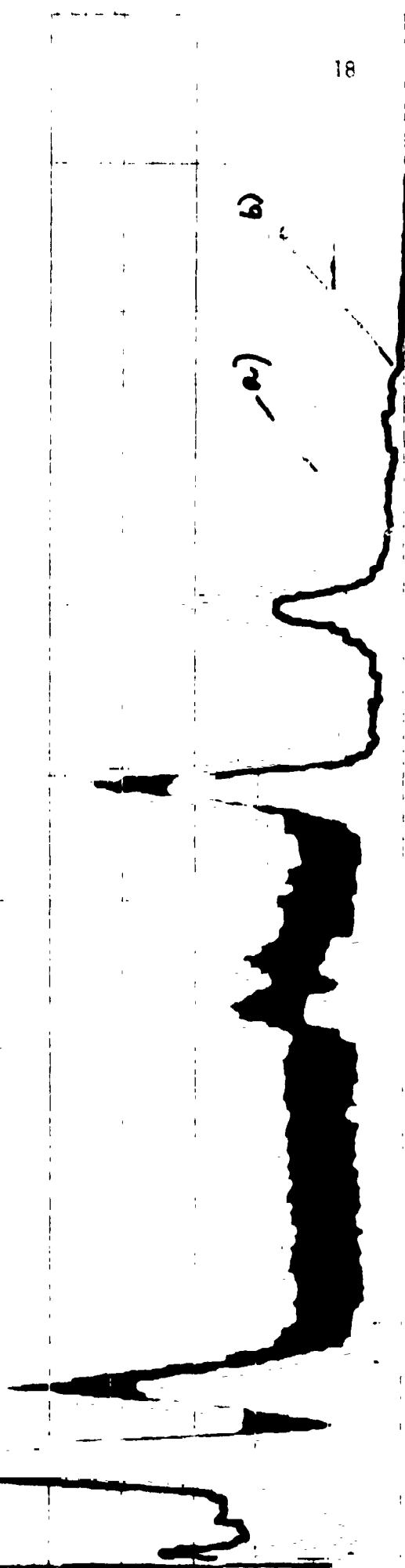
The eutectic used for the Apollo demonstration on eutectic solidification was the lower melting eutectic (72°C) with 22 atomic percent bismuth.

As indicated in Fig. 5, the phase width of $In_{1+x}Bi_{1\mp x}$ has not yet been established. Since intermetallic compounds frequently have phase widths of several atomic percent, and on the other hand excess of one component can lead to constitutional supercooling especially under solely diffusion controlled conditions, we have inv gated the compositional variation that the InBi lattice can tolerate. Alloys rangir from +1 to -1 weight percent excess indium and bismuth in increments of 0.1 wt % were prepared by alloying and casting in high vacuum. Part of the alloy was then uni-directionally solidified by an unseeded horizontal boat technique in quartz boats in high vacuum. Powders, < 10 micron grain size, were prepared from cast material and beginning and end of the samples solidified in the horizontal boats. Out of these 60 samples, 30 have now been analyzed by powder diffraction (Debye-Scherrer). Since one of the neighboring phases to InBi, namely In_5Bi_3, is superconducting and InBi is not, this phase could readily be detected by electrical measurements at low temperatures. Forty samples for resistivity measurements were prepared; however, the studies are incomplete. Our preliminary results by X-ray and optical methods indicate possible compositional variations of InBi of $<\pm$ 0.1 wt %.

Areas of lower reflectance found on cleaved surfaces (001) of crystals prepared from the same batch as used for Apollo 14 samples were of concem to SSL staff and NASA headquarters representatives. We have investigated these areas by optical micros-copy, scanning electron microscopy and electron microprobe analysis, in cooperation with Mr. D. W. Gates, S&E-SSL-TT. Characteristic X-ray spectra of the different areas on a crystal surface are shown in Fig. 6. The results indicate that no different phase was present.

A summary of properties of InBi that are of importance as far as solidification is concerned is given in the Table I.

Property	Value, Unit	Temp (^{o}K)	Ref.
Formula	InBi phase width ± 0.1 wt %	(our preliminary value)	
Molecular weight	323.82		
Symmetry	P 4/n mm (PbO(B10) type structure)		3
Lattice parameters	$a_o = 5.015$ Å	T_R	$\backsim$
	$c_o = 4.781$ Å	T_R	3
Melting point	110 ± 0.5		7
Thermal conductivity	0.011 W/cm^{o}K	T_R	8
Electrical resistivity	10^{-4} ohm-cm		8
Resistivity ratio	60 - 300		9
Electron mobility	30 cm^2/V sec		10
Coefficient of self diffussion of In in InBi	$(1.21 + 0.05) \, 10^{-5}$ to $(9.6\overline{4} \pm 0.48) \, 10^{-6}$ cm^2/sec	112°C to 800°C resp.	11
Enthalpie of formation (from In,Bi, solid)	$\wedge$ H" = -563 cal/g - Atom		12
Entropie of formation	ΔS" = 0.26 cal/g - Atom		12

Table I

c. Growth of InBi Single Crystals

Since only qualitative information on growth was available,[13-17] we have processed about 90 samples at various growth conditions using Bridgman, Czochralski

and horizontal boat technique. The quality of the samples was studied, optimal growth conditions were established, and the perfection of the samples obtained by the different techniques was compared.

Growth by Bridgman and Horizontal Boat Techniques*, **

Single crystals up to 20 cm length and 4 cm diameter were grown by the Bridgman technique b, passing the crucibles through a gradient furnace. Quartz, Pyrex and carbon (5N) crucibles were used as hard molds. Soft mold arrangements consisted of samples cast in carbon split molds and packed with high-purity carbon powder (5N, 325 mesh) into a Pyrex container. All crystals were self-nucleated; sample geometries with constrictions and/or pointed ends were used. The Pyrex containers were sealed off in high vacuum, whereas growth in carbon and quartz crucibles was simply done in air. Gradients at the melting point ($1C9.5^\circ$C) of $10 - 35^\circ$C/cm and growth rates from 0.3 cm/hour up to 5 cm/hour were applied.

For horizontal boat growth, high purity quartz was used as boat material. The experiments were performed under high vacuum at $10^{-6} - 10^{-7}$ torr. The cylindrical, single coil furnace with gold reflector surrounding the vacuum tube was traveled at 1 to 5 cm/hour. The molten zone was about 2 cm wide; the solid-liquid interface was slightly convex toward the melt.

Out of about 60 self-nucleated samples grown by hard and soft mold Bridgman and horizontal boat technique, about 90% of the crystals and grains were oriented with the (001) plane parallel within 10 degrees with the growth axis. See Table II.

---

* Starting material: Bi: 5N +, In: 6N, alloying in high vacuum, stochiometric composition within $\pm$ 0.01 wt. %.

** All temperatures controlled with current proportioning controllers to $< \pm 1^\circ$C.

Angular deviation [°]	0-1	1-2	2-3	3-4	4-5	5-6	6-7	7-8	8-9	9-10	> 10
Number of Samples	10	6	8	7	5	6	7	5	4	2	7

Table II. Orientation of (001) of self-nucleated crystals with respect to crucible axis in degrees of arc.

Growth by Czochralski Technique*

All crystals were grown in inert atmosphere (N_2) at atmospheric pressure. To enable us to apply pulling rates greater than 5 cm/hour, the seeds were mounted in a watercooled sample holder. The seed crystals were oriented perpendicular to the c-axis. No difference in growth rate and growth behavior could be observed within these $\langle hk0 \rangle$ directions. Growth rates from 2 to 10 cm/hour were used; at high growth rates, > 6 cm/hour, a tendency was observed to form additional grains at the periphery of the samples. Similar to self-nucleated crystals, these grains were generally oriented with the (001) planes about parallel to the direction of growth. No variation in growth rates could be observed within the $\langle hk0 \rangle$ directions of the (001) planes. Interface shape was found to be convex towards the melt. Crystals grown with seed rotation (2 - 6 rpm) had elliptical cross sections, the larger axis of the ellipse being parallel to the (001) plane. Axis ratios were between 1.1 to 1.2. This effect was more outspoken with crystals grown without seed rotation; ratios between 1.3 to 1.9 were observed. This indicates higher growth rates parallel rather than perpendicular to (001).

---

*Bridgman, horizontal boat and Czochralski setups were designed and constructed at UAH under this contract.
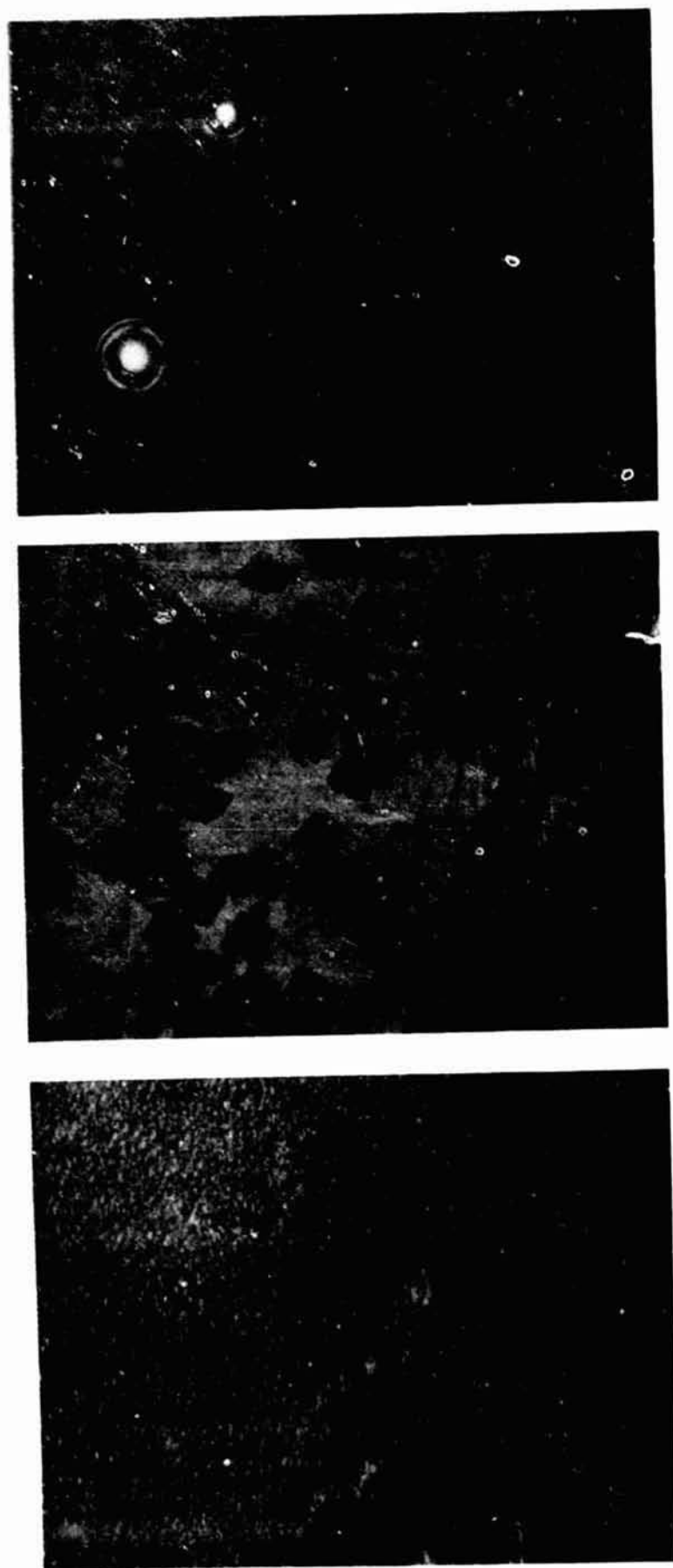
(a) Modified CP-4A etchant   (b) HNO_3/H_2O_2/tartaric acid etchant   (c) Br_2/Methanol etchant

Fig. 7. Etch pits obtained with different solutions (Magnification 600X)

(d) Characterization of the Crystals

The quality ⸀ the crystals was studied in terms of subgrain misorientation and dis-
location densities. In general, observations were done on cleaved (001) planes.

The mirror-like cleavage planes allow determining of grain and subgrain mis-
orientations very readily. A two-circle optical goniometer readable to 1 min. of
arc was used to determine larger misorientations. Misorientations below 1 min.
of arc were measured by probing the surfaces with a laser beam and scanning the
crystals. Tilt angles to about 20 seconds of arc could thus be observed by splitting
and displacement of the reflected beam. This approach, backed up by Laue and
Berg-Barrett photographs, enables one to obtain quantitative and statistical informa-
tion on the mosaic structure exposed at cleaved surfaces.

Dislocation densities were determined by counting etch pits on (001) planes.
Several chemical etchants were found to produce pits (see Table III).
Solution #2 and modifications thereof were reported to produce valid results for
InBi.[17] This etchant has also been successfully applied for etching of InAs (111).[18]
CP-4 etchants have been widely used for etching of other III-V compounds, and
alcoholic solutions of oxidizing agents such as chlorine, bromine, etc. were re-
ported to reveal reliably dislocations on cleavage planes of zinc.[19] Solution #1
produced square, pyramidal pits, the sides of the squares being parallel to [110]
as determined by Laue photographs. Besides preferential etching, the surfaces were
attacked in general (see Fig. 7a) and it was sometimes difficult to discriminate
pits from the background. Etching in solution #2 resulted in square, flat bottom
pits (Fig. 7b), a tendency to oxidize the surface was observed and the squares tended
to overlap since lateral growth took place rather fast. Irregular shaped pits were formed

Table II. Chemical etchants for InBi (001)

Etchant	Time	Result
1. CP-4A: H_2O: CH_3COOH – 1:1:1	1 Min, T_R	Square, pyramidal pits plus general attack of surface.
C -4A = HNO_3: HF: CH_3COOH – 5:3:3		
2. HNO_3: H_2O_2: [40% aq.solution tartaric acid] – 1:1:6	1 Min, T_R	Square, flat pits, tendency to oxidize surface.
3. I_2 (concentrated methanol solution): Methanol – 1:10	1 Min, T_R	Irregularly shaped pits.
4. Br_2: Methanol – 1: 12.5	25 sec, T_R	Conical pits.

26
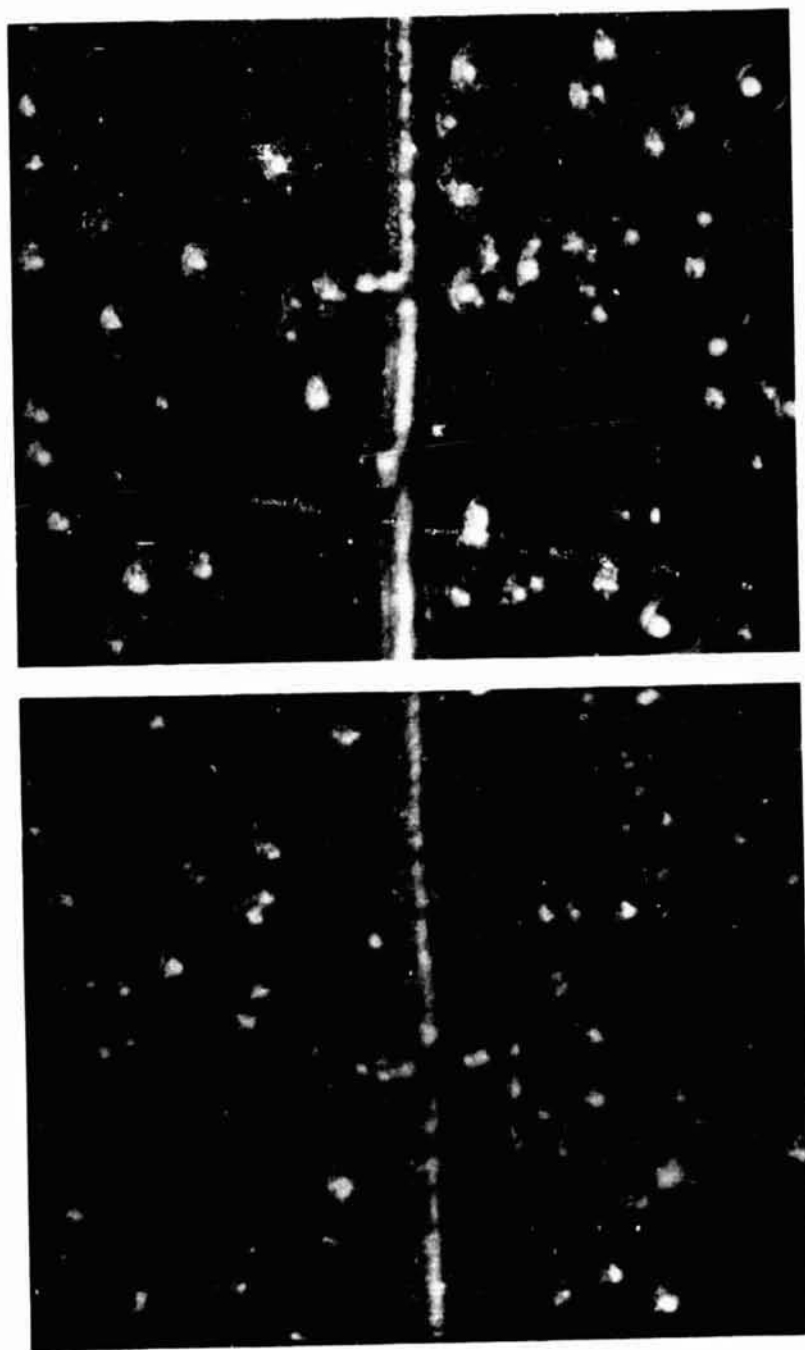
Fig. 8. Etch pit patterns on matching cleavage planes, crystal cleaved at liquid nitrogen temperature. Magnification 100X.

by solution #3, the surface was otherwise not attacked. Best defined pits of coni-

cal shape were obtained by etching with solution #4. The remaining part of the

surface was unaffected (Fig. 7c).

To ascertain that the pits correspond to crystal defects, matching cleavage

planes were etched with solution #4 and the patterns were compared. Unlike other

III – V compounds, InBi does not have a polar structure and, therefore, planes

equivalent by symmetry are also chemically identical. Except for grain boundaries,

the matching of the pit patterns was, however, only qualitative (Fig 8). This

indicates low activation energies for dislocations to be moved; evidently the

cleavage process causes rearrangement of dislocations. Consequently, mechanical

deformation experiments were performed. Etching, bending and reetching of speci-

mens showed that strain caused the appearance of many new pits. In addition, a

large percentage of the original pits showed flat bottoms. Since slip lines and grain

boundaries (Fig. 8) were also decorated and annealing reduced the pit density con-

siderably, it was concluded that the pits obtained correlate with crystal defects.

(e) Quality of the Crystals

As already indicated, the overwhelming majority of self-nucleated crystals

grew with the (001) plane parallel to the axis of the crucible or rather to the growth

direction. The substructure generally also consists of long grains and subgrains

parallel to the direction of growth. The subgrain width was of the order of 1-2 mm

and the average misorientation about 14 minutes of arc for crystals grown in hard

molds. Cleaved samples are shown in Fig. 9. The best hard-mold Bridgman crystals

were grown at rates of 10 to 12 mm/hour and gradients between 15° and 25°C/cm.
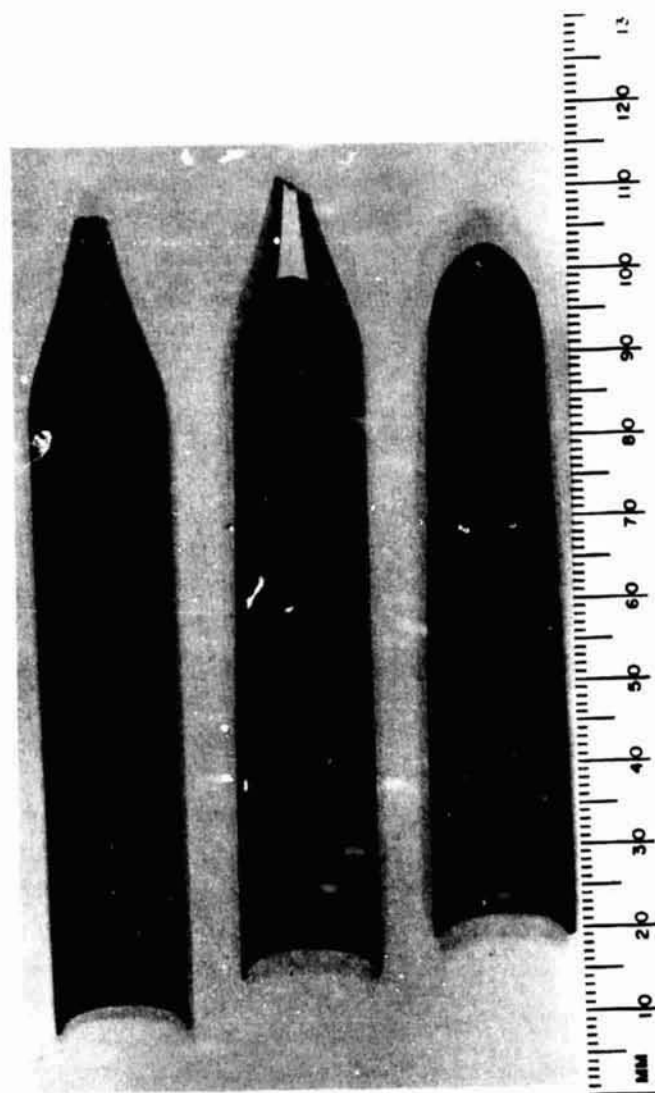
Fig. 9. InBi single crystal grown by hard-mold Bridgman technique in Pyrex crucible, sample cleaved in three slabs.
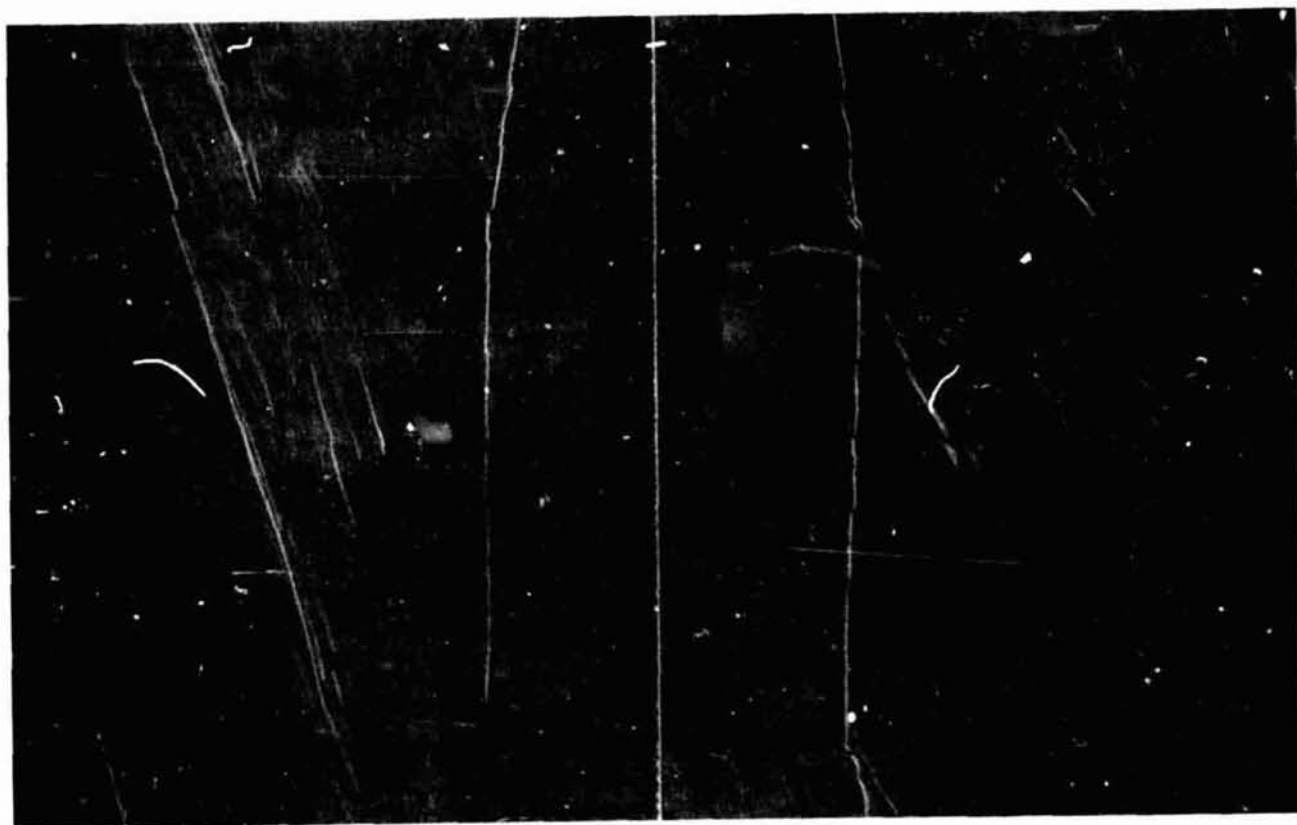
Fig. 10. Effect of annealing on etch pit density on matching cleavage planes. Left side annealed, pit density $2.5 \cdot 10^3$; right half not annealed, pit density $5 \cdot 10^4$. Linear magnification 120X. Crystal grown by Czochralski technique.

Dislocation densities in as-grown crystals ranged from $0.9 \cdot 10^4$ to $2.3 \cdot 10^4$ per cm^2; the average was $1.6 \cdot 10^4$ dislocations/cm^2. These counts include the dislocations at grain and subgrain boundaries. Crystals grown in soft molds were of considerably better quality. Best crystals were grown at low growth rates (≈ 1 cm/hour) and relatively steep temperature gradients (25 to 35°C/cm).

Average misorientation of grains was about 5 min. of arc, with grain width being 1 mm to several cm. Dislocation densities were also somewhat lower, $0.6 \cdot 10^4$ to $2 \cdot 10^4$ with an average of $1.3 \cdot 10^4$ dislocations/cm^2. Growth by the Czochralski technique produced single crystals only with seed orientation along the $\langle hk0 \rangle$ directions. Growth along $\langle 001 \rangle$ resulted in polycrystals. The best crystals were obtained by growing at a rate of 3 - 4 cm/hour and by tapering the seed to 1 to 2 mm diameter and then constantly increasing the crystal diameter at an angle of 10 to 15 degrees. Crystals as large as 6 cm in length and 1 cm diameter with no observable subgrains were obtained. The average dislocation density was about the same as it was for soft mold Bridgman-grown crystals, namely $1.3 \cdot 10^4$/cm^2.

Annealing of samples at 100°C for 4 - 8 hours and returning to room temperature at a constant rate of about 20°C/hour resulted in considerably lower etch pit density. The density was reduced by a factor of 20 to 30; crystals with less than 1000 counts per cm^2 could be obtained (Fig. 10).

It should be mentioned that single crystals of InBi were given to Dr. R. Kroes (SSL-T) for optical reflectance studies, to Dr. L. Lacy (SSL) for measurements of elastic properties and to Mr. T. White (UAH) for studies on thermal expansion.

References

1. H. U. Walter, J. Crystal Growth 10 (1971) 309.

2. H. U. Walter and R. S. Snyder, J. Less Common Metals 24 (1971) 467.

3. W. P. Binnie, Acta Cryst. 9 (1956) 686.

4. O. H. Henry and E. L. Badwick, Trans. AIME, 171 (1947) 389.

5. E. A. Peretti and S. C. Carapella, Trans. Am. Soc. Metals, 41 (1949) 947.

6. C. Giessen, M. Morris, N. J. Grant, Trans. Met. Soc. AIME, 239 (1967) 883.

7. M. Hansen and K. Anderko, Constitution of Binary Alloys, 2nd Ed. N.Y.
   McGraw Hill Publishing Co., 1958.

8. M. A. Krivor et al, Electrophysical Properties of the InBi Compound, IZV.
   VYSSHIKH.ZAVEDENii, Fiz., V. 10, No. 6, 1967. p. 152-154. FF. No. 672,
   1965, 3 p. N67-35140.

9. R. B. Lal, H. U.Walter, J. H. Davis, Bull. Am. Phys. Soc., Series II, Vol 17, No. 4
   (1972) 520.

10. G. S. Cooper et al, The Electrical Resistivity and Thermoelectric Power of InBi
    and In_2Bi, J. of Phys. and Chan. of Solids 25 (1964) 1277.

11. N. Petrescu, Z. Metallkunde 61 (1970) 19.

12. B. Predel and H. Sandig, Mater. Sci. Eng. 6 (1970) 110.

13. A. C. Thorsen, T. G. Berlincourt, Nature 192 (1961) 959-960.

14. S. Fischler, Trans. TMS-AIME, 230 (1964) 340-341.

15. Y. Shapira, S. J. Williamson, S. Fischler, Phys. Rev. 144 (1966) 715-719.

16. S. Asanabe, Memoirs of the Faculty of Science, Kyusyu University Ser. B, Vol 2,
    No. 2 (1956) 82-86.

17. U. Roy, Final Report, NASA Contract No. NAS8-25120 (1972).

18. J. W. Faust, A. Sagar, J. Appl. Phys. 31 (1960) 331.

19. H. S. Rosenbaum, M. M. Saffren, J. Appl. Phys., 32 (1961) 1866.

I.A.2. ELECTRICAL MEASUREMENTS ON InBi CRYSTALS*

The characterization of the crystals of indium bismuth compound started with NASA's interest in growing this material in one of the Apollo Flyback missions. The intermetallic compound InBi, in contrast to other III-V compounds which are semiconducting and have zinc blende or diamond structure, is metallic in nature and exists in three different phases.[a] The purpose of these studies is to differentiate the effect of reduced gravity environment on the growth of single crystals. The studies will provide background data that can be used to compare and differentiate the quality of crystals grown in space and on earth.

Electrical resistance arises whenever the regular periodicity of the lattice is disturbed. The resistivity of a pure perfect crystal is low since there are no defects to scatter or stop the electrons moving through the lattice under the influence of the applied voltage. In a real crystal, though, there are several types of deviations from this perfection which scatter electrons and this contributes to the resistivity ρ. These contributions act independently of one another, and are due to thermal oscillations of the atoms, $\rho(T)$, scattering due to impurity atoms, $\rho(c)$, scattering due to vacancies, $\rho(v)$, and relatively small contribution for dislocations, $\rho(d)$. Thus

$$\rho = \rho(T) + \rho(c) + \rho(v) + \rho(d) \tag{1}$$

For the most part, contributions due to impurities and physical defects are treated independently in theoretical discussions, but, in general of course, both are present in any physical experiment. The residual resistance in metals is the limit of the observed resistance when extrapolated to absolute zero (with many metals a measure-

* Person in charge - R. B. Lal

ment at $\sim 4^\circ$K is quite adequate) which is assumed to be due solely to chemical and physical imperfections. Correspondingly, the remainder of the resistance $\rho(T)$ (often called the ideal resistance) is assumed to arise solely from thermal vibrations of the unperturbed lattice and hence to be characteristic of the ideally pure and physically perfect metal crystal. Dislocations as well as point defects cause scattering of the conduction electrons in metals, and thus are responsible for an increase of the electrical resistivity over the residual resistivity and thermal resistivity. One usually assumes validity of the Matthiessen's rule.

For measurement of resistivity, the following two methods were used:

(a) Two-point probe method

(b) Four-point probe method

Experimental arrangements were made for setting up the two-point probe method of resistivity.[3] Basically the procedure involves making ohmic contacts to the ends of the sample, passing a known current through the sample and then measuring the voltage drop across the two probes applied to the surface. The resistivity is then calculated:

$$\rho = \frac{V}{I} \cdot \frac{A}{L} \quad \text{ohm cm} \tag{2}$$

where A = cross sectional area normal to current

L = distance between two probes

I = constant current

V = potential measured across the two probes

The four probe technique developed by Veldes,[4] was used to determine resistivity of samples in the form of flat discs. According to Valdes, the resistivity ρ is given by,

$$\rho = 2 \pi a \frac{V}{I} \text{ ohm cm} \tag{3}$$

where the distance between each of the four equidistant probes "a" is usually about 0.13 cms, V is the potential measured across the inside probes and I is the current passing through the outer probes.

The low temperature work down to 4.2°K was done using a glass cryostat. The temperatures were measured using Cu – constantan and Au + .07% Fe – chromel thermocouples. The values of voltages, current and thermocouple voltage were recorded using a Hewlett Packard data acquisition system having 2402A integrating digital voltmeter, 2547A coupler, 2911B crossbar scanner and a teletype system. Data could also be taken on a tape which can directly go to a computer to calculate the value of resistivity and to plot the curve for the temperature variation of resistivity.

Since indium bismuth is a very low melting compound (109°C) special care was taken in making ohmic contacts on the sample. For current contacts electrical leads were soldered using a low melting solder #B20E2 (mp 204°F) made by Alpha Metals, Inc. The crystals were mounted on alumina substrate. The potential probes were pressure contacts for samples of definite rectangular geometry.

For Apollo Flyback samples of InBi a special crystal holder was made from teflon where the whole cast sample could be used for resistance measurement (see Fig. 1). All the electrical leads were pressure contacts. The sample holder was tested by using samples of stainless steel 303 and high purity aluminum rods of about 0.62 cm diameter. The values of resistivities for stainless steel and aluminum were found within 5% of the available values in literature (Table 1).

TEFLON CRYSTAL HOLDER

T.C.

holder rod

Wiring connector

Copper contacts

copper contacts

Sample

Fig. 1

V+   V−

Sample

I+   I−

T.C.
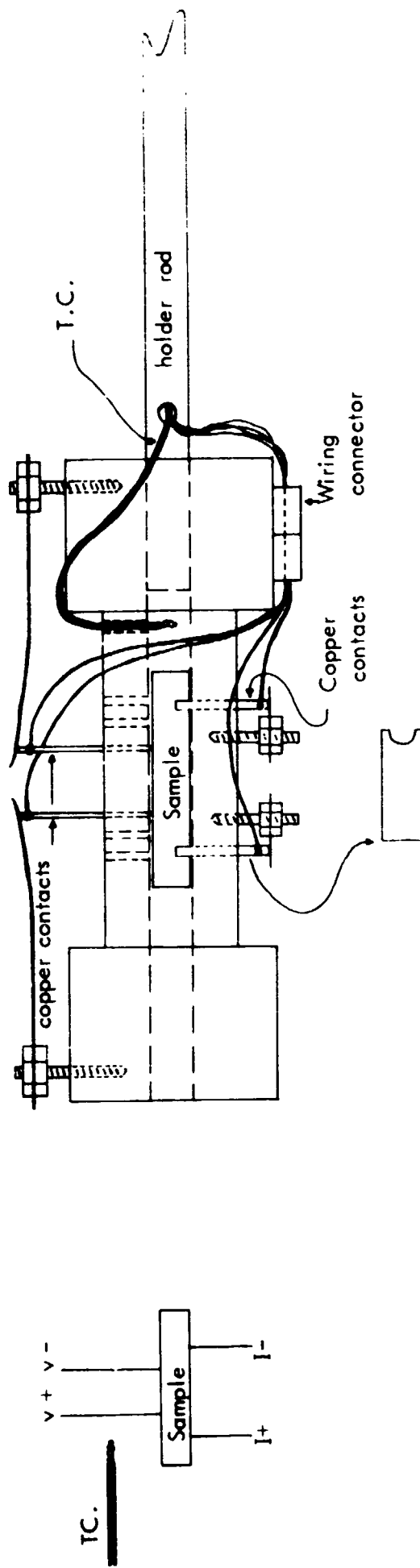
Table I

Test of Teflon Crystal Holder

Sample	Measured Resistivity by ρ in ohm cm	Reported Value of ρ (ref 5)
Stainless Steel 303	75.48×10^{-6}	73.5×10^{-6}
High purity Aluminum 6061	2.52×10^{-6}	2.67×10^{-6}

Results for Cast Polycrystalline Samples (Destructive Effects of Thermal Cycling)

Cast samples of InBi were solidified from the high purity molten indium and bismuth in a cylindrical, 5.4 mm diameter split graphite mold. Sample dimensions were measured with a traveling microscope. The melting point of one of the samples was checked and found to be $109 \pm 1^{\circ}C$ as expected. This eliminates the possibility that the presence of heterogeneous phase,[8] such as In or Bi, caused the results reported here. The results of resistance measurements on polycrystalline InBi samples at room temperature and at $77^{\circ}K$ are shown Table II. The sample current density is no longer uniform because of internal fractures noticed after cooling the samples down to $77^{\circ}K$; therefore, symbol ρ' for the apparent resistivity is used.

Table II

Resistance Ratios of Indium Bismuth Samples

Sample	$\dfrac{\rho'_{77}}{\rho_{295}}$	$\dfrac{\rho'_{295}}{\rho_{295}}$
Single Crystal 1	.20	1.0
InBi Polycrystal 2	.47	1.8
3	.55	2.0
4		2.3
5	.69	2.2

In general, the resistance decreased by about 1/2 instead of 1/5 (as seen for single crystal) as the temperature was lowered from $295°K$ to $77°K$ as seen in column 1. When the samples were warmed back to room temperature, ρ' was about two times greater than it was before quenching to $77°K$ as seen in column 2. Table II covers only the first cycle; however, repeated quenchings further increased the value of ρ'_{295}. These changes were independent of the rate of cooling from 50 to $1°K/sec$.

Several of the samples which had been quenched several times were annealed at $50°C$. The resistivity decreased by up to 20% in several hours, but the amount and rate of recovery was not reproducible from sample to sample. Annealing one sample at $80°C$ did not produce additional recovery.

Microscopic examination of the InBi polycrystals after cycling revealed surface cracks, which had not been observed on monocrystals. In order to study the morphology more carefully, samples of InBi polycrystals were polished on one side. This removed the

outer layer of material which might have been affected by the mold and pro-vided a flat surface for examination.

The appearance of the original polished surface is shown in Fig. 2. Fig. 3 shows the same after seven cycles to 77°K. Note that (1) the grain boundaries have darkened considerably, (2) that grains appear to have subdivided and (3) that new, long vertical straight fractures have appeared which pass through several grains.

Several samples actually fractured in half after about 10 cycles to 77°K. The fractured ends consisted of several smooth facets which presumably were the (001) cleavage planes of each grain.

Similar, but more subtle, morphology results have been reported for other non-cubic materials by Boas and Honeycomb[7,8,9] who studied the deformation of poly-crystals of tin, zinc, cadmium, and other materials by cyclic heating and cooling. Their results indicated that the anistropy of thermal expansion causes plastic deforma-tions which resulted in changes of the morphology of grain boundaries of noncubic materials. Cyclic treatment of materials having cubic symmetry or small differences in thermal expansion coefficients (such as magnesium) did not produce deformations. Their X-ray examination of samples, for which the surface layers had been etched away to remove slip lines, indicated that the deformation occurred throughout the specimen. Epprecht[6] has studied the behavior of heterogeneous alloys by thermal treatment and has found deformations when the thermal expansion coefficients of the components were considerably different. Likhachev[10] has studied the problem of stresses generated in crystals theoretically in terms of the temperature variation,
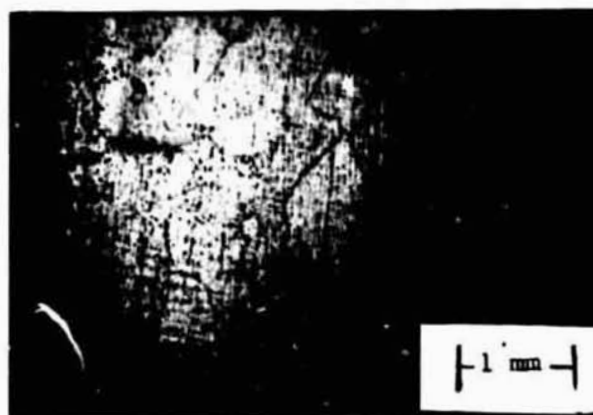
Fig. 2

InBi polished surface before thermal cycling

Fig. 3

The same InBi surface after seven thermal
cycles to 77°K

the elastic constants, and the differences of thermal expansion constants.

The present results in polycrystals of InBi are attributed to an anisotropy in the thermal expansion and the good cleaveability in the (001) plane. The deformation resulting from the temperature change produced the irreversible change of the resistivity and morphology. The observation that there were no changes of the resistivity or morphology of single crystals of InBi is compatible with this analysis because a single crystal would not have surrounding grains on which to exert stress.

Obviously any experimentalist contemplating using polycrystalline InBi at low temperature should consider using single crystal samples or take into account the effects of stress on his results. Polycrystalline InBi appears unreliable upon cooling to cryogenic temperatures structurally or as an electrical solder. The results of the above measurements were published in open literature.[11]

Results for InBi Single Crystals (Correction of Hashimoto's Data)

The electrical resistivity of InBi single crystals were measured by two-point probe method. The current contacts were soldered with low melting solder (mentioned earlier) and the potential probes were two pressure type contacts or in some cases lightly pressed screw in contacts. Special probe assembly was designed and fabricated at UAH (fig 4). Samples were mounted on alumina substrates. Samples used for these measurements were single crystals grown at UAH by different growth techniques. Other experimental details were the same as mentioned earlier in the report. Temperature variation of electrical resistivity down to 4.2°K was measured in a number of crystals cleaved along (001) plane and cut by a special wire cutter into a regular

COPPER CRYSTAL HOLDER

Teflon

Leads soldered on

Substrate

SAMPLE

wiring
board
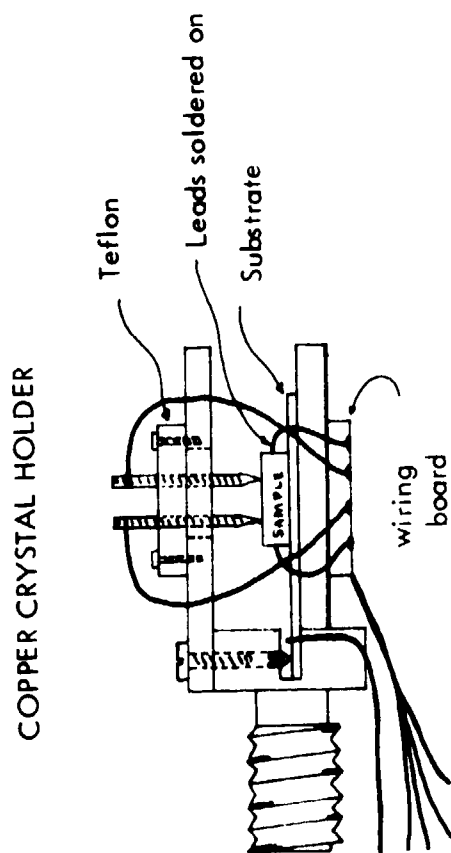
Fig. 4

rectangular shape. Sample dimensions were measured with a travelling microscope. In some samples resistivity was also measured down to 2.5°K by pumping on the liquid helium. Temperatures below 4.2°K were measured by noting the vapor pressure of helium and using the table given by Hoare et al.[12] X-ray Laue pattern shows that all the crystals studied belong to a tetragonal system. The crystal structure has been reported earlier by Binnie.[13] Result of measurement of temperature variation of resistivity for samples #5, 6, Cz(1), Cz(11) are given in Table III and the curves are shown in Figs. 5, 6, 7 and 8, respectively.

The room temperature resistivity in all cases compares with the only available values reported by Asanabe.[14] From the curves of temperature variation of resistivity it is evident that in the case of InBi the behavior is metallic and the residual resistivity occurs around 4°K. The values of resistance ratios $\left(\frac{\rho_{300}}{\rho_{4.2}}\right)$ for different crystals are given in Table IV.

Table IV

Resistivity Ratio $\frac{\rho_{300}}{\rho_{4.2}}$ for InBi Crystals

Sample	$\rho_{300}/\rho_{4.2}$
#5	275
#6	70
#Cz(1)	45
#Cz(11)	98

Table III

Temperature Variation of Resistivity of InBi

Temperature	Sample #5 Resistivity $\rho_\perp$ ohm cm	#6 Resistivity $\rho_\perp$ ohm cm	#Cz(1) Resistivity $\rho_\perp$ ohm cm	#Cz(11) Resistivity $\rho_{\parallel}$ ohm cm
2.6	3.60×10^{-7}	10.91×10^{-7}	1.73×10^{-6}	
3			1.72	
3.4		10.91		
3.6	3.60			
4.2	3.6	1.19×10^{-6}	1.72	1.37×10^{-6}
5	3.7	1.21	1.7	1.6
10	7.3	1.49	1.9	3.2
20	2.3×10^{-6}	2.70	3.2	6.0
40	7.0	5.8	6.1	1.4×10^{-5}
60	1.3×10^{-5}	9.5	1.0×10^{-5}	2.2
80	2.0	1.4×10^{-5}	1.5	3.0
100	2.8	1.8	1.9	3.8
120	3.8	2.4	2.5	4 6
140	5.0	2.9	3.0	5.6
160	5.6	3.4	3.5	6.5
180	6.4	4.0	4.2	7.5
200	7.3	4.6	4.7	8.2
220	7.8	5.2	5.2	9.1
240	8.0	6.0	5.8	1.0×10^{-4}
260	8.8	6.5	6.5	1.1×10^{-4}
280	9.2	7.2	7.0	1.25
300	9.9	7.7×10^{-5}	7.7×10^{-5}	1.35×10^{-4}

TEMPERATURE VARIATION OF RESISTIVITY OF InBi SINGLE CRYSTAL
5
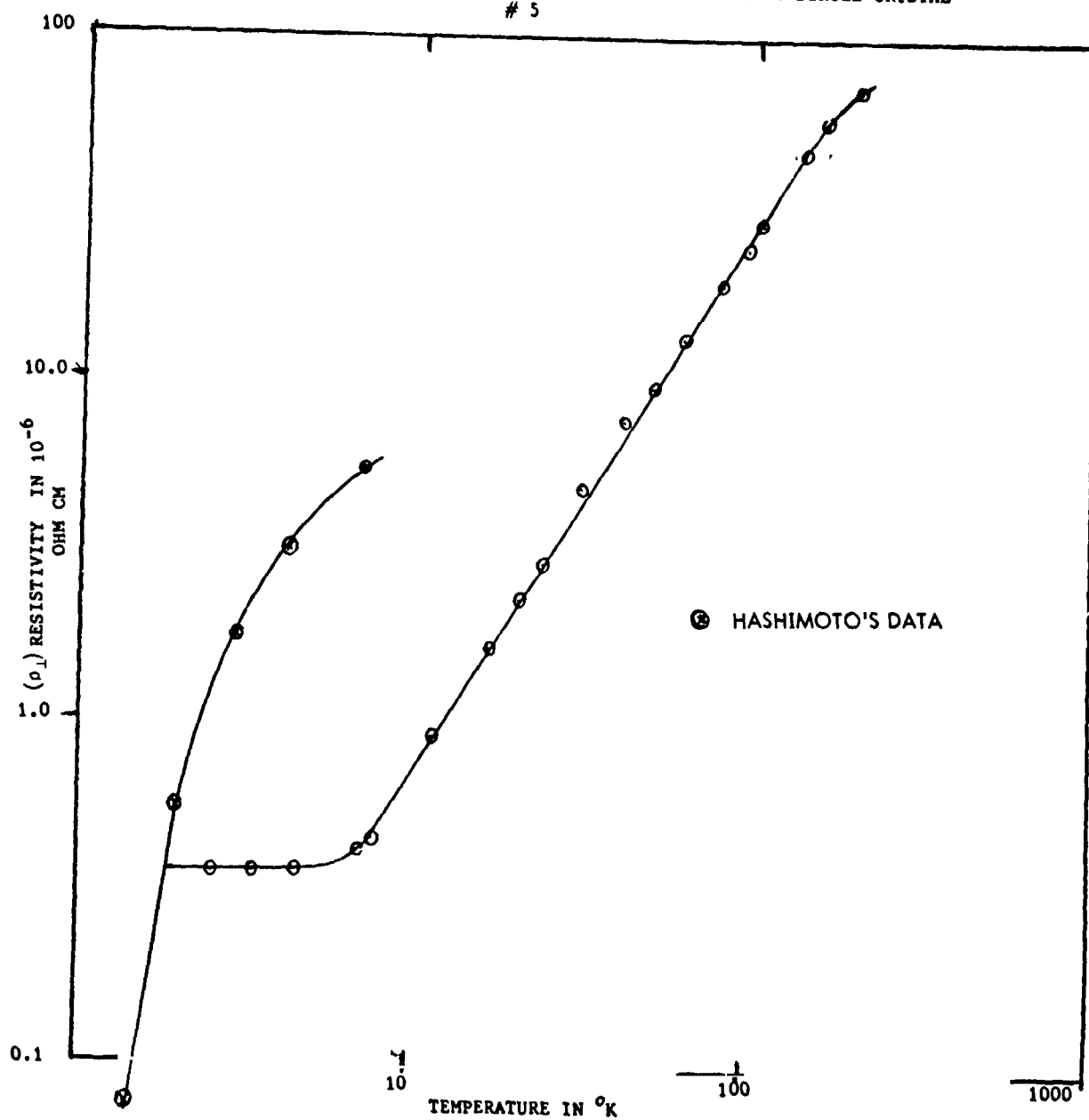
Fig. 5

InBi Cleaved Crystal #6
Residual Resistivity ratio = 60
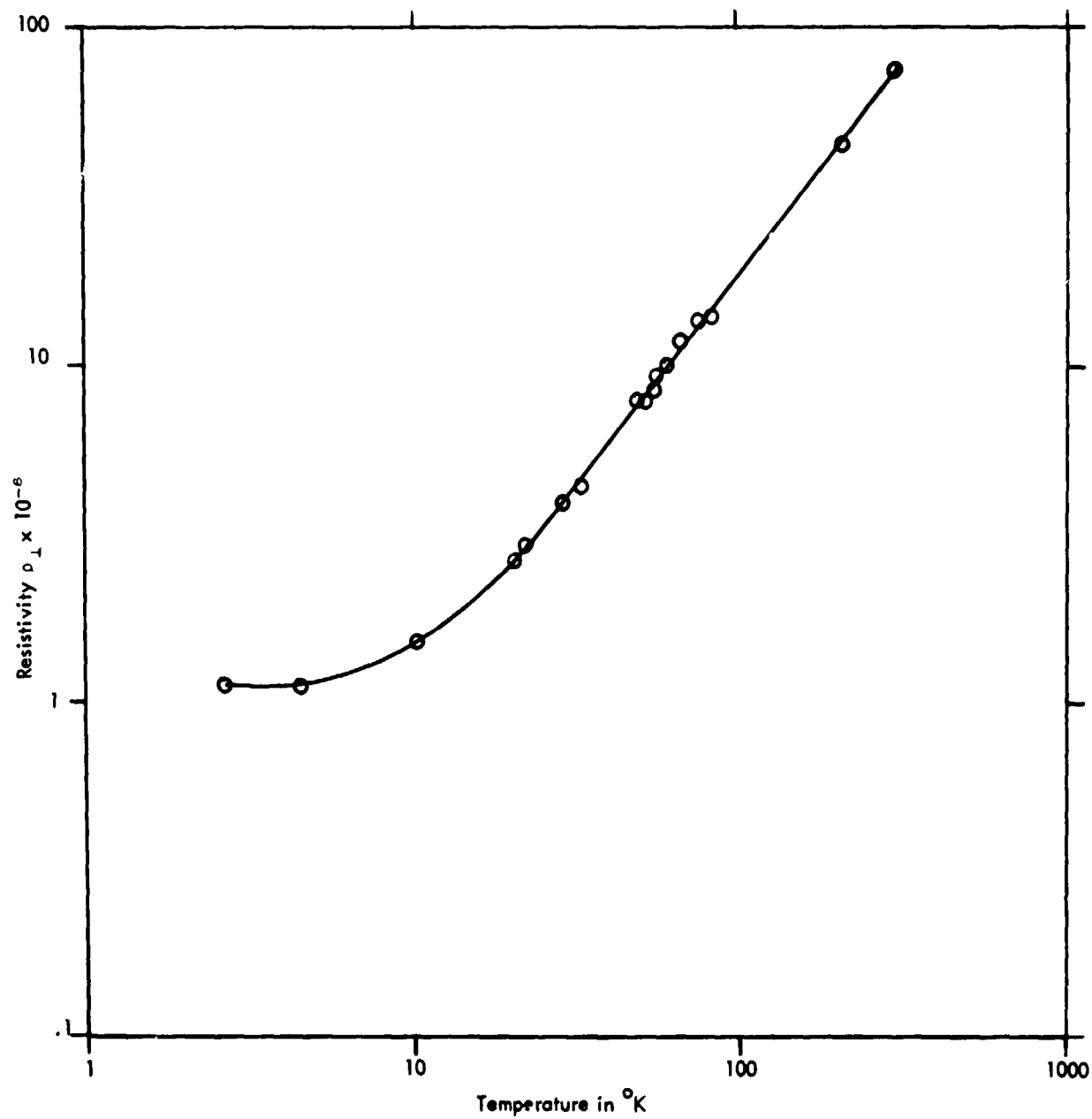
Fig. 6

InBi SINGLE CRYSTAL

CZ (111) 1

RESISTIVITY RATIO = 46

Fig. 7

InBi Crystal #CZ(11)
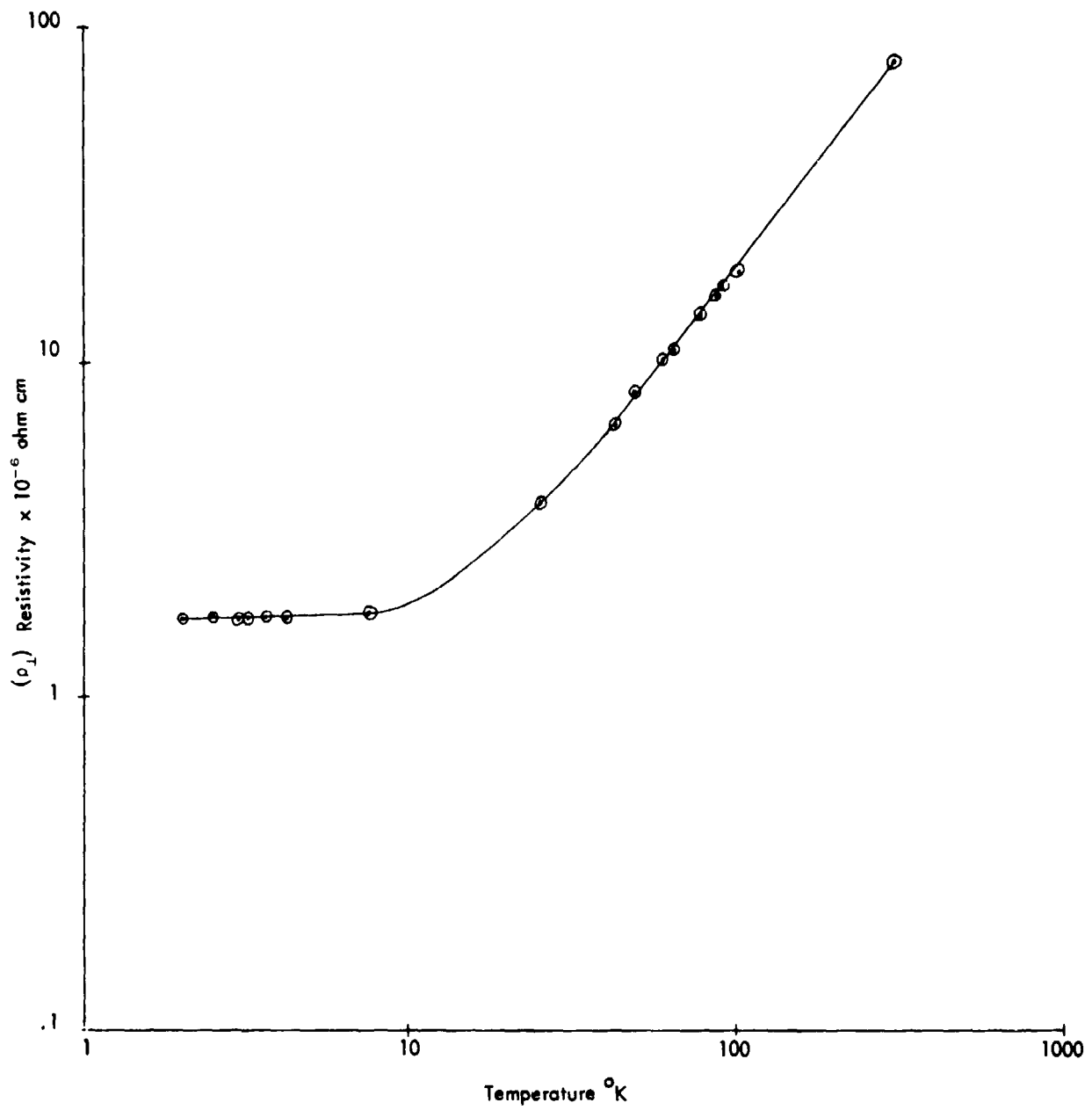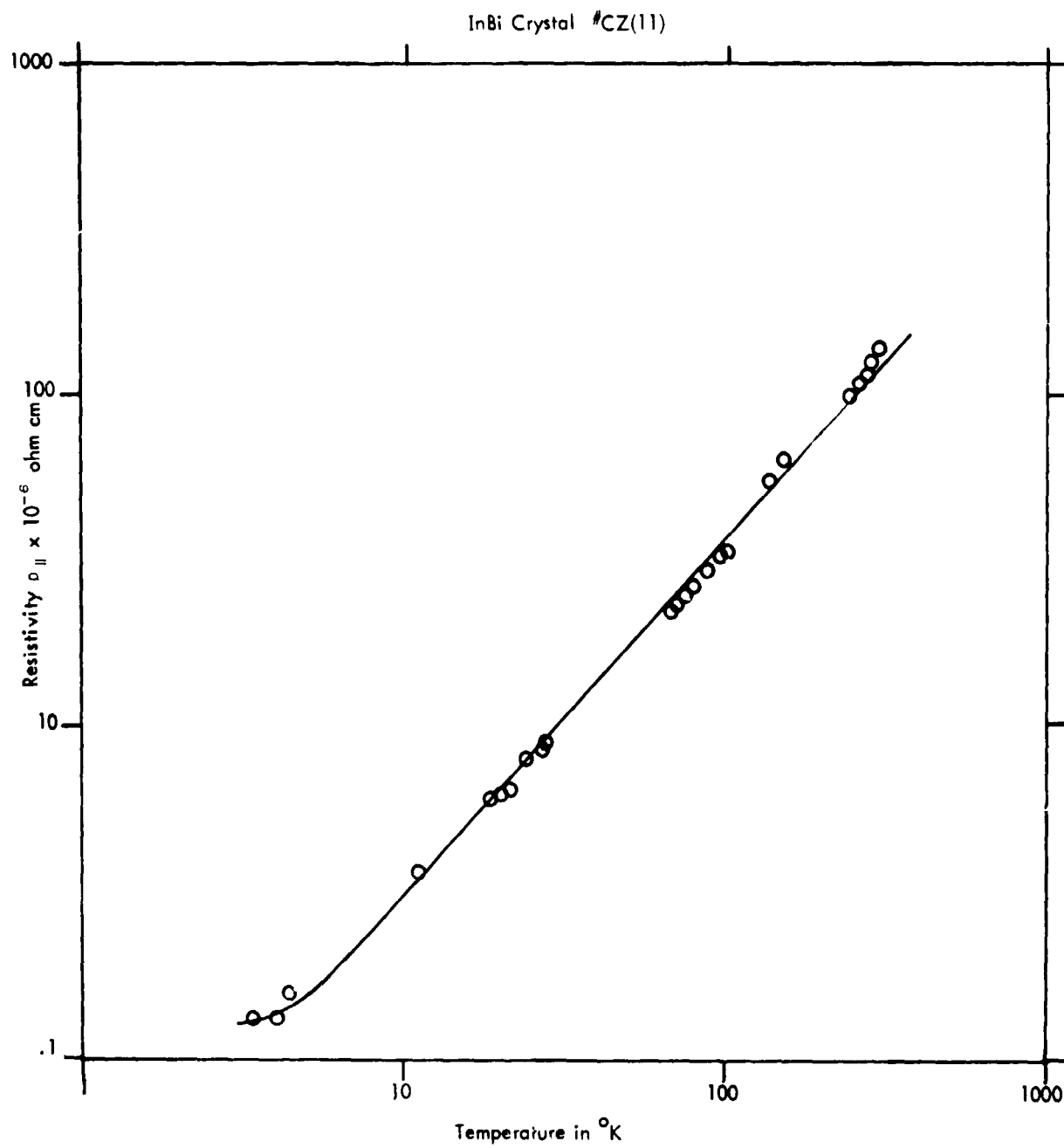
Fig. 8

In samples #5, 6 and Cz(1), resistivity data were taken down to 2.6°K. No appreciable change of resistivity was found in going from 4.2°K down to 2.6°K. The high values of resistivity ratio is a good indication of the crystal purity and can be regarded as a measure of crystal quality.

The data reported here for InBi single crystals do not agree with the resistivity data reported by Hashimoto.[16] Hashimoto measured the resistivity ($\rho_\parallel$) down to 2°K (Fig.5) in one of the samples of Asanabe. Hashimoto did not observe residual resistivity even at 2°K and found a sharp fall in his resistivity curve around 8°K. This seems unlikely for a metallic sample where no residual resistivity is seen even at 2°K and a considerable departure of Mathiessen's rule is observed. These results developed considerable doubt of the validity of Mathiessen's rule in the case of InBi samples. Although samples used by Hashimoto had the tetragonal structure of InBi but their mp was reported to be 103°C (as compared to 109.5°C). The most probable source of error expected in the measurements of the above workers is the possibility of having an excess of one of the phases. To check on the above results, some cast samples were grown with 1 at % excess of indium. The result of measurement of resistivity for one of such samples is shown in Fig. 9. The sample was found to be superconducting, but the transition width was much smaller as compared to Hashimoto's results. At the time when Hashimoto published his paper, superconductivity in indium bismuth compounds were not reported. It was reported later by Jones and Ittner[16] that In_2Bi is superconducting with a transition temperature of $5.6 \pm 0.1^{\circ}$K; also Hutcherson et al. and Cruceanen et al.[18] reported a transition temperature of 4.1°K for In_5Bi_3. This makes us believe that Hashimoto's crystals might have had a trace of In_5Bi_3 phase which, in turn, gave rise to superconductivity. This gives a very good indication that an InBi single
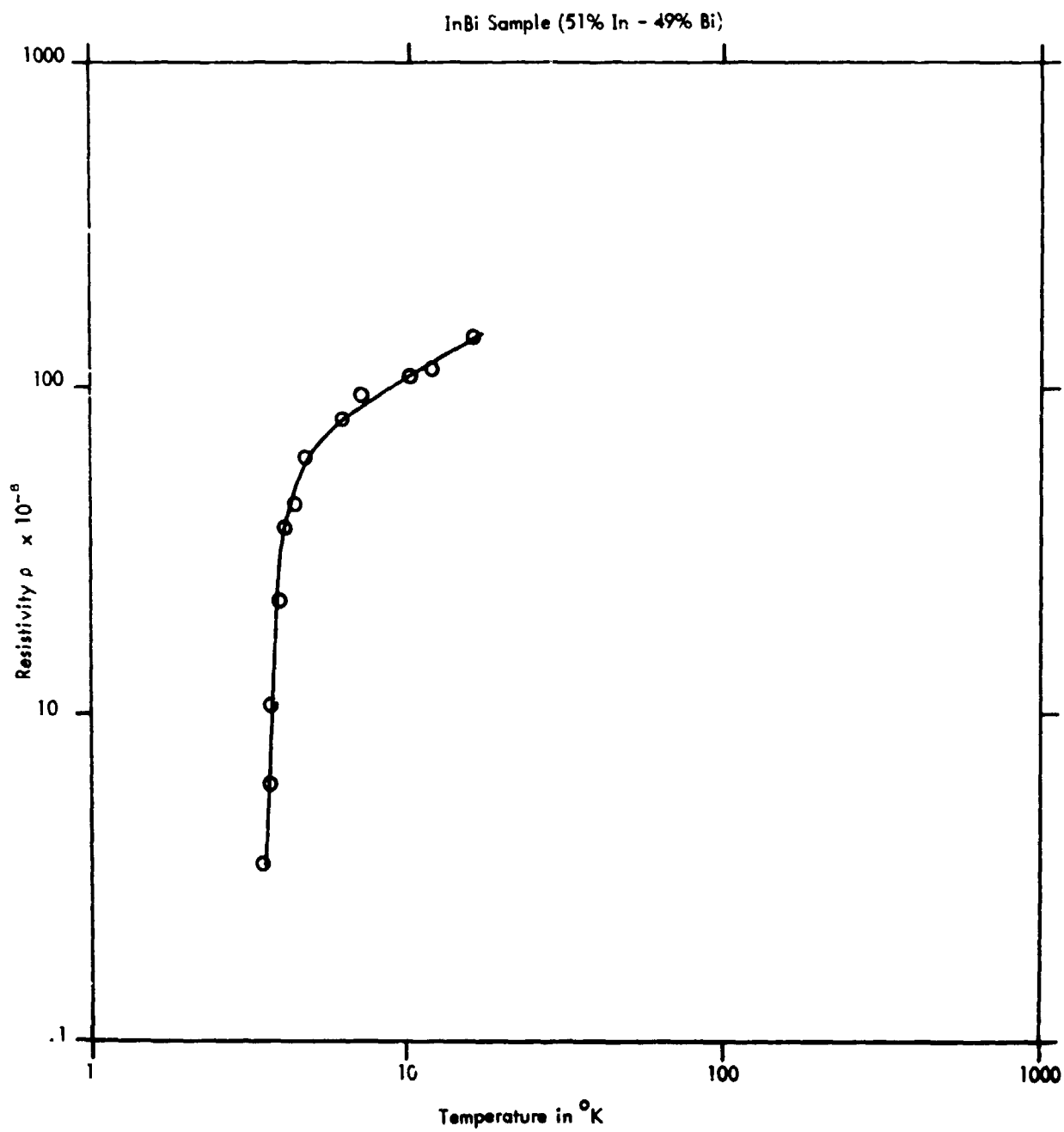
Fig. 9

crystal, if perfect, should not exhibit any superconductivity, and should have almost

a line type compound in the phase diagram. From the results of temperature varia-

tion of resistivity in InBi single crystals it can be concluded that this intermetallic

compound, unlike other compounds of the same series, is metallic. The compo-

sition width of InBi is extremely narrow. The high value of resistivity ratio is a

good indication of the overall crystal quality. No appreciable change in the

value of the resistivity ratio was detected for some single crystals of InBi after

they were annealed at room temperature for a few months.

Estimate of Lorenz Number for InBi

The electrical resistivity versus temperature curve may be used in interpreting thermal

conductivity data in transformation regions. The data are correlated by the Wiedemann-

Franz Lorenz equation as follows:

$$K = \frac{L_0 T}{\rho}$$

where

K = thermal conductivity in watts/cm$^\circ$K

T = temperature in absolute K

ρ = electrical resistivity in ohm-cm.

L_0 = constant, known an Lorenz number

The chief use of the above equation is to determine both thermal conductivity

and electrical conductivity on one or a few specimens of an alloy or metal to establish

the constant for that particular system. For metals, the value of L_0 has been found

to be constant and the theoretical value to be 2.45×10^{-8} watts ohm/K^2.

No reliable data are available for the thermal conductivity of InBi crystals. We have tried to estimate the value of L_0 using the thermal conductivity data of Weighardt (ref. 19) and our data of electrical conductivity. The value of L_0 was found to be 2.33×10^{-8} watts ohm/K^2. Krivov et al.[20] have also measured the thermal conductivity of InBi single crystals from 110° K to 330°K. They found that their crystals had a melting point of 105°C, which is different from the reported mp of InBi. Using their value of thermal conductivity (3.2×10^{-3} cal/cm. sec. deg.), we calculated a value of L_c equal to 0.38×10^{-8} watts ohm/K^2. This value of L_0 is very different from the theoretical value of L_0. If we try to estimate the value of thermal conductivity of InBi at 4.2°K using our value of electrical resistivity and estimated value of $L_0 (2.33 \times 10^{-8}$ watts ohm/K^2), we find a value of $\approx 50 \times 10^{-3}$ cal/cm. sec. deg.). This suggests that the behavior of thermal conductivity of InBi is not only electronic but also has a significant lattice contribution similar to metals like antimony and bismuth. More accurate measurements of the thermal conducitivity of InBi at room temperature and at lower temperature are needed to resolve the behavior of thermal and electrical condutivities.

Computerized Data Handling and Curve Plotting

During the previous year data were taken on a teletype printer and graphs were hand drawn only after manual calculations and chart interpolation had been made at each point. Now we can take parallel data in the form of punched paper which may be fed directly into the computer for calculations and automatic graphing. The variables are usually sample resistance (voltage) and temperature (thermocouple output). The
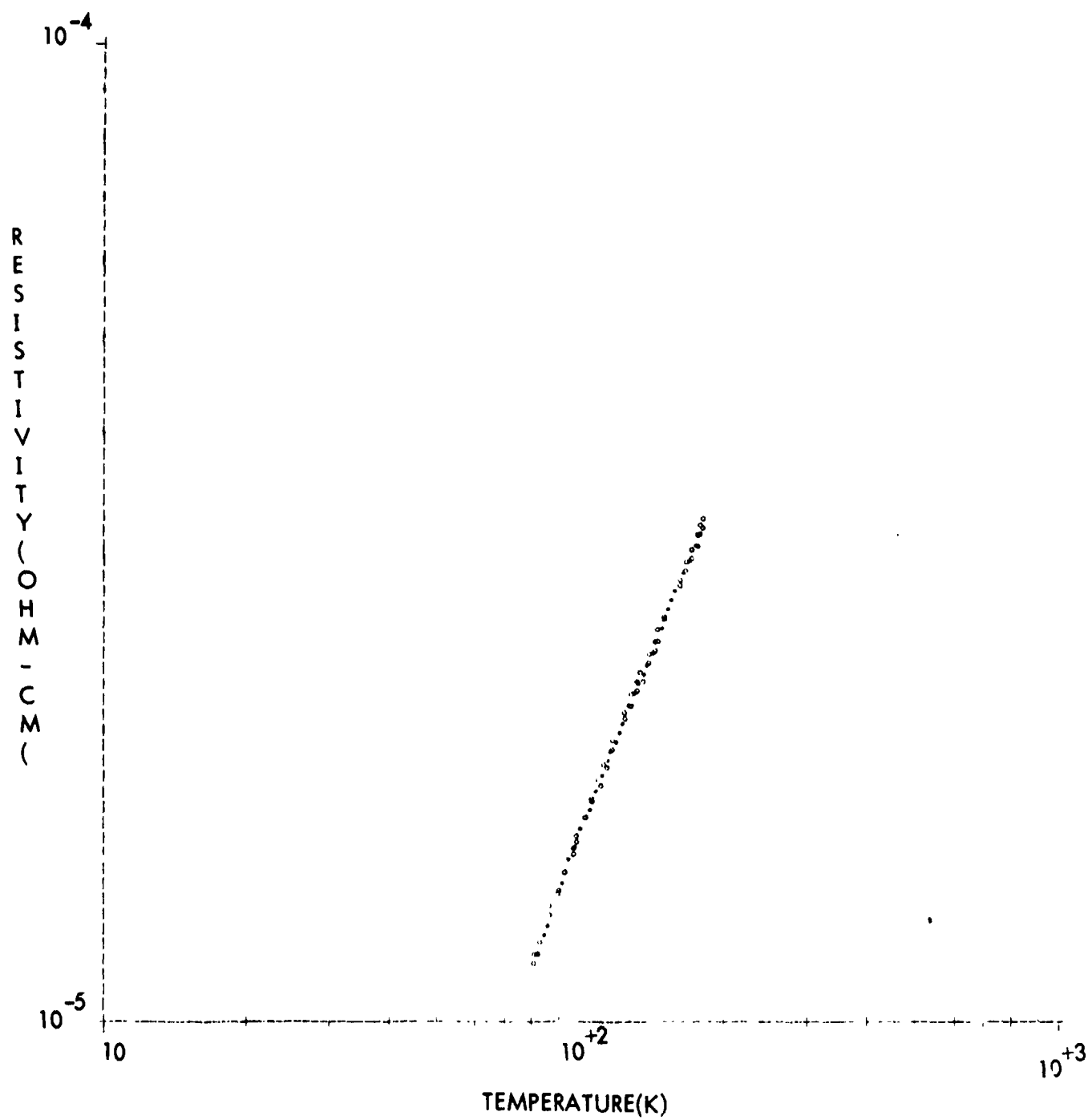
Figure 10. Sample data computer analyzed and plotted for InBi single crystal.

direct use of an X-Y recorder was not meaningful since the thermocouple and germanium resistor voltages are not linear in temperature.

The first test results, displayed in Fig. 10, show the change in resistivity of an InBi sample cooled from about 120 to 80°K. Only slight program changes will permit germanium resistance thermometer output to be used.

Table for Properties of InBi, In_2Bi and In_5Bi_3

During the course of work the attached tables (V, VI and VIII) were compiled which list important properties of indium bismuth compounds.

Conclusion

From the results of electrical resistivity measurements reported earlier, it can be seen that InBi intermetallic compound behaves like a metal, unlike other III-V compounds. The residual resistivity in single crystals appears around 4°K and does not support the results reported earlier by Hashimoto. It appears that the composition width of InBi is very narrow and the other two compounds, In_2Bi and In_5Bi_3, are superconducting. Polycrystals are extremely susceptible to thermal cycling effects. Resistivity ratios $\rho_{295}/\rho_{4.2}$ in the case of single crystals can safely be regarded as an indicator of overall quality of a crystal.

REFERENCES (Part 1.A.2)

1. T. C. Bannister, R. B. Lal and H. U. Walter, Characterization Plan for Apollo 14 Flyback Demonstration No. 15, 16, 17 and 18, SSL/UAH.

2. B. C. Giessen, M. Morris and N. G. Grant, Trans. Met. Soc. AIME, 239, 883 (1967).

3. "1968 Book of ASTM Standards," ASTM, Philadelphia, Penn., 1968.

4. L. B. Veldes, Proc. of I.R.E. 42, 420 (1959).

5. George T. Meaden, Electrical Resistance of Metals, Plenum Press, New York, 16, (1965).

6. W. Epprecht, Z. Metallkde 59, 1 (1968).

7. W. Boas and R. W. K. Honeycombe, Proc. Roy. Soc.,(London) A186, 57 (1946).

8. W. Boas and R. W. K. Honeycombe, Proc. Roy. Soc.,(London) A188, 427 (1947).

9. R. W. K. Honeycombe, Plastic Deformations in Metals, St. Martins Press, N. Y. (1968).

10. V. A. Likhachev, Sov. Phys. Solid State 3, 1330 (1961).

11. R. B. Lal, J. H. Davis and B. E. Powell, J. Less Common Metals 27, 367 (1972).

12. F.E. Hoare, L. C. Jackson and N. Kurte, Eds., Experimental Cryophysics, Butterworths, London 351 (1961).

13. W. P. Binnie, Acta. Cryst. 9, 686 (1956).

14. S. Asanbe, Mem. of Faculty of Science, Kyuyu Univ., Ser B 2, 82 (1956).

15. K. Hashimto,J. Phys. Soc., Japan 12, 1423, (1957).

16. R. E. Jones and W. B. Ittner, Phys. Rev. 113, 1520 (1959).

17. J. V. Hutcherson, R. L. Guay and J. S. Harold, J. Less Common Metals 11, 296 (1966).

18. E. Cruceanu, E. Hering and H. Schwarz – Phys. Letters 32A, 295 (1970).

19. Von G. Wieghardt, Z. Metallkde, 57, 76 (1966).

20. M. A. Kirov, E. V. Malisova and V. A. Presnov, Sov. Phys. J. 10, 109 (1967).

TABLE V

54

PROPERTIES OF INTERMETALLIC COMPOUND InBi

Property	Description	Comments	Reference
Melting point	109.5°C	The compound melts congruently	1. Constitution of Binary Alloys, 2nd ed. McGraw Hill Book Co., New York, 1950. 2. Trans. of Metallurgical Society of AIME, 239, 883, (1967).
Crystal Structure	Tetragonal $a = b = 5.00$ Å $c = 4.773$ Å $c/a = 0.955$ Å	Each Bi atom has four In atoms as nearest neighbors. The structure consists of layers of like atoms normal to C - axis. Marked cleavage plane normal to C - axis. Density measurements show there are two molecules of InBi in unit cell.	3. Acta. Cryst., 9, 686 (1956).
Space Group	P4/nmm		4. Ref. 2
Electrical Resistivity $\rho = 1/2 (\rho_{11} + \rho_{33})$ (Mean)	$\approx 8.8 \times 10^{-6}$ ohm cm at 300°K	Electrical resistivity increases proportionally to temperature	5. Memoirs of the Faculty of Science, Kyusyn Univ. Ser. B, 2, No. 2 82 (1956).
$\dfrac{\rho_{33}}{\rho_{11}}$	1.6	Values are at 300° K	6. Same as ref 5.

Properties of Intermetallic Compound InBi

Property	Description	Comments	Reference
Electrical Resistivity (Molten)	$\approx 8 \times 10^{-5}$ ohm cm	The measured resistivities of In Bi alloy was shown to satisfy the linear relation to temperature and the parabolic relation to concentration	7. Trans. JIM, 3, 35, (1962).
Hall Coefficient and Free Electron Density	$\sim 1.3 \times 10^{-3}$ cm^3 / coulomb $\sim 10^{21}$ cm^{-3}	The Hall coefficient (R_{33}) remains constant for the range 80° C to -170° C	8. Same as 5
Residual Resistivity ρ/ρ_0 (Quick freeze method) ρ/ρ_0 (Bridgman)	~ 40 ~ 80	The quick freeze method of growing involves use of a graphite boat and mixture of In and Bi is melted in air. Few tentative conclusions concerning the Fermi surface of InBi are given.	9. Phys. Rev. 144, 715, (1966).
Superconductivity	NO	InBi (y phase) has been found non-superconducting down to 0.5° K (by adiabatic demagnetization)	10. J. Less Common Metals, 11, 295 (1966).
Diffusion Coefficient D for In [114]	$D = 1.21 \times 10^{-6}$ cm^2/sec at 112°C $D = 9.64 \times 10^{-5}$ cm^2/sec at 800°C	The self diffusion coefficient of In^{114} in the molten InBi compound was measured by capillary reservoir method between 112° C to 800° C.	11. Z. Metallkde 61, 19 (1970).
NMR Studies (Molten State)	Activation energy for the dissociation of InBi grouping = 2 kcal $mole^{-1}$.	(a) The results indicate the existence of intermetallic compound in liquid state. (b) Knight shift is sensitive to the short range atomic order. (c) The axial component of Knight shift and the isotropic knight shift is small compared to bare metal.	12. Proc. Phys. Soc. 87 473 (1966). 13. Advances in Phys, 16, 275 (1967). 14. Proc. Phys. Soc., 90 495 (1967).
Phase Diagram		Three stable phases have been reported, $InBi$, $In_2 Bi$, $In_5 Bi_3$	15. Same as ref. 1 and 2.

Properties of Intermetallic Compound InBi

Property	Description	Comments	Reference
Debye Temperature			
Specific Heat			
Heat of Fusion			
Vapor Pressure			
Absolute Thermal Conductivity in Cal/cm sec°C	~ 0.019 at 100°C		16. Z. Metallkde, <u>57</u>, 76, (1966).
Enthalpy of Formation	$\Delta H'' = -563$ cal/g – atom	Enthalpies of melting was determined by quantitative differential thermal analysis.	17. Z. Metallkde, <u>55</u>, 97 (1964).

Properties of Intermetallic Compound InBi

Property	Description	Comments	Reference
Entropy of Formation	$\Delta S'' = 0.26$ cal/g – atom$^\circ$C	The value of $\Delta S''$ is very low as compared to ΔS_{ideal}, which indicates an ordered arrangement of the atoms in the lattice	18. Same as ref. 16.
Coordination number	(a) 8	(a) Number of neighbors in first coordination shell	19. Same as ref. 2.
	(b) 4	(b) Number of close neighbors	

TABLE VI

PROPERTIES OF INTERMETALLIC COMPOUND In_2Bi

Property	Description	Comments	Reference
Melting Point	$8\text{Y}.0^\circ C$	(a) Peritectic reaction α + InBi – cooling In_2 Bi (ref. 1). (b) Later it was reported that compound melts congruently (ref. 2)	1. Trans. Am. Soc. Metals 41, 947 (1949). 2. Growth and Imperfections of Metallic Crystals, Eds D.E.Ovsienko Consultant Bureau (1968) p. 47.
Crystal Structure Space Group	Hexagonal Symmetry $a = 5.496$ Å $c = 6.579$ Å $c/a = 1.197$ $P_{63/mmc}$	Holohedral class D_{6h}. Structure of the Ni_2In type	3. Sou. Phys. Cryst, 3, 3 (1958).
Electrical Resistivity (at the melting point)	$\rho = 2.4 \times 10^{-5}$ ohm cm	Results suggested that at mp the In and Bi atoms are in exactly the same positions as in the solid state.	4. Phys. Metals and Metallogr, 14, 132 (1962).
Hall Coefficient (Molten State)	$R_{expt} = -4.6$ cm^3/$^\circ$C Mobility $\mu = 1.80$ R_c (theoretical cm^2/V.sec $= -5.0$ cm^3/$^\circ$C $\frac{R}{R^o} = 0.92$		5. Soviet Phys. Solid State, 8, 2950 (1967).
Superconducting T_c	$T_c = 5.6 \pm 0.1$ $^\circ$K		6. Phys. Rev., 113, 1520 (1959)
Superconducting Energy Gap	(3.4 ± 0.2) kT$_c$	Determined by ultrasonic attenuation method.	7. J. Appl. Phys., 25, 3322 (1964).

Properties of Intermetallic Compound In_2Bi

Property	Description	Comments	Reference
Debye Temperature	$\theta_D = 80^\circ K$ $\dfrac{T_c}{\theta_D} = 0.07$	Determined by specific heat measure-ments, assuming the electronic contri-bution to be small and considering only acoustic modes of vibration	8. Same as 7.
Phase diagram		Three stable phases have been reported. Reports a 3% HCl solution in water used as an etchant for alloys of In and Bi concentrations range 30 to 33% Bi.	9. Same as 1. 10. Trans. Metallurgical Society of AIME, 239, 883, (1967). 11. AIME Trans, 171, 389 (1971).
Thermal Conductivity in Cal/cm sec$^\circ$C	0.025 at 90°C	The conductivity isotherm exhibit a minimum at the concentration of In_2Bi phase. This indicates exis-tence of relation between liquid and solid state.	12. Z. Metallkde, 57, 76, (1966).
Enthalpy of Formation	$\Delta H'' = -222.0$ cal/g-atom	Enthalpy of melting was determined by quantitative differntial thermal aralysis.	13. Z. Metallkde, 55, 97 (1964)
Entropy of Formation	$\Delta S'' = 0.7$ cal/g-atom $^\circ$C	$\Delta S_{ideal} = 1.26$ cal/g - atom $^\circ$C is of the same order of magnitude as $\Delta S_{experimental}$, which indicates a statistical distri-bution of atoms in the crystal lattice is expected.	14. Same as 13.
NMR Studies (molten alloy)	Knight shift data is presented	In_2Bi atomic grouping persists in liquid state.	15. Advances in Phys., 16, 275 (1967).
Kinematic Viscosity	$\nu = 0.85$ centi stokes	Marked increase of kinematic viscosity was observed between 120°C to crystallization temperature. These results suggest that at mp the In and Bi atoms in In_2Bi are exactly in same position as in the solid state	16. Phys. Metals and Metallogr, 14, 132 (1962). 17. Soviet Phys. Sol. State, 7, 1780 (1966).
Coordination Number	11 to 14.	Number of Neighbors in first coorina-tion shell.	18. Same as 10.

TABLE VII

PROPERTIES OF INTERMETALLIC COMPOUND $In_5 Bi_3$

Property	Description	Comments	Reference
Melting point	$\sim 89^\circ C$	(a) Melts congruently with an open melting point maximum, slightly above $89.0^\circ C$. (b) Later it was reported that it formed peritectically.	1. Trans. Metallurgr. Soc. AIME, 239, 883 (1967). 2. Phys. Letters, 32A, 295, (1970).
Crystal Structure Space group	Tetragonal $a = 8.544$ Å $c = 12.68$ Å $c/a = 1.484$. 14/mcm	Large tetragonal unit cell. Structure like $Cr_5 B_3$ type (T_a). Axial ratio smallest for $Cr_5 B_3$ structure. 32 atoms per unit cell.	3. Zeit. Kntst, 128, 277 (1969)
Residual Resistance Ratio $\dfrac{\rho_{398^\circ K}}{\rho_{4.2^\circ K}}$	75	Residual resistivity at $4.2^\circ K$ was measured by field dependence of electrical resistance. Behaves metallic.	4. Same as 2.
Hall Coefficient $R_H (10^{-4} \, cm^3/c)$	3.0 at $298^\circ K$ 17.3 at $4.2^\circ K$	Hall coefficients positive for whole temperature range and almost constant above $200^\circ K$.	5. Same as 2.
Characteristic Temperature θ_R	$70 \pm 5^\circ K$	Using a Gruneisen–Bloch function.	6. Same as 2.
Superconducting T_c	$4.2^\circ K$	(a) Temperature variation of resistivity (ref. 7). (b) $In_5 Bi_3$ alloys show two transitions 5.6 and $4.1^\circ K$.	7. Same as 2. 8. J. Less Common Metals, 11, 295, (1966)
Phase Diagram		First detected in 1966 and later studied in 1967. It lies between $In_2 Bi$ and InBi concentration range 37.5% Bi.	9. Same as 1 and 8 (1966).
Coordination Lumber	9 to 14	Number of neighbors in first coordination shell.	10. Same as 1.
Ginzburg – Landau Parameter K	2·6	Consequently $In_5 Bi_3$ represents a type II superconductor	11. Same as 2.

I.A.3. InBi and In_2Bi WHISKER CRYSTAL GROWTH

A good supply of crystal "dry run" samples was needed as the task of characterizing InBi, which was to be solidified on the Apollo 14 mission, was undertaken. Although both the Bridgman and Czochralski techniques were being used (see Part A.!.1) to produce large (up to 2 cm diameter) crystals, there was an obvious need for a less expensive source of hundreds of oriented single crystals. Single crystal whiskers fit that description; however, there was no information in the literature on InBi whiskers. Although numerous techniques for whisker growth are known, the squeeze technique, which works well for other soft, low-melting point metals, was tried first. At that time, no compound had ever been grown by this "squeeze technique." Our first attempt was successful and whisker samples were immediately used in generating InBi X-ray patterns which would later serve useful in characterization. Whiskers, with their long thin dimension pointing in a low index crystallographic direction, are ideally suited for rotating crystal X-ray analysis.

Whiskers were also used to measure InBi and In_2Bi resistivity and its dependence on strain.

Since this is the first time the "squeeze technique" has been used to grow compound whiskers, the results were published or a "Letter" in Applied Physics Letters, Vol. 19, #7, p. 220, October 1, 1971, indicating that the results were especially "timely and/or important." A copy of the manuscript is included in Appendix V.

Since our In_2Bi whiskers grew much faster than InBi whiskers, they were observed, investigated and reported first. The growth and properties of InBi whiskers

were reported in a later article, "Growth and Morphology of InBi Whisker Crysials," J. Crystal Growth, Vol. 16, 1972, which is attached as Appendix VII. An unsalaried graduate student, Mr. James Huckle, provided the X-ray analysis of the whiskers which was used as his thesis subject.

I.A.4. HIGH ANISOTROPIC THERMAL EXPANSION DISCOVERED IN InBi

As discussed under I.A.2., Electrical Measurements in InBi Crystals, poly-crystalline samples of InBi developed fine cracks and fractures under thermal cycling from 300 to $77^{\circ}K$. This fracturing was attributed to highly anisotropic thermal expansion coefficients of InBi in our article, "The Effect of Thermal Cycling on the Resistance and Morphology of InBi Single Crystals and Polycrystals," Journal of Less Common Metals, Vol. 27, p. 367, 1972, which is enclosed as Appendix VI.

The linear thermal expansion coefficients $\alpha_\perp$ and $\alpha_{||}$ are defined as follows:

$$\alpha_\perp = \frac{1}{\ell_\perp}\left(\frac{d\ell_\perp}{dT}\right)$$

$$\alpha_{||} = \frac{1}{\ell_{||}}\left(\frac{d\ell_{||}}{dT}\right)$$

$\ell_{||}$ is the length of the crystal parallel to the 4-fold axis and $\ell_\perp$ is a length of the crystal measured perpendicular to the 4-fold axis. T is temperature.

Since the above publication, nc' measurements of $\alpha_\perp$ and $\alpha_{||}$, the thermal expansion coefficient perpendicular and parallel, respectively, to the InBi C axis, were carried out by an unsalaried graduate student (Mr. Timothy White) as part of

his M.S. thesis. His results have greatly exceeded our expectations: we were expect-

ing only that $\alpha_\perp$ is not equal to $\alpha_{\parallel}$. He actually found that $\alpha_{\parallel}$ is large and negative.

He also found that $\alpha_{\parallel}$ and $\alpha_\perp$ have opposite signs and are both extremely large and

increase in magnitude with increasing temperature. The following preliminary values

were found at 50°C.

$$\alpha_\perp \approx 60/°C$$

$$\alpha_{\parallel} \approx -100/°C$$

These α's are unusual in comparison with other α's in the American Institute of Physics

Handbook. (1) The magnitude of the α's is about an order of magnitude larger than the

average α. (2) Only one material in ten has a negative α. (3) $\alpha_{\parallel}$ is about 100 times

larger than the other negative α's listed in the above handbook.

Conclusions: Care must be exercised in the use of materials or alloys containing

polycrystalline InBi in situations involving temperature changes. Because of the above

fracturing, InBi polycrystals should not be characterized using any cryogenic technique

such as residual resistivity or superconductivity measurements. For example, the

three times too large InBi resistivity found by the University of California Group

(J. Phy. Chem. Sol. 25, 1277, 1964) is probably due to their subjecting polycrystalline

InBi to cryogenic temperatures.

I. B. BISMUTH SINGLE CRYSTALS

I.B.1. GROWTH AND ETCHING OF BISMUTH SINGLE CRYSTALS *

In support of a soft mold Bridgman experiment that was proposed for flight on Apollo 16 by Mr. Mirt Davidson (S&E-SSL-T), a similar study as described for InBi (I.A.1.) was performed on bismuth.

Since bismuth was the material that was used by Bridgman to establish the growth technique named after him and in the following, a series of articles on growth [1..10] and etching [11..16] of bismuth single crystals has been published, no development was required and only little experimentation was needed to establish growth and etching procedures.

Large single crystals (up to 20 cm length and 2 cm dia.) were grown in Pyrex and carbon powder molds. Samples were given to Dr. U. Roy (UAH) and to SSL for their studies.

Etching was generally done on cleavage planes (111); on these planes the pits have trigonal or pseudohexagonal symmetry. The pit geometry can be used to determine crystallographic directions within the planes.

Etchants employed are as follows:

(1) Concentrated HCl, etching time 5 - 15 min at TR.

(2) Tartaric acid (40%): H_2O_2 (30%): H_2O = 6:1:1 (by volume)

(3) Methanol plus 1 part iodine

Best results were obtained with the methanol/iodine solution. Etching time was 10 to 30 seconds at room temperature. Chemical polishing was best done with a solution consisting of 6 parts HNO_3 (68%), 6 parts acetic acid (50%) and 1 part H_2O at room temperature.

---

*In charge: H. U. Walter

REFERENCES

1. J.V.D. Planken, J. Crystal Growth 6, 352 (1970).

2. J. P. Issi, A. Moureau: J. Less Common Metals 20, 67 (1970).

3. S. Bednarski, J. Crystal Growth 6, 193 (1970).

4. E. M. Porbansky, Jour. Appl. Phys. 30, 1455-56 (1959).

5. R. S. Wagner and H. Brown, TMS-AIME 224, 1185-88 (1962).

6. R. E. Slonaker, Jr., M. Smutz, H. Jensen and E. Olson, Jour. Less-Common Metals, 7, 165-168 (1964).

7. S. Fischler, TMS-AIME 230, 34-341 (1964).

8. C. J. Creasy and J. E. Aubrey, Jour. Less-Common Metals 12, 508-510 (1967).

9. W. A. Nordland, TMS-AIME 23?, 2002-2004 (1967).

10. P. Issi and A. Moureau, Jour. Less-Common Metals 20, 67-69 (1970).

11. C. Stee G. Muller, J. S. Daniel, J. Less Common Metals 27, 81 (1972).

12. J. J. Frawley, J. Appl. Phys. 41 (4), 1862 (1970).

13. U. Roy, Final Report NAS8-25120 (1972).

14. L. C. Lovell and J. H. Wernick, Jour. Appl. Phys. 30, 234 (.

15. L. S. Palatnik, A. A. Levchenko and V. M. Kosevich, Soviet Phys. Cryst. 6, 472 (1961-62).

I.B.2. ELECTRICAL MEASUREMENTS ON BISMUTH CRYSTALS*

Studies on the characterization of bismuth single crystals were initiated during the summer of 1971. It was proposed to grow bismuth, a typical semi-metal, in space environment during the flyback mission of Apollo 16. The work mentioned here concerns itself with the electrical resistivity measurements to identify the role of 0-gravity in the crystal growth process

The electrical techniques used for such measurements were the same as mentioned in Part I.A.2. Some samples were studied by four-point technique also for quick estimate of resistivity values.

Bismuth has a rhombohedral crystal structure which has been described by three different unit cells. The primitive cell contains two atoms. Precise measurement of lattice parameters have been made by Barrett.[1] The physical properties of bismuth are highly anisotropic and far from what one might expect from an almost cubic structure. It is probable that atoms in a layer perpendicular to the trigonal axis are held together by mostly covalent bonds and that these layers are weakly held together by Van der Waal's forces. Single crystals can be cleaved in this plane (111) much more easily than in any other.

Resistivity of Bi Samples Supplied by SSL

The resistivities of three samples supplied by SSL were measured by the four-probe technique at room and liquid nitrogen temperatures. All the samples used were cleaved alo₁ (111) plane. The values reported are not the absolute values because the surfaces of the samples were not polished or specially made for such measurements. The values reported herein can be used as a comparison between different crystals of bismuth with different amounts of impurities.

*Person in charge - R. B. Lal.

SAMPLE NO. 1 (Alfa Ventron crystal 99.999+% pure)

Room temperature value of resistivity ρ_{295} = 112 micro ohm cm.

Liquid nitrogen value of resistivity ρ_{80} = 21 micro ohm cm.

The above values of resistivities are corrected for thickness according to Valdes[4] Part I.A. The above values of resistivities are slightly lower than the reported values for ultra pure bismuth crystals.[a]

SAMPLE NO. 18.

Room temperature value of resistivity ρ_{295} =142 micro ohm cm.

Liquid nitrogen temperature resistivity ρ_{80} =271 micro ohm cm.

SAMPLE No. 17.

Room temperature value of resistivity ρ_{295} =144 micro ohm cm.

Liquid nitrogen temperature resistivity ρ_{80} =235 micro ohm cm.

The resistivities of samples 17 and 18 increased to almost double when the samples were cooled down to $80^{\circ}K$. This indicates that the samples have negative temperature coefficients. This is not surprising, since small amounts of lead produce humps in the resistance curve and it passes through a maximum, the position of which moves to lower temperature as the lead content is decreased. For these samples, the room temperature and LN_2 temperature values correspond to the values reported by Thompson[3] for lead impurity of 0.2%. It is likely that these samples contain lead impurity of about 0.2%.

Resistivity of Bismuth Cast Samples and Single Crystals

a. Cast sample

A crystal of bismuth was cast (No. 2) from 99.999% purity bismuth using a graphite

Resistivity of Bismuth 99.999% sample (cast)
in graphitemold (UAH) Sample # 1

$$\frac{\rho_{285}}{\rho_{4.2}} = 22$$

$\rho \times 10^8$ ohm cms

120
110
100
90
80
70
60
50
40
30
20
10

4.2   77   100   200   300

T^oK
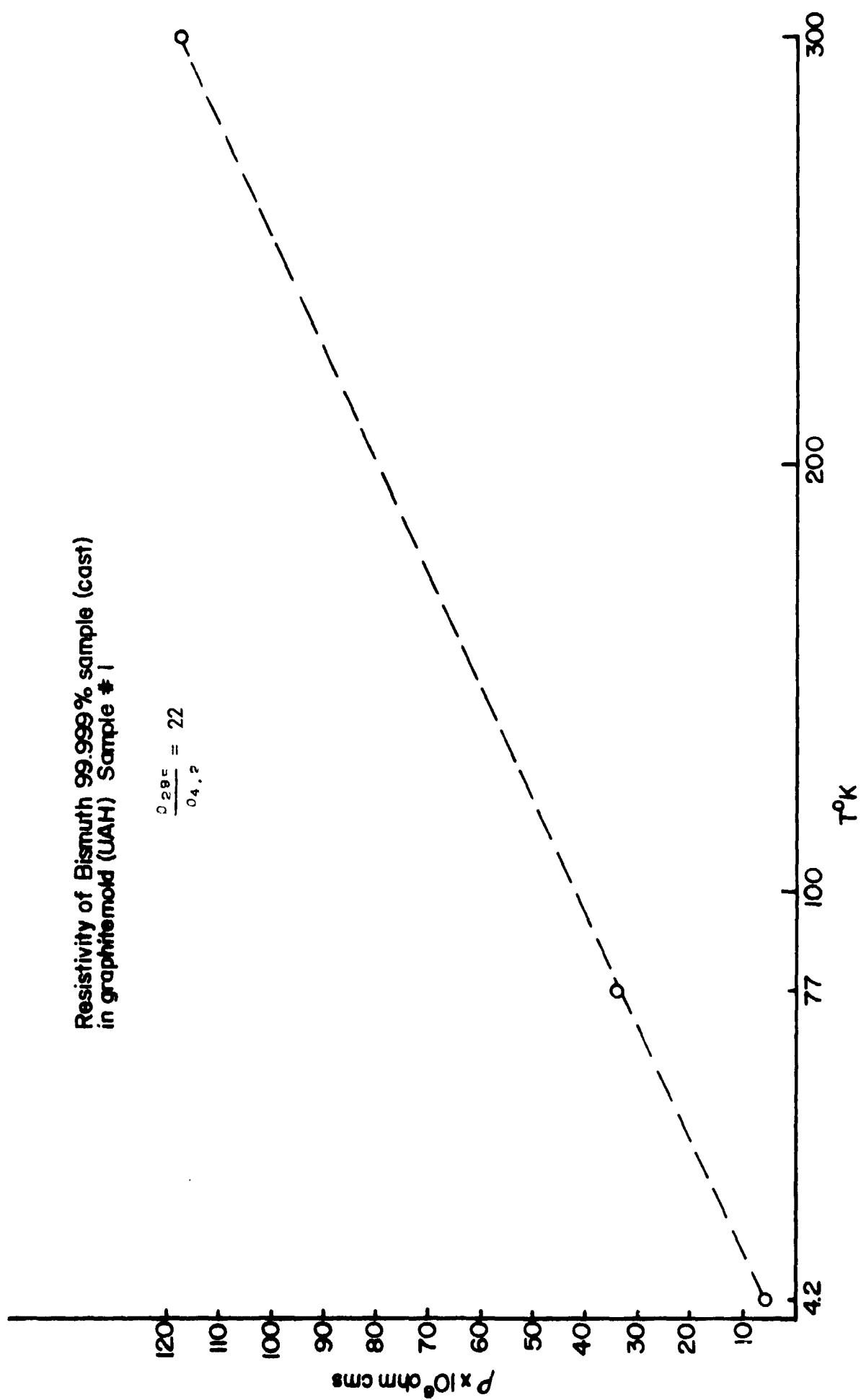
FIG. 1

mold. The resistivity of this sample was measured at room temperature, $77^{\circ}K$ and $4.2^{\circ}K$ using a glass helium dewar and a specially designed teflon crystal holder (reported in Part I.A.2.). The resistivity of the sample at the above three temperatures is given in Fig. 1. This sample has a residual resistivity ratio $\frac{\rho_{295}}{\rho_{4.2}} = 22$. The sample comes back to initial room temperature resistivity value after cooling down to $4.2^{\circ}K$. The resistivity ratio of this sample is very low compared to the reported ratio for single crystals $\frac{\rho_{291}}{\rho_{4.2}} = 290$, ref 5, Part I.A.2. The measured value for the cast sample compares with the value reported by White and Wood.[4]

b. Single Crystal (Alfa Ventron supplied by SSL)

A single crystal of bismuth obtained from Alfa Ventron Company was supplied by SSL. The crystal was cleaved at LN_2 temperature along (111) plane. A required shape of a rectangle was cut. Crystal dimensions were measured using a travelling microscope. The crystal (No. 3) was mounted on an Al_2O_3 substrate, soldered contacts were made for current leads, and silver paint was used for potential probe.

with a travelling microscope taking the center distance from the silver paint area. The resistivity was measured at RT, $77^{\circ}K$ and at $4.2^{\circ}K$. The results are given in Fig. 2. The sample has a residual resistivity ratio $\frac{\rho_{299}}{\rho_{4.2}} = 34$. It is surprising that the sample has only a ratio of 34, although the initial purity of the sample was 99.999 +%. The low resistivity ratio for this sample may be due to the possibility that the sample has been damaged during the cleaving and cutting processes.

Also, resistivity was measured on a sample (No. 4) from the same crystal, but the cleavage steps were removed by scraping with a knife. Such a sample gave only a residual resistivity ratio of 26. Results are given in Fig. 3. It is apparent that more damage was

Resistivity of single crystal of Bismuth
(Alfa Ventron) cleaved (III) plane
Sample recovers to RT value after
cooling down to 4.2°K. Sample #2

$$\frac{\rho_{299}}{\rho_{4.2}} = 34.$$

FIG. 2

Resistivity of single crystal of Bismuth
(Alfa Veltron) cleaved (III) plane surface
scrapped. Sample #3

$$\frac{\rho_{295}}{\rho_{4.2}} = 26.$$

$\rho \times 10^8$ ohm cms

$T^\circ K$
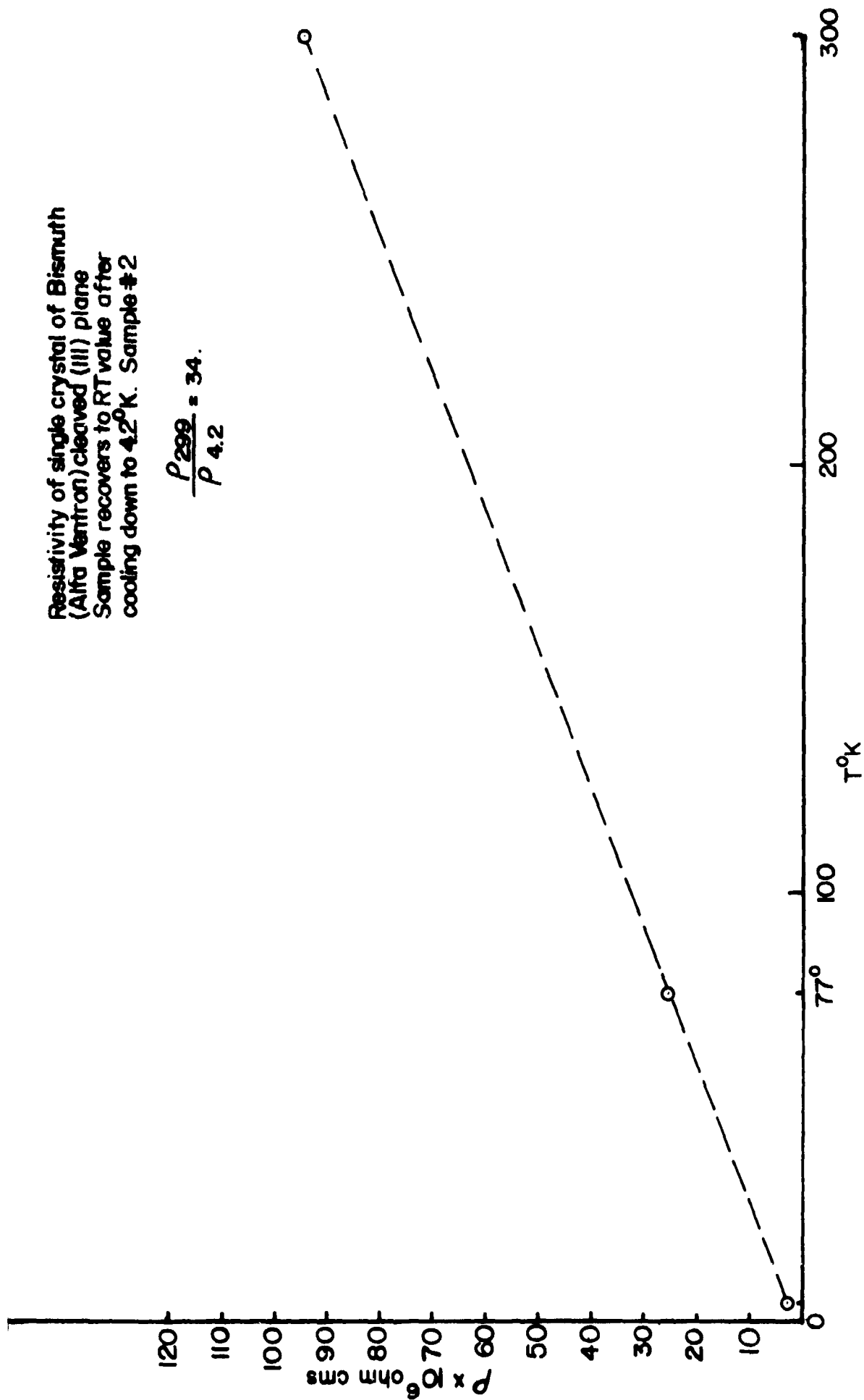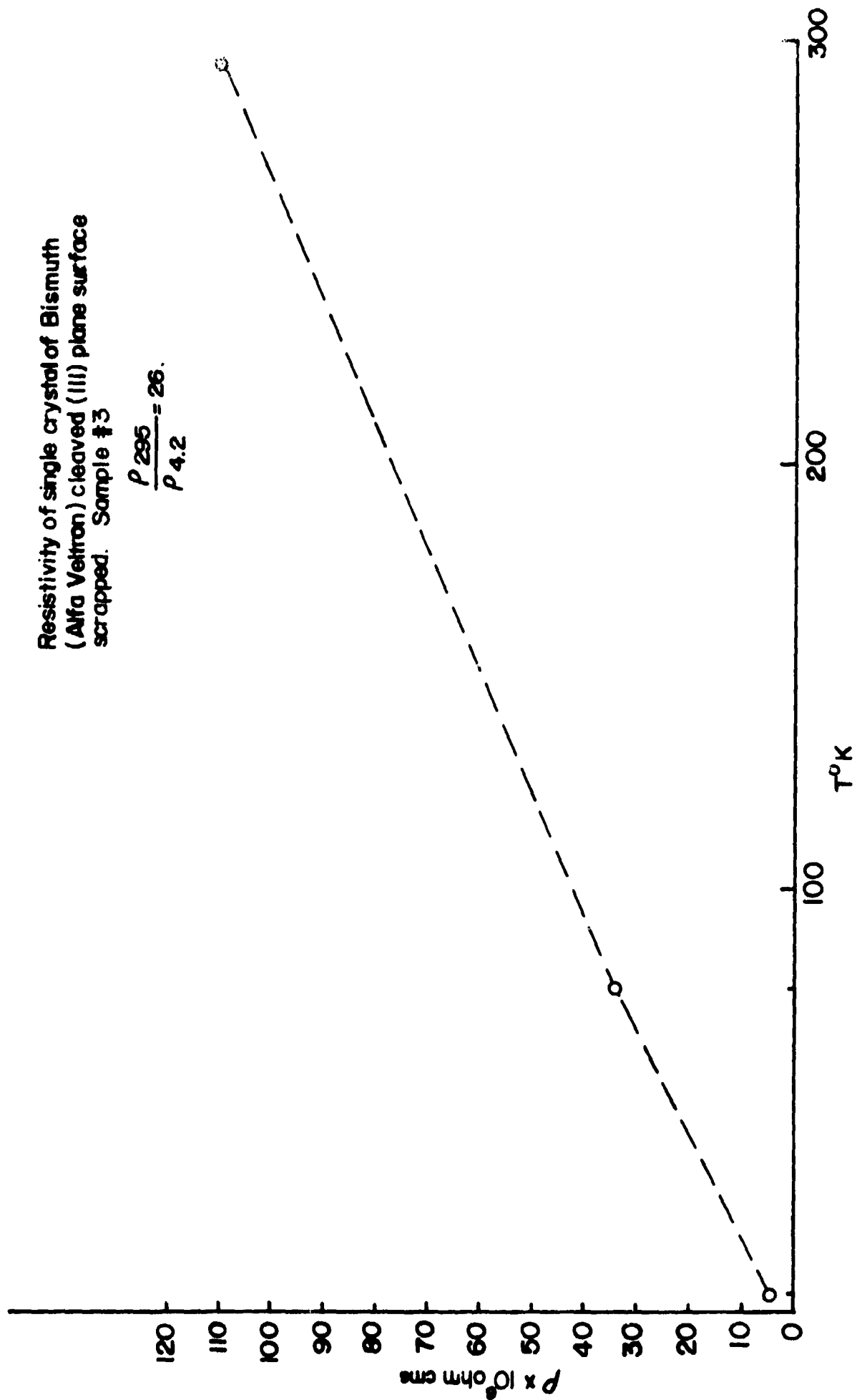
Fig. 3

done to the sample during scraping with a knife and, in turn, a lower value of resistivity ratio was obtained. At this stage it is difficult to say how much of the resistivity is due to damage. Since the residual resistivity (ρ_0) values for the two crystals (No. 3 and 4) are different (2.8×10^{-6} ohm cm and 4.2×10^{-6} ohm cm it appears that the increased value of ρ_0 for sample No. 4 may be due to the structural damage, because at liquid helium temperature, the residual resistivity is assumed to be due solely to chemical and physical imperfections. Since samples No. 3 and No. 4 have similar amounts of chemical impurities, it can be understood that part of the re-sisitivity in sample No. 4 may be due to physical imperfections.

Resistivity of Bismuth Crystals (Effect of Annealing)

Resistivity has been measured on four different crystals of bismuth (Alfa Ventron crystals). Two crystals, Nos. 5 and 6 (similar to Nos. 3 and 4), were chemically polished and annealed at 240°C in a vacuum for two hours. The resistivity was measured at room temperature, 77°K and 4.2°K. Also, crystal No. 4 (reported earlier) was chemi-cally polished and its residual resistivity ratio was measured again. Results are given in Table I. After annealing, the ratio $\frac{\rho_{295}}{\rho_{4.2}}$ for crystals 5 and 6 (similar to 2 and 3) in-creased to 133 and 216 from the previous value of 26 and 34. It appears that by anneal-ing, certain defects were annealed out and this, in turn, gave a higher value of resistivity ratio. Sample No. 4, which was just chemically polished, did not have any significant change in the residual resistivity ratio.

Etch pit counts were made at SSL and at UAH for crystal No. 6 before and after cutting into the shape of a rectangle. The dislocation density/cm^2 was found to be 2×10^6 and 1.2×10^7, respectively.

TABLE I

RESISTIVITY OF BISMUTH CRYSTALS

SAMPLE	$\rho_{295} \times 10^6$ OHM CM		$\rho_{77} \times 10^6$ OHM CM		$\rho_{4.2} \times 10^6$ OHM CM		$\rho_{295}/\rho_{4.2}$		BEFORE ANNEALING DISLOCATION DENSITY/CM^2
	BEFORE ANNEAL-ING	AFTER ANNEAL-ING	BEFORE ANNEAL-ING	AFTER ANNEAL-ING	BEFORE ANNEAL-ING	AFTER ANNEAL-ING	BEFORE ANNEAL-ING	AFTER ANNEAL-ING	
VENTRON BI CLEAVED AND SCRAPPED No. 5	110.4	133.0*	34.03	30.87*	4.27	0.996*	25.9	133*	1.2×10^7 (after cutting)
VENTRON BI CLEAVED No. 6	95	178*	25.3	36	2.80	0.826*	34	216*	2×10^6
VENTRON BI CLEAVED AND SCRAPPED No. 7		153.3		31.03		1.55		99	
VENTRON BI CLEAVED No. 4	110.3		34		4.27		25.9		
No. 4 AFTER CHEMICAL POLISHING	114.4		36.4		3.96		28.8		
POLYCRYSTALLINE BISMUTH No. 2 (Cast) 99.999% pure	118.2		34.0		5.32		22		

* MEASUREMENTS WERE MADE ON DIFFERENT SAMPLES BUT FROM THE SAME CLEAVED PIECE.

After annealing at 240°C in vacuum, crystals were analyzed under a metallurgical microscope. One of the crystals was found to contain large single grain boundaries. Some areas of the crystal were found to have a high dislocation density as compared to that before annealing, while many areas were found to have lower dislocation density values. In further experiments lower annealing temperatures were tried to anneal out the damage.

A rectangular shaped bismuth crystal ($\#$ 8) was cut from a cleaved piece (also scraped to remove cleavage steps) of a Ventron single crystal. The crystal dimensions were measured with a travelling microscope. Before any leads were put on the sample, the dislocation density was measured by the etch pit count method. The average value of dislocation density on (111) surface was found to be 5×10^{5}/cm^2. A similar crystal from the same batch has been found to have a residual resistivity ratio $\frac{\rho_{295}}{\rho_{4.2}} = 26$. The above crystal ($\#$8) was then annealed for 1 hour at 80°C in a vacuum of 2×10^{-4} Torr. The dislocation density was again measured and found to be 2.2×10^{5}/cm^2. The residual resistivity ratio was measured for this crystal using a specially designed crystal holder. The ratio $\frac{\rho_{295}}{\rho_{4.2}}$ was found to be equal to 58. This indicates that annealing at 80°C could remove some structural defects which gave a higher resistivity ratio. The above sample was again annealed at 140°C and the dislocation density count was found to be equal to 1.9×10^{5}/cm^2. No significant change in the residual resistivity could be detected for this crystal. No grain boundaries were observed after the annealing process.

From the above results it can be concluded that 140°C is an optimum temperature for annealing bismuth crystals before producing any large angle grain boundaries. The

resistivity of bismuth shows metallic behavior in that it decreases almost linearly with decreasing temperature until impurity scattering dom. iates. With the purest samples (about 99.9999% pure) the residual resistance become: important at liquid helium temperature. A qualitative estimate of structural damage can be made by measurement of residual resistivity ratios; Otake [5] has shown that a correlation can be made between dislocation density measurements and the resistiv· y of the sample. Since the material deforms and cleaves easily, care must be taken in cutting samples. A thin, fine grit, high speed abrasive wheel may be used if cutting rates of less than one inch per hour are used, but cutting with a stri. y saw is preferable.

Table for Properties of Bismuth

During the course of the above work the attached Table No. 2 was compiled which lists important properties of bismuth.

TABLE II

PROPERTIES OF BISMUTH (Bi)

PROPERTY	DESCRIPTION	COMMENTS	REFERENCE

Basic parameters	Atomic no. = 83
	Atomic weight = 208.980
	Atomic radius = 1.70 Å
	Covalent radius = 1.46 Å
	Electronegativity = 1.9
	Heat of vaporization
	   = 42.7 Kg - cal/g-
	     atom at boiling
	     point
	Heat of fusion = 2.6 Kg -
	    cal/g - atom
			1) E. H. Sargent Co. Table

Melting point Boiling point	271.16° C or 544.16° K 1560° C		2) American Institute of Physics Handbook, McGraw Hill Co., N. Y. (1963)
Crystal Structure at 25° C	Rhombohedral a = 4.546 Å c = 11.862 Å Type A7	Interatomic distance is equal to 11.862 Å Each atom has three nearest neighbors. The structure consists of two interpenetrating face centered sublattices, nearly cubic, one sublattice being slightly displaced from the mid edge position of other	3) Acta. Cryst, 15, 865, (1962)
Space group	$R \bar{3} m$		4) Structure of Metals McGraw Hill, N.Y., 1966, p. 626.
Density g per cm^3	9.803 at 25° C		5) Same as ref 4.
Electrical resistivity in μ ohm cm.	ρ_{mean} = 116 at 295° K $\rho_{\shortparallel}$ = 138 at 293° K $\rho_{\perp}$ = 109 $\frac{\rho_{\perp}}{\rho_{\shortparallel}}$ = 0.79	a) The mean value is related to poly-crystalline sample b) In ref 7, the authors measured the temperature dependence of electrical conductivity from 80° K to 540° K. The dependence was non-linear. An emperical formula is given.	6) Electrical Resistance of Metals, ed. George Meaden, Plenum Press N.Y. (1965) p 55 7) Sov. Phys. Sol. State, 7, 633, (1965).

PROPERTY	DESCRIPTION	COMMENTS	REFERENCE
Resistance ratio	1) $\dfrac{\rho_{300}}{\rho_{4.2}} / 200$ for rapid freeze crystals 2) $\dfrac{\rho_{290}}{\rho_{4.2}} = 1000$	a) b) Zone ref'ned in 11 slow passes (0.7 mm min^{-1})	8) Trans. Metall. Soc. of AIME, 230, 340, (1964) 9) J. Phys. (D), 2, 753, (1969).
Crystal growth technique	1) Rapid freeze 2) Directional freezing 3) Spherical crystal in Pyrex mold 4) Flexible mold	a) Residual resistivity ratio $\rho_{300}/\rho_{4.2}$ > 200 b) Single crystal of diameter 75 mm and 180 mm of length are grown c) Crystal of 25 mm diameter were grown. d) Dislocation density $\approx 10^4\,cm^{-2}$	10) Same as ref 8. 11) Phys. Stat. Sol., 9, 839, (1965). 12) J. Less Common Metals, 20, 67, (1970). 13) Phys. Metal. Mettalgr, 21, 147, (1966) 14) J. Crys. Growth, 6, 352, (1970).
Phasediagram Pressure - temperature		The density of the melt close to the melting point, is higher than density of the crystalline phase.	15) Kristallografia 5, 154, (1960). 16) Phys. Rev, 110, 314 (1958). 17) Phys. Rev, 131, 632, (1963).
Superconductivity	i) Amorphous Bismuth (films at 1.5° K) is a strong coupling supe conductor with $T_c = 6.17 \pm .03$°K 2) Under high pressure possesses crystal modification and is superconducting $T_c = 3.9$°K at 25 Kb $T_c = 7.2$°K at 27 Kb		18) Phys. Letters, 25A 679, (1967). 19) Same as ref. 6, p. 57.

Properties of Bismuth (Bi)

PROPERTY	DESCRIPTION	COMMENTS	REFERENCE
Hall Coefficient	R_H (polycrystalline) $= -41\text{ to } -1078 \times 10^{-11}$ V-c-^{3}/amp - Maxwell μ_n (Hall mobility) = 3200 to 8700 cm^2/V-sec $R_{\shortparallel}$ and $R_\perp$ for pure bismuth are both negative (ref 21)	According to Jain and Koenig (ref 22) $R_{\shortparallel}$ is positive and $R_\perp$ is negative.	20) Ind. J. Pure Appl. Phys. 2 349, (1964) 21) J. Phys Soc. Japan 17, 1900, (1962) 22) Phys. Rev., 127, 442, (1962)
Debye Temperature Specific Heat	$\theta = 120^\circ$ K below 2° K $\theta = 95^\circ$ K at 10° K $\theta = 150^\circ$ K at RT Sp Heat - 0.034 ca/a/$^\circ$C		23) Progress in Semi-conductors, 7, 1, (1963) 24) Can. J. Res., A27, 9, (1949).
Thermal Expansion	$\alpha_{\shortparallel} = 16.5 \times 10^{-6}$ $^\circ$C^{-1} $\alpha_\perp = 12.4 \times 10^{-4}$ $^\circ$C^{-1}	The notation $\alpha_{\shortparallel}$ and $\alpha_\perp$ refers to expansion parallel and perpendicuiar to the triogonal axis. The volume of bismuth contracts 3.5 percent upon melting.	25) Same as 23
Elastic Constants	$K_{\shortparallel} = 17 \times 10^{-13}$ cm^2/dyne $K_\perp = 6.5 \times 10^{-13}$ cm^2/dyne	Rhombhedral structure of bismuth requires six independent elastic constants. The discrepancies between theoretical and expt. individual elastic constant is beyond expt. error. Linear compressibilities agrees.	26) Same as 23
Thermal Conductivity	$K_{\shortparallel} = 0.054$ W cm^{-1} K^{-1} $K_\perp = .093$ W cm^{-1} K^{-1} at room temp.	a) Thermal conductivity was measured from 25° C to 150°C	27) Same as 23 28) Phil. Mag, 3, 342, (1958).

Properties of Bismuth (Bi)

PROPERTY	DESCRIPTION	COMMENTS	REFERENCE
Thermal Conductivity (Contd)	$K = .041$ cal/cm$^\circ$ C at 300° C.	b) White and Wood (ref 28) have shown that lattice contribution dominates the electronic below 150°C. Thermal conductivity has $1/T$ tempture dependence to about 5°K c) Later it was reported that there is a sizable additional term in the electronic thermal conductivity due to bipolar diffusion. Between 100° K and 300° K thermal conduction by electrons and holes is the dominant mechanism (ref 29).	29) J. Appl. Phys., 34, 144 (1963)
Magnetic Susceptibility	$\chi = -155$ and -133×10^{-7} c.g.s. emu at 85° K and at 300° K. $\chi_\perp = 143 \times 10^{-7}$ c.g.s. emu at 300° K $\chi_{\|} = 100 \times 10^{-7}$ c.g.s. emu at 300° K	χ - values are for polycrystalline material. The temperature variation of χ is quite large.	30) Theory of Metals (Cambridge Univ. Press, London), 53, p. 169.
Magnetostriction	In a field of 250 K gauss along the trigonal axis, increase in length by a factor of 2×10^{-4}. H$\perp$ to trigonal axis length decreased by a factor of 2×10^{-6}.	In both cases, the change in length was measured along the direction of field. At low fields, the change of length was proportional to H^2 for both orientation.	31) Proc. Roy Soc. A135, 537, (1932)

PROPERTY	DESCRIPTION	COMMENTS	REFERENCE
Chemical Polishing	6 parts fuming HNO_3, 6 parts glacial acetic acid and 1 part water	Immersion times of 1 - 5 minutes are used and removal rate is 10^{-3} in/min	32) J. Appl. Phys. 30, 234, (1959). (quoted in ref. 23)
Electro-polishing	Soln consisting of 25 g potassium iodide, 1 g iodine, and 10 cc hydrochloric acid dissolved in 200 cc of water.	Current density of $1A/cm^2$. Best results are obtained using polishing period of 1 min during which approx 1 mil of material is removed. The sample must be dipped in HCl to remove a water insoluble film which accumulates and then rinsed in distilled water and/or alcohol.	33) Phys. Rev., 115 1501, (1959).
Etchant	1) 1 percent iodine in methyl alcohol after polishing	a) Etching time of approx. 15 sec. This is also useful for showing grain boundaries in polycrystalline material.	34) Same as ref. 23. 35) J. Appl. Phys, 41, 1862, (1970)
	2) Conc Hydrochloric acid	b) Different etching time and temperatures were used. Can be used to etch preferentially different crystallographical planes.	

REFERENCES

1. C. S. Barrett, Austr. J. Phys., $\underline{13}$, 209 (1960).

2. V. I. Prokoshin, Phys. Metals and Metallogr, $\underline{20}$, 56 (1965).

3. N. Thompson, Proc. Roy. Soc. A$\underline{155}$, 111 (1936).

4. G. K. White and S. B. Wood, Phil. Mag., $\underline{3}$, 342 (1958).

5. Otake, Shuichi, J. Sci. Hiroshima, Univ. Ser. A-II, Vol. 25 [#]3, 385 (1962).

I.C. GaAs CHARACTERIZATION FOR SKYLAB   M555

1. SURFACE PREPARATION AND DISLOCATION ETCH PITS ON SINGLE CRYSTALS OF GaAs *

In support of the approved experiment M555 for Skylab on diffusion con-
trolled solution growth of epitaxial films of gallium arsenide, literature on de-
termination of dislocation densities by etch pits on single crystals of GaAs was
surveyed. The various reported techniques in preparing the surfaces mechani-
cally and chemically and finally etching techniques have been studied for (111),
(100) and (110) surfaces. The following is an outline of our findings and recommen-
dations for surface preparation and etching.

Mechanical Polishing and Lapping

After cutting with a diamond saw, which is a generally accepted procedure for
GaAs, mechanical polishing with 600 grit SiC paper followed by lapping with 0.3
micron Al_2O_3/H_2O suspension yields excellent results. Ca e should be taken to re-
move all scratches originating from the 600 grit SiC polishing by lapping. Such tracks
would show up later as lines of etch pits, indicating dislocations arising from mechani-
cal damage of the crystals.

The depth of the damaged layer is relatively low for GaAs. Compared with
other III-V compounds such as InSb, InAs, GaSb, gallium arsenide has a high hardness.
The depth of the damage layer was studied by Gatos;[11] for abrasive particle sizes of
10, 20, 45 μ, the layer thickness is 3, 4, 8 μ on ($\bar{1}\bar{1}\bar{1}$) and 6, 9, 14 μ on (111) sur-
faces, respectively.

Chemical Polishing

The damaged surface layer has to be removed by chemical means. Flat sur-
faces obtained by lapping tend to become rounded and somewhat wavy; chemical

*Investigator in charge: H. U. Walter

polishing time should, therefore, be minimized. After lapping with a 0.3 micron Al_2O_3 suspension, 3 - 5 seconds of chemical polishing is sufficient to remove the damage layer and results in sufficiently flat surfaces.

Chemical polishing by rubbing the sample against a felt cloth soaked with a chemical polishing solution was tried   the samples become somewhat lens-shaped, waviness of the surfaces is reduced.

Different crystallographic planes require different reagents for nondiscriminate etching. The following solutions and procedures have been reported:

Cryst. Plane	Etchant and Procedure	Reference
(111)	$HF:HNO_3 H_2O = 1:1:1$	1
$(\bar{1}\bar{1}\bar{1})$, (100), (110)	$HCL:HNO_3:H_2O = 3:1:2$	1
Polycrystalline, (111)	Only mechanical (M7 powder)	2
(111), $(\bar{1}\bar{1}\bar{1})$, (100), (110)	Only mechanical polishing (3200 mesh Alundum)	3
(111), $(\bar{1}\bar{1}\bar{1})$	$HF:HNO_3:H_2O = 1:3:2$	4, 5
(111), $(\bar{1}\bar{1}\bar{1})$, (100), (110)	$H_2SO_3:H_2O_2 (30\%):H_2O = 3:1:1$ 3 min, hot	6
All faces:	$NaOCl - H_2O$	7
(100)	$Br_2:CH_3COOH = 1:4$ T_R)	
(111)	$H_3PO_4:HNO_3 = 49:11$ $60^{\circ}C$)	8

Modifications of these approaches have been applied by a series of investigators. We have found that the solutions reported by Grabmaier and Watson (8) yield very good results. Both (111) and $(\bar{1}\bar{1}\bar{1})$ GaAs surfaces are polished in a $H_3PO_4:HNO_3 = 49:11$ solution at $60^{\circ}C$ (10-30 sec.) and (100) and (110) surfaces are polished in a $Br_2:CH_3COOH = 1:4$ solution at room temperature within 5 - 10 seconds.

Etching

For III – V compounds with Zinkblende structure (space group $F\bar{4}3m$) that do not have an inversion center, etching imposes more of a problem but is also more revealing than it is for materials that do not have polar structures. Certain planes are composed entirely of group III or group V atoms. Most importantly, the $\{111\}$ planes are split into two groups, (111), $(\bar{1}1\bar{1})$, $(\bar{1}\bar{1}1)$ and $(1\bar{1}\bar{1})$ exposing only group V atoms and $(\bar{1}\bar{1}\bar{1})$, $(\bar{1}11)$, $(1\bar{1}1)$ and $(11\bar{1})$ exposing only group III atoms at the surface. $\{100\}$ surfaces consist of both group III and group V atoms, there is only one type of $\{100\}$, this is similarly so for $\{110\}$ surfaces.

Of the various approaches to reveal dislocations, chemical etching has been applied for GaAs rather exclusively. The following table gives a summary of basic chemical etchant procedures for GaAs. We have found that the best reproducible and interpretable results are obtained by etching in potassium hydroxide melt – at slightly higher temperatures, $350^{\circ}C$ rather than 300 as indicated in ref. 8. Photographs of various types of etch pits on different crystallographic planes are shown in Fig. 1 – 5. The dislocation densities of the seed crystals used by Westinghouse were between 1.10^5 to $6.10^5/cm^2$. Orientation of the GaAs wafers was done by back reflection Laue, some experimentation with Berg–Barrett technique was initiated and topographs were obtained. Since our X–ray source was not well suited to Berg–Barrett studies, the quality of the micrographs was relatively poor. A microfocus X–ray tube with Ag–target was then obtained by SSL, the use of which will allow us to perfect our Berg–Barrett studies. To enable us to study dislocation
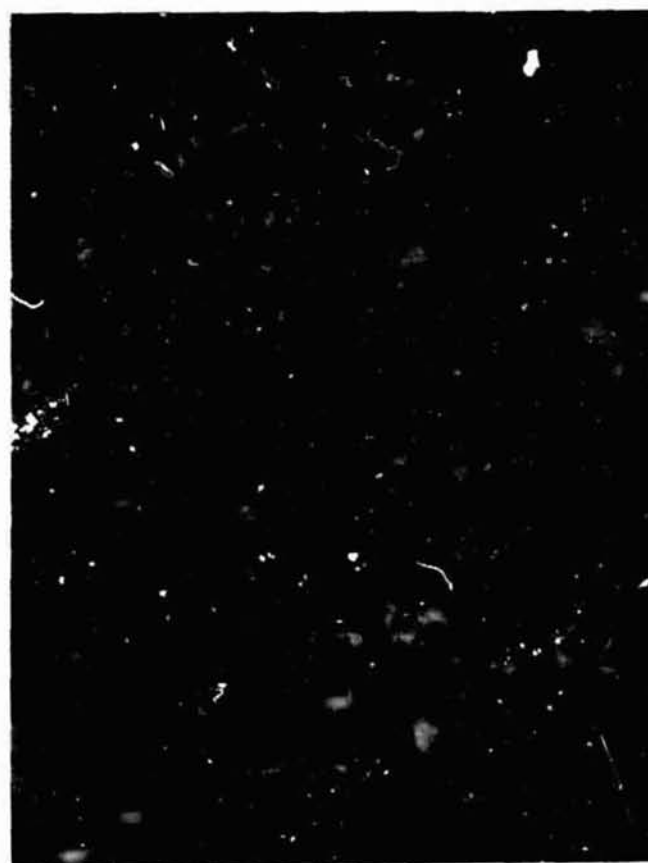
Fig. 1. (a) Pits and hillcocks on epitaxial GaAs grown from gallium
solution in the Westinghouse M-555 growth tube. Orienta-
tion of substrate (100). Magnification: 100.

Fig. 1. (b) Cracks on GaAs (111) wafer caused by freezing liquid
gallium with one side of the wafer immersed. A possible
occurrence with M-555 due to comparable seed-melt
arrangement.
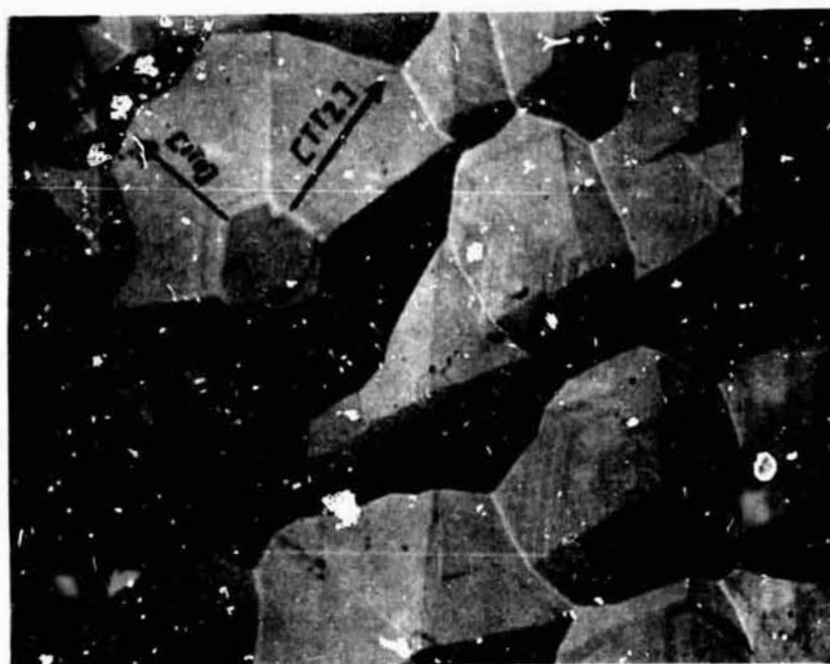
Fig. 2. Etch pits obtained by etching in KOH melt (350°C,
10 min) on ($\bar{1}\bar{1}\bar{1}$) (Dewalt nomenclature). Pits have
pseudohexagonal symmetry crystallographic direc-
tions [$1\bar{1}0$] and [$\bar{1}\bar{1}2$] are indicated in the photo-
graph. Magnification 600X.

88
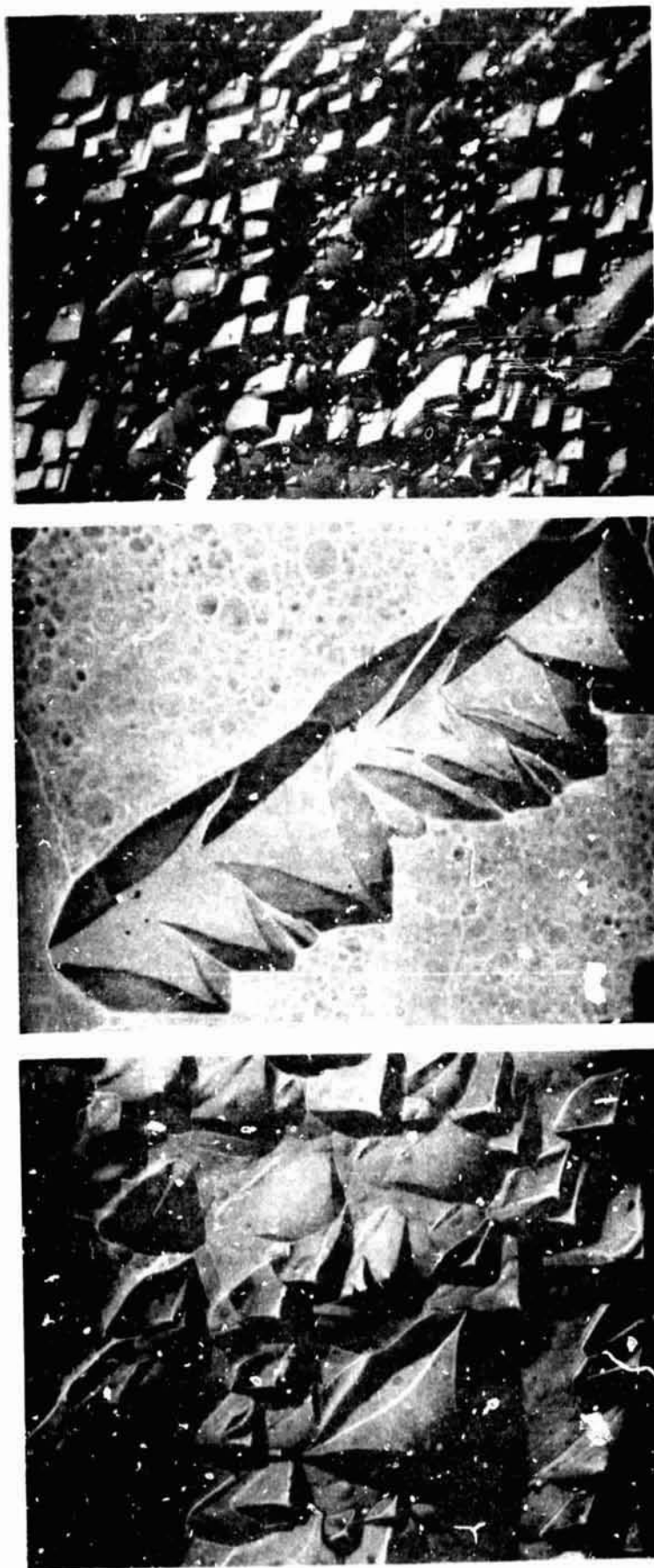
(a) Pits have trigonal symmetry. Crystallographic directions $[1\bar{1}0]$ and $[112]$ are indicated.

(b) Line dislocation parallel to surface.

(c) Area of high dislocation density: $\approx 10^{5}/cm^{2}$.

Fig. 3. Etch pits obtained by etching in KOH melt (350°C, 10 Min on (111)).
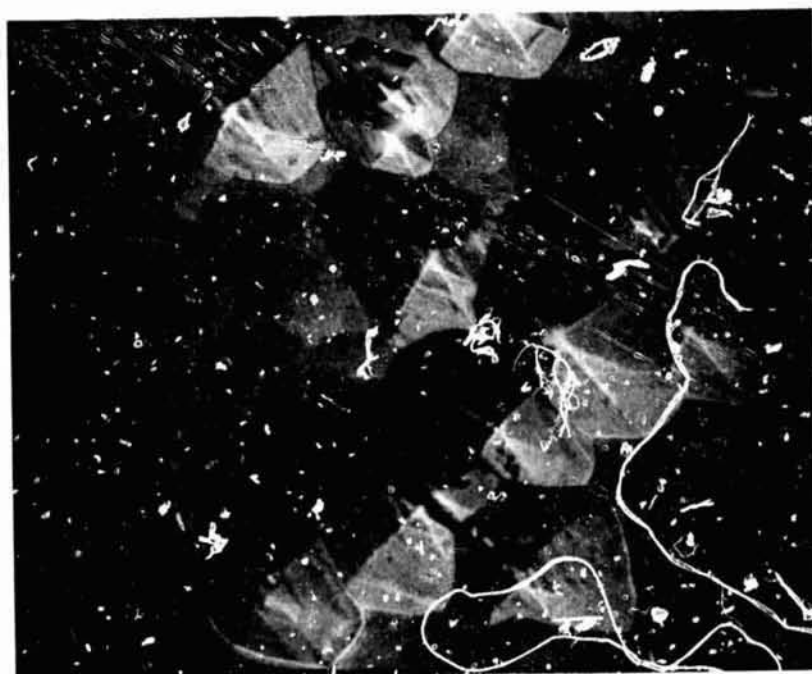
Fig. 4. Etch pits on (100), KOH etch (350°C, 10 min).
Crystallographic directions $[1\bar{1}0]$ and $[\bar{1}\bar{1}0]$
are indicated.

Fig. 5. Etch pits on (100), Richardson-Crocker etch, dislocation density $4.10^5/cm^2$.

Cryst. Plane	Etchant	Reference
(111), (100), (110)	HNO_3:H_2O = 1:2 (15 Min, T_R)	1.
	H_2O_2:HF:H_2O = 1:1:2 (10 – 20 Min, T_R)	1.
polycrystalline, (111)	5% NaOH:H_2O_2 = 5:1 (boiling)	2.
(111), ($\bar{1}\bar{1}\bar{1}$), (100)	H_2O_2: HF:H_2O = 1:1:4 ⎫ HNO_3: tartaric acid = 3:1 ⎬ (5 – 30 Min, T_R) HNO_3: HCl: H_2O = 1:1:2 ⎪ H_2O_2: NaOH = 3:1 ⎭	3.
(111), ($\bar{1}\bar{1}\bar{1}$)	HNO_3: H_2O = 1:3 ⎫ HF: HNO_3 = 1:7 ⎬ HF: HNO_3: H_2O = 1:3:0 – 4 ⎭	4.
($\bar{1}\bar{1}\bar{1}$)	HCl: HNO_3: H_2O = 3:1:2 ⎫	
(111)	H_2SO_3: H_2O_2 (30%): H_2O = 3:1:1 ⎪	
(111)	NaOH(5%):H_2O_2 (30%) = 5:1 ⎬ 6.	
(111)	KOH–6g, $K_3[Fe(CN)_6]$ –4g, 50 ml H_2O ⎪	
(111)	HNO_3: H_2O = 1:3 ⎭	

(111), ($\bar{1}\bar{1}\bar{1}$)	Schell's etchant plus inhibitors: ⎫
	   1) Butylamine 0.5% ⎬ 5.
	   2) $AgNO_3$: 0.5% ⎭	

(111), ($\bar{1}\bar{1}\bar{1}$)	H_2O: HF: HNO_3 = 5:2:3 ⎫ plus 2.4 x 10^{-3} molar solution ⎬ 9. of $AgNO_3$ as inhibitor ⎭	
(111), ($\bar{1}\bar{1}\bar{1}$), (100), (110)	2 ml H_2O, 8 mg $AgNO_3$, 1 g CrO_3 1 ml HF	10.

(111), ($\bar{1}\bar{1}\bar{1}$)	Schell's etchant plus inhibitors: ⎫
	   1) Amylamine ⎬ 5.
	   2) $AgNO_3$ ⎭	

(111), ($\bar{1}\bar{1}\bar{1}$), (100)	KOH (350°C, 30 Min)	8.
{111}	0.2 N Fe^{3+} in 6N HCl (10 Min, 82°C)	12.

density and distribution of dislocations in the bulk of a wafer, we have proposed

for SSL to obtain a Lang camera, which will enhance our capabilities in crystal

characterization in terms of structural perfection. (See Appendix XI)

References

1. H. A. Schell, Z. Metullkde, $\underline{48}$ (1957) 158.

2. D. N. Nasledov, A. Patrakova, B. V. Tsarenkov, 779 (1958) Soviet Physics – Technical Ph. 3, p. 726.

3. J. W. Faust, A. Sagar, J. Appl. Phys. $\underline{31}$ (2) (1960) 331.

4. J. L. Richardson, A. J. Crocker, J. Appl. Phys. $\underline{31}$ (1960) 611.

5. P. L. Petrusevich, E. S. Sollertinskaya, Soviet Physics–Crystallography $\underline{8}$ (2) (1963) 182.

6. P. L.Petrusevich, E. S. Sollertinskaya, O. F. Pavlova, Soviet Physics – Solid State $\underline{4}$ (1962) 1013.

7. A. Reisman, R. Rohr, J. Electrochem. Soc. $\underline{111}$(12) (1964) 1425.

8. J. G. Grabmaier, C. B. Watson, Phys. Stat. Sol. $\underline{32}$ (1969) K13.

9. M. S. Abrahams, J. Appl. Phys. $\underline{35}$ (1964) 3626.

10. M. S. Abrahams, C. J. Binocchi, J. Appl. Phys. $\underline{36}$ (1964) 2855.

11. H. C. Gatos, M. C. Lavine, E.D. Warekois, J. Electrochem. Soc., $\underline{108}$ (1961) 645.

12. H. C. Gatos, M. C. Lavine, Phys. and Chem. of Solids $\underline{14}$ (1960) 169.

I.C.2. <u>OHMIC CONTACTS ON GaAs {100} and {111}</u>*

Electrical characterization of GaAs generally requires reliable, ohmic, low resistance contacts to be made on the crystal surface. The contact area has to be defined and small as compared to the contact distances. Pressure contacts are not suitable for GaAs and high frequency electrical characterization that avoids the use of contacts is not yet well established.

In support of DC electrical characterization, our goal was to provide samples with suitable contacts for resistivity and Hall measurements. We have established a new technique for making contacts that are ohmic to temperatures as low as liquid helium temperature by alloying an In-Pt alloy to extremely carefully prepared surfaces of GaAs under high vacuum conditions. Since GaAs has a technological potential as a device material for Gunn mode oscillators, amplifiers, switching devices, etc. for which low resistance ohmic contacts are a basic requirement, our results do have meaning other than for electrical characterization only.

A frequently applied approach to form metallic contacts on GaAs is to mask part of the surface and to vapor deposit a metallic film (e.g. In). Following heat treatment is applied to diffuse into the surface and to form a contact. A series of experiments were done by this approach, the results were generally unsatisfactory. Both deposition on heated substrates and subsequent heat treatment at various temperatures were tried.[†] The contact resistance was in the order of $K\,\Omega$ up to infinite and nonohmic.

A different approach that has been used by other investigators involves alloying of tin, indium and gold and combinations thereof to the surfaces. Applying these

_____

*In charge: H. U. Walter

techniques yielded nonreproducible contacts; we have been searching for a better alloy combination and procedure.

It was found that a platinum-indium alloy that was alloyed under high vacuum conditions to carefully prepared surfaces gave excellent results. By varying platinum content, alloying time and alloying temperature (at a vacuum of $\approx 10^{-7}$ torr), optimal concentration and conditions were established. To verify that the C-V plots were linear within the temperature range of the electrical measurements, the current voltage plots were monitored with a curve tracer at room temperature and liquid nitrogen temperature. To minimize passivation of all surfaces involved, all operations and preparations were carried out under pure methanol. Fresh indium surfaces were produced by cutting indium ribbons under alcohol. Alloying of platinum with indium was done in high vacuum at $\approx 600^{\circ}C$. 8 - 10 wt % Pt in In was determined to be optimal alloy composition (close to saturation). Surface preparation of GaAs surfaces prior to alloying was found to be most critical. The following procedure was established.

1. Boil in acetone 5 min.
2. Boil in ethanol 5 min.
3. Polish in $\langle 100 \rangle$ Br/Acetic Acid 1:4 at T_R
   $\langle 111 \rangle$ Br/Methanol 1:4 at T_R
4. Boil in distilled H_2O, 3 successive boils, 2 min. each.
5. Boil in acetone 5 min.
6. Boil in ethanol 5 min.
7. Decant into cool ethanol and store until ready for use. Sample must not be prepared more than 2 - 3 hours before contact alloying.
8. Contact alloying.
   a. Place In/Pt chips on surface, evacuate to 10^{-6} torr.
   b. Soak at $125^{\circ}C$ for 5 min.
   c. Heat to $350^{\circ}C$, hold for 2 - 3 min. and allow to cool to room temperature before withdrawing from vacuum.

Excellent, perfectly ohmic contacts with contact resistance of about 0.5 - 1 Ω (in-

cluding sample) could be prepared reproducibly by this procedure. An example of

four contacts is shown in Fig. 1.

Fig. 1. Current-voltage plots of
electrical contacts on GaAs.
Ordinate: 10 ma/Div.
Abscissa: .01 V/Div.
Resistance about .5 Ω each.

Samples with four or six contacts were prepared from wafers obtained from

Westinghouse Electric Corporation, Wacker Chemie and Ventron. There was no

problem encountered to reproducibly form contacts on these substrates by our tech-

nique. Samples were used for electrical characterization between T_R and liquid

helium temperature by Dr. R. B. Lal and by SSL-T personnel for their studies.

I.C.3. <u>POSSIBLE OPTICAL MAPPING TECHNIQUES</u>

a. <u>Method of Mapping GaAs Homogeneity by Photoluminescence</u> *

Fabre [1] has used scanning photoluminescence technique at 4.2°K for investigating locally the compensation variations in n-type gallium arsenide. Earlier, Williams[2] had also reported photoluminescence of epitaxial n-type GaAs at 20° K. The samples used by the above author were epitaxial layers of high purity n-type gallium arsenide with a doping level of about 10^{15} cm^{-3} on a semi-insulating substrate or n^{+} doped with silicon or tellurium. It is possible to study the homogeneity of compensation by scanning the laser excitation. Correlation between the relative intensities of two recombination peaks can be used to give information about the homogeneity along the surface of the sample.

We have attempted to set up such a technique with the available equipment at UAH. Preliminary results at room temperature indicate that the equipment we have can be adapted for such measurement. Some refinements in the optics or cooling of the sample to a low temperature may be necessary.

Such a technique, being completely non-destructive, will be extremely useful for characterizing the epitaxial layer of GaAs in the M-555 experiment

---

*Person in charge - R. B. Lal

I.C.3.b. Photo-voltaic Effect in GaAs*

The resistivity gradient may be measured in a material by producing a conduction cloud of electrons which diffuse faster in the direction of higher conductivity. Such a preferred diffusion gives rise to a net transport of charges producing a few microvolts which may be detected on a sample having two ohmic contacts at the end.[3] Oroshmic, et al,[4] evaluated inhomogeneities in germanium crystals by scanning the whole crystal with a photon beam. In one of the samples of GaAs we found some indications of photo voltage on the order of a few microvolts by shining light from a He-Ne laser source. We are looking into more details of the setup so that we can use it for our program.

Latest refinements in photo-voltaic measurements have been partially successful. In order to minimize the noise to signal ratio, a light chopper coupled to a PAR 50 nanovolt lock in amplifier has been used to detect the photo voltage. The voltage produced by a 1 mw HeNe laser is still too weak; however, by using a Hg light source, a signal is easily detected in GaAs. However, the laser does produce a voltaic response on our Ge crystals. Efforts are presently being directed toward (1) improving the system's noise shielding and (2) doping the GaAs with different Cr concentrations to produce higher resistivity gradients.

_____

* Person in charge - J. H. Davis

REFERENCES

1. E. Fabre, Solid State Commun. $\underline{9}$, 635 (1971).

2. E. W. William, Solid State Commun. $\underline{4}$, 585 (1967).

3. H. Frank, Cz. J. Phys. $\underline{6}$, 433, (1956).

4. J. Oroshmic and A. Many, J. Electrochem. Soc. 106, 361 (1959).

I.C.4. ELECTRICAL MEASUREMENTS ON GaAs CRYSTALS*

Electrical measurements find a significant role in the evaluation of single crystals of high purity. These are direct measurements of the chemical and physical imperfections in the host crystal. Each type of measurement provides a different type of information about the crystal. The resistivity of a semiconductor is a basic material parameter whose measurement is required for determining the density and interaction of charge carriers with the host crystal lattice and with impurities. If the semiconductor type is known the resistivity can be used, along with resistivity carrier concentration curves, to yield an approximate net majority carrier concentration. The Hall coefficient and resistivity yield the mobility and net majority carrier concentration. The sign of the Hall coefficient gives the carrier type, positive for p-type and negative for n-type. Lifetime measurements give information about neutral impurities and imperfections which acts as recombination centers for minority carriers.

The measurement of electrical parameters in an epitaxial film is aggravated by a number of difficulties. A large number of measurements are required for the characterization of a $A_{III}B_V$ semiconducting film. The composition, structure, electrical and galvanomagnetic properties of the films can often be determined by means of conventional measurement techniques used on bulk materials. However, extreme care has to be taken of the small mass of the films, of their irregular topography, the strong effect of included micro-inhomogeneities, the large surface-to-volume ratio and the presence of

---

*Person in charge – R. B. Lal

the substrate. On the whole, the accuracy of measurements made on films is con-

siderably smaller than similar measurements made on bulk materials. For this reason,

several different measurement procedures should be used to determine the same film

parameter.

In the case of semiconductors, as in GaAs, the number of charge carriers, as

well as mobilities, depend upon temperature and also on the presence of defects and

impurities. In such a case the most common measurement made of the properties of a

semiconducting solid is the electrical conductivity. In the case of an n-type material,

the expression for conductivity reduces to,

$$\sigma = n e \mu_n \tag{1}$$

where σ (the reciprocal of resistivity) is the conductivity, e is the electronic charge,

and μ_n is the drift mobility of electrons. Since σ can be measured experimentally, we

can determine majority carriers if drift mobility can be determined.

In order to determine the type, concentration and mobility of charge carriers,

the measurements made on the resistivity must be supplemented by galvanomagnetic

measurements over a wide temperature range.

In the work described under this report the measurement of resistivity and Hall

effect (dc-dc) was done by the method developed by Van der Pauw.[1] The Van der Pauw

method requires plane parallel samples of arbitrary shape with four ohmic contacts on

the surface. A current is passed between two adjacent contacts while potential

differences between the other two are measured. By cyclic permutation, two inde-

pendent pseudo-resistances R_1 and R_2 are obtained as voltage current ratios.

It has been shown by Van der Pauw that between R_1 and R_2, the resistivity ρ and

the thickness of the platelet "d", the following relation exists,

$$\rho = \left\{ \frac{\pi d}{2 \ell n_2} \right\} \left\{ R_1 + R_2 \right\} f \frac{R_1}{R_2} \tag{2}$$

The function $f \frac{R_1}{R_2}$ is given by Van der Pauw and only depends on the ratio $\frac{R_1}{R_2}$ and is given in a graphical form (the maximum error in the curve is $\sim 2\%$).

The Hall coefficient R_H was determined by passing the current in the non-adjacent contacts. The change in voltage was measured across the other contacts when a magnetic field was applied perpendicular to the sample. The Hall coefficient R_H is given by

$$R_H = \frac{d}{B} \Delta R_3 \tag{3}$$

where B is the magnetic induction and ΔR_3 is the change in resistance R_3 with magnetic field and d is the thickness of the sample. Also, $R_H = \frac{1}{ne}$ so that carrier concentration can be calculated. The mobility μ_H can be calculated from the expression,

$$\mu_H = \frac{R_H}{\rho} \tag{4}$$

The temperature variation of ρ and R_H was done using glass liquid helium cryostat. Temperatures were measured with Cu - const and Au + .07% Fe and chromel thermocouples. Data was recorded on a teletype using a Hewlett Packard data acquisition system. Ohmic contacts on GaAs samples were made in high vacuum using In-Pt alloy (details in section I.C.2.). Considerable time was spent in setting up and making preliminary checking of the apparatus.

The following measurements were made on different crystals of GaAs

(a) dc electrical resistivity at different temperatures by the Van der Pauw method.

(b) dc-dc Hall effect.

(c) Calculation of Hall mobility and carrier concentration.

(d) Determination of total ionized impurity density $(N_D + N_A)$, N_A by taking use of mobility calculated at $77^{\circ}K$

(e) Checking the electrical homogeneity of various crystals.

Measurement of Resistivity and Hall Effect in GaAs #1

The GaAs crystal #1 supplied by SSL was used for these measurement. X-ray Laue pattern indicated that the sample face was oriented towards (111) orientation. Ohmic contacts were made with platinum wire using indium as the alloying metal. The four contacts made on the circumference of the GaAs disc were found ohmic when tested with a curve tracer. The Hall effect was measured by the Van der Pauw method.[1]

At first measurements were only made at two temperatures, i.e., at room temperature and LN_2 temperatures. A magnetic field of only 3000 gauss was used. The results of measurement are given in Table I. The values in the parenthesis are from the data sheet supplied by the Westinghouse Corporation. Note that our value of μ_H is only 60% of the Westinghouse value suggesting that defects have been introduced in GaAs #1. This drop is not surprising since GaAs #1 had been contaminated during handling, etching, polishing, X-raying, and studying under the electron microscope and had been broken in half in the process.

To give a check on our measurements the value of Hall mobility was also measured in a magnetic field of 2000 gauss and the values calculated for R_H and μ_H were found within 5%. The value of Hall coefficient at 3000 gauss is slightly lower than the value calculated at 2000 gauss field which is expected for a homogeneous sample.

TABLE I

		RT Value								LNa Value					
Sample		$\rho \times 10^{-2}$ ohm cm	R_H in cm³/coul		μ_H in cm²/volt sec		$n \times 10^{-16}$ cm³		$\rho \times 10^{-2}$ ohm cm	R_H in cm³/coul		μ_H in cm²/volt sec		$n \times 10^{-16}$ cm³	
			2000 gauss	3000 gauss	2000 gauss	3000 gauss	2000 gauss	3000 gauss		2000 gauss	3000 gauss	2000 gauss	3000 gauss	2000 gauss	3000 gauss
GaAs #1		3.82 (4.0)	109.3	108.7	2859 (5000)	2837	5.72 (3.1)	5.78	4.15	167	166	4031	4004	3.73	3.76

Resistivity of Hall Data for GaAs 1

Temperature Variation of Resistivity of GaAs #1 Down to $4.2°K$

The liquid helium dewar was tested on the Hall set-up. Temperature varia-
tion of resistivity of GaAs sample #1 was measured from room temperature down to $4.2°K$.
Fig. 1 gives the variation of resistivity ρ from room temperature down to $4.2°K$. Simi-
lar variation of resistivity for a high purity n-type GaAs epitaxial film has been reported
by Whitaker, et al.[2]

Wolfe, et al.[3] have determined the total ionized impurity concentrations $(N_D + N_A)$
from 7×10^{13} to 3×10^{17} cm^{-3} for n-type GaAs by analyzing mobility and carrier con-
centration data as a function of temperature with the Brooks-Herring formula for ionized
impurity scattering. An optimum temperature for the mobility analysis was thus determined
for each concentration and the results were used to determine empirical curves for the total
ionized impurity density to be expected for a given $77°K$ mobility.

Following Wolfe, et al.[3] the value for $(N_D + N_A)$ was calculated for sample #1 .
The results are given below in Table II.

Table II

Sample	Hall Mobility μ_H at $77°K$	Total Ionized Impurity Density $(N_D + N_A)$	N_D	N_A	N_A/N_D
GaAs #1	4031 $cm^2/$ volt sec	3×10^{17} cm^{-3}	1.78×10^{17} cm^{-3}	1.22×10^{17} cm^{-3}	0.68

Homogeneity of Sample #1

In the case of sample #1 (which is the Westinghouse seed sample) the ratio of two
pseudo resistances in Van der Pauw's expression, $\frac{R_1}{R_2}$ changes from 1.3 at room temperature
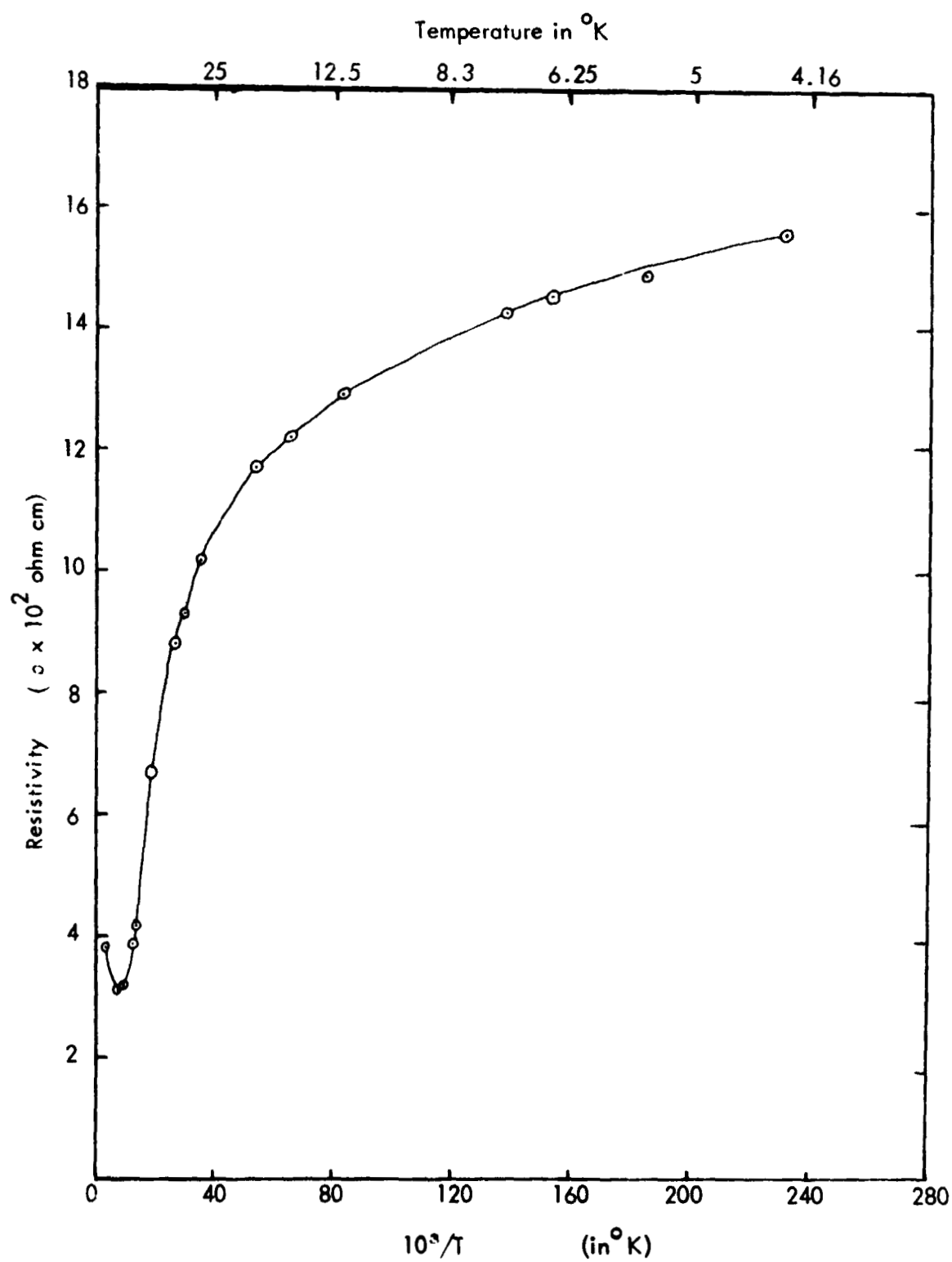
Figure 1   Temperature variation of resistivity of gallium arsenide crystal #1.

to only 1.5 at liquid helium temperature. This indicates that the sample is homo-geneous, because the ratio $\frac{R_1}{R_2}$ is apt to change for samples which contain some inhomogeneities (details in next paragraph).

Resistivity and Hall Effect Measurements on GaAs Crystals #5 and 6

Ohmic contacts (four) were made on two different samples (#5 and 6) of GaAs cut and polished on (100) face from the same ingot of GaAs. The resistivity and Hall effects measurements were made using the Van der Pauw technique. The room tempera-ture results for sample #5 and #6 are given in Table III.

Table III

Sample	ρ ohm cm	R_H cm³/coul		μ_H cm²/volt sec		n/cm³	
		2000 g	3000 g	2000 g	3000 g	2000 g	3000 g
GaAs #5	0.2734	1030	1030	3733	3767	6.1×10^{16}	6.1×10^{16}
GaAs #6	0.264	722	715	2737	2709	8.6×10^{16}	8.7×10^{16}

Homogeneity of Samples #5 and 6

It is to be noted that the value R_H and μ_H of both samples are quite different although the samples were parts of the same ingot. It has been reported by many workers [4,5,6] that the Hall mobility in semiconductors and insulators can be greatly affected by inhomogeneous impurity distributions. This is due to the formation of large space-charged regions surrounding local inhomogeneities. Anomalous mobility effects have been observed in GaAs by these workers.

Also, in an inhomogeneous sample the activation energy for conduction is not

generally a constant throughout the whole material. When measuring an in-
homogeneous material, even constant current, the current pattern will generally
change with the temperature. The resistances R_1/R_2 (measured in Van der
Pauw method to evaluate the value of resistivity ρ) are sensitive to changes
in ucrrent pattern. For a homogeneous sample the ratio R_1/R_2 should be a
constant, only determined by the geometry of the sample and the contacts.
A variation of the ratio R_1/R_2 with temperature, therefore, points to
the presence of macroscopic inhomogeneities. H. J. Van Daal [7] has reported
similar effects in SiC crystals. He also reported a model where intentional inhomo-
geneities were introduced in a crystal. In almost all cases the introduction of in-
homogeneities results in a reduction of the measured mobility. Where relatively
small regions with higher conductivity are introduced intentionally, the reduction of
mobility is mainly due to a decrease of the Hall coefficient, while no influence is
found on the resistivity. In our measurements also as indicated in Table III for
samples #5 and #6, the value of ρ is almost the same, while the value of μ_H is
considerably lower in #6. The ratio of R_1/R_2 also changes considerably in going down
to $77^{\circ}K$. While for sample #1 (reported earlier), the ratio R_1/R_2 remains almost con-
stant down to $4.2^{\circ}K$. These results indicate that the samples #5 and #6 contain
large amounts of inhomogeneities.

The exact location of inhomogeneities in these crystals is not known because
facilities were not available (like micro-beam Laue) to locate these inhomogeneities.

The data at low temperatures were not meaningful because these samples showed
large amounts of inhomogeneities at $77^{\circ}K$.

Resistivity and Hall Effect in GaAs #8 and GaAs #9 and Checking the Homogeneity

A sample of GaAs (called here as #8) was obtained from Mr. Mirt Davidson of SSL/TR.

X-ray Laue pattern indicated that wafer was oriented on (100) face. The sample was chemically polished by usual techniques and six ohmic contacts were alloyed in vacuum using In-Pt

alloy. All the contacts were found to be ohmic down to $77^\circ K$. The geometrical location of

the contacts on the sample is shown in Fig. 2. In order to test the homogeneity of the sample,

the resistivity of ρ was measured using different combinations of the six contacts on the sample.

Also, Hall mobility and carrier concentration were measured at room temperature. The results

of measurement are given below:
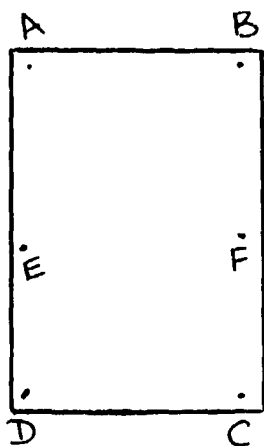
$$R_{AB, EF} = 9.993 \times 10^{-1} \text{ ohm}$$

$$R_{BF,EA} = 1.394 \text{ ohm}$$

$$\rho_1 = 2.814 \times 10^{-1} \text{ ohm cm}$$

$$\rho_2 = 2.826 \times 10^{-1} \text{ ohm cm}$$

(ρ_2 values are after interchanging current and potential leads)

$$R_{EF,CD} = 9.891 \times 10^{-1} \text{ ohm}$$

$$R_{FC,DE} = 1.887 \text{ ohm}$$

$$\rho_1 = 3.274 \times 10^{-1} \text{ ohm cm}$$

$$\rho_2 = 3.297 \times 10^{-1} \text{ ohm cm}$$

$$R_{AB,CD} = 1.516 \times 10^{-1} \text{ ohm}$$

$$R_{BC,DA} = 4.929 \text{ ohm}$$

$$\rho_1 = 3.173 \times 10^{-1} \text{ ohm cm}$$

$$\rho_2 = 3.166 \times 10^{-1} \text{ ohm cm}$$

Fig. 2

$$R_{AB,CE} = 5.714 \times 10^{-1} \text{ ohm}$$

$$R_{BC,EA} = 1.951 \text{ ohm}$$

$$\rho = 2.636 \times 10^{-1} \text{ ohm cm}$$

$$R_{BE,CD} = 4.518 \times 10^{-1} \text{ ohm}$$

$$R_{BC,DE} = 2.724 \text{ ohm}$$

$$\rho = 2.975 \times 10^{-1} \text{ ohm cm}$$

$$R_{AB,ED} = 5.32 \times 10^{-1} \text{ ohm}$$

$$R_{BD,EA} = 2.088 \text{ ohm}$$

$$\rho_1 = 2.675 \times 10^{-1} \text{ ohm cm}$$

$$\rho_2 = 2.694 \times 10^{-1} \text{ ohm cm}$$

The values of resistivity measured using different combination of contacts on the cryastal vary appreciably indicating that the crystal is inhomogeneous. The values of ρ_1 and ρ_2 in each case are almost the same. The above results suggest that there are some regions of inhomogeneity in the crystal which, in turn, tend to increase the resistivity. The overall values of Hall mobility and carrier concentration measured at room temperature for the above sample are:

Hall constant $R_H = 1071 \text{ cm}^3/\text{coul}$

Hall mobility $\mu_H = 3912 \text{ cm}^2/\text{volt sec.}$

Carrier concentration $= 5.8 \times 10^{15}/\text{cm}^3$

Another sample of GaAs #9 (ventron 41721-7) supplied by Mr. Davidson
was also used for measurement of resistivity and Hall constant. Laue pattern indi-
cated that the sample was oriented on (111) face. The results of room temperature
and 77°K resistivity, Hall constant, etc. are given in Table IV.

Table IV

Sample	Resistivity ρ in ohm cm		R_H in cm^3/coul		μ_H cm^2/ volt sec		n/cm^3		$N_D + N_A$	N_D	N_A
	Room Temp. (RT)	LN$_2$	RT	LN$_2$	RT	LN$_2$	RT	LN$_2$			
GaAs #9	1.066×10^{-1}	8.997×10^{-2}	-570	-863	5352	9592	1×10^{16}	7×10^{15}	2.78×10^{16}	1.89×10^{16}	0.89×10^{16}

Following Wolfe, et al.,[3] and taking into account the screening factor, the
total ionized impurity density was calculated and is included in the Tavle IV above.
The compensation ratio $\frac{N_A}{N_D}$ was found to be 0.47 for this sample thereby indicating
that the analysis used by Wolfe, et al.,[2] can be safely applied in this case.

The ratio of $\frac{R_1}{R_2}$ changes by a factor of 5% in going from room temperature down
to 77°K. This indicates that the sample is homogeneous. Wolfe, et al.,[2] have indi-
cated that resistance ratio $\frac{R_1}{R_2}$, an indication of electrical homogeneity, was typically
1 and 2 in their crystals and did not vary by more than about 30% over the measured
temperature range (room temperature to 4.2°K).

Magnetic Field Dependence of Hall Effect

Although the Hall effect is much less sensitive to inhomogeneity than is the magnetoresistance, pronounced anomalies could be observed when gross inhomogeneities occur. Bate, et al.,[8] observed an anomalous magnetic field dependence of the Hall coefficient in an n-type InSb sample containing a step function discontinuity in carrier concentration ($n - n^+$ junction). If the junction is near the Hall probes, the Hall voltage will be an average of the Hall voltages in the two regions. Wolfe, et al.,[6] have reported that since intentionally introduced conducting inhomogeneities result in anomalously high measured mobilities, similar effects may be observed in samples with other conducting inhomogeneities such as accumulation layers, metallic inclusions and precipitates and doping variations due to polycrystalline growth or faceting effects. For a homogeneous sample, the Hall constant should decrease with increasing field as expected by the magnetic field dependence of the Hall coefficient factor. Anomalous magnetic field dependence was observed by these workers for GaAs samples with intentional inhomogeneities. This casts doubt on the use of mobility as a figure of merit for a material unless homogeneity can be established. In samples #1 and #9, no appreciable change of measured Hall coefficient was found between the magnetic field values of 300 to 4000 gauss. Due to limited magnetic field value in our set-up, we could not obtain magnetic field values of the order of 10^4 gauss, where the above workers found anomalous effects in the Hall coefficient.

Resistivity and Hall Effect in GaAs #10(2) and 10(3) and Check on the Electrical Homogeneity

GaAs #10(2) and 10(3) were supplied by SSL after chemical polishing. X-ray Laue

pattern indicated (111) orientation for both the samples. Four ohmic contacts were made with In-Pt alloy on sample #10(2) and six on sample #10(3), for Van der Pauw measurements. All the contacts were found to be ohmic down to $77^{\circ}K$. Sample thickness was measured with a travelling microscope. Hall effect was measured at 3000 gauss and 2500 gauss magnetic field values. The two values of Hall coefficient were found to be nearly the same (within 5%). The results of measurement are given in Table V.

Table V

	Resistivity ρ in ohm cm		R_H in cm^3/coul		μ_H cm^2/ volt sec.		n/cm^3	
Sample	RT	LN_2	RT	LN_2	RT	LN_2	RT	LN_2
GaAs #10(2)*	9.05×10^{-2}	7.567×10^{-2}	312	467	3443	6172	2×10^{16}	1.2×10^{16}
#10(3)*	2.62×10^{-3}	2.95×10^{-3}	3.76	3.86	1431	1307	1.6×10^{18}	1.62×10^{18}

Following Wolfe, et al.,[8] the total ionized impurity density was calculated for sample #10(2) and is given in Table VI. The above method could not be applied for the sample #10(3) because the Brooks-Herring [9] formula is not valid at concentrations higher than 3×10^{17} cm^{-3}.

Table VI

Sample	$(N_D + N_A)$ cm^{-3}	N_D cm^{-3}	N_A cm^{-3}	N_A/N_D
GaAs #10(2)	6.54×10^{16}	4.27×10^{16}	2.27×10^{16}	0.53

Resistivities at room temperature were measured for GaAs #10(3) using five possible combinations of contacts giving five independent values of resistivity ρ. The results are given in Table VII.

Table VII

Pseudo Resistance	Resistivity ρ in ohm cm
$R_{DA} \cdot ED$ $R_{AE} \cdot DB$	2.492×10^{-3}
$R_{AB} \cdot CD$ $R_{BC} \cdot DA$	2.651×10^{-3}
$R_{FD} \cdot BC$ $R_{BD} \cdot FC$	2.519×10^{-3}
$R_{DA} \cdot EF$ $R_{AE} \cdot DF$	2.527×10^{-3}
$R_{FE} \cdot BC$ $R_{EB} \cdot CF$	2.549×10^{-3}

From Table VII, it is evident that five different resistivity values are within 6% of each other. Brice, et al.,[10] have reported that in a laminar sample the values of different resistance, although not true spreading resistances, depend only on the logarithm of contact-to-contact distance. Hence, provided the contacts are not grossly unsymmetrical, a wide variation of resistance indicates an inhomogeneity normal to the plane of the slice. In measuring the resistiv   ...e variation of contact positions is taken into account and so very little variation ... istivity values indicates that the sample does not contain inhomogeneities normal to the plane of the slice.

The ratio $\frac{R_1}{R_2}$ changed only by a factor of 5% in going from room temperature down to 77°K. This indicates that the sample is quite homogeneous.

It is recommended that each crystal be tested for inhomogeneities before deciding on a seed material for epitaxial growth of GaAs.

Table for Properties of GaAs

During the course of the above work the attached table was compiled which lists important properties of GaAs.

Conclusion

The data generated on ground based samples can be used to evaluate the over-all role of the space environment on the growth of GaAs single crystals and epitaxial films, although during this reporting period no measurements were made on epitaxial films. The following parameters could be used to elucidate the role of gravity:

(a) The overall carrier concentration and mobility of the sample.

(b) Type of material grown, n or p type

(c) Homogeneity of the sample.

(d) Total ionized impurity density $(N_D + N_A)$ and the compensation ratio N_A/N_D.

In the case of an epitaxial undoped film grown on a doped substrate or a doped film on an undoped substrate, the results of measurement of the above mentioned parameters can give information about the overall quality of the grown film. The resistivity and Hall constant of the film in both cases can be several orders of magnitude different than the substrate, thereby making the results more meaningful. I some cases of epitaxial growth by vapor phase method, a region of high resistance was detected by Hasegawa [11] between the layer-substrate interface. The measurements are also especially useful in evaluating the prior quality of the seed material used for the M-555 experiments of GaAs epitaxial film growth. In the case of epitaxial growth of films, the quality of seed on which the film is grown is of utmost importance, because defects present in the seed can emerge out in the film making the quality of the film poor. [12]

Errors Introduced in Van der Pauw's Method Due to Finite Size of the Contacts and the

Contacts Not Lying Exactly on the Circumference of the Sample

In order to calculate the errors introduced if the contacts are of finite size and not at the circumference of the sample, Van der Pauw derived special formulas for these special cases. Taking those particular cases, we have calculated the percentage of error involved. In all cases it was assumed that the sample had a shape of a circular disc and that contacts are at right angles to each other. Three special cases are discussed and are represented in Fig. 3.

I. One of the contacts is of finite length "d" and is assumed to lie on circumference.

Case I   Case II   Case III
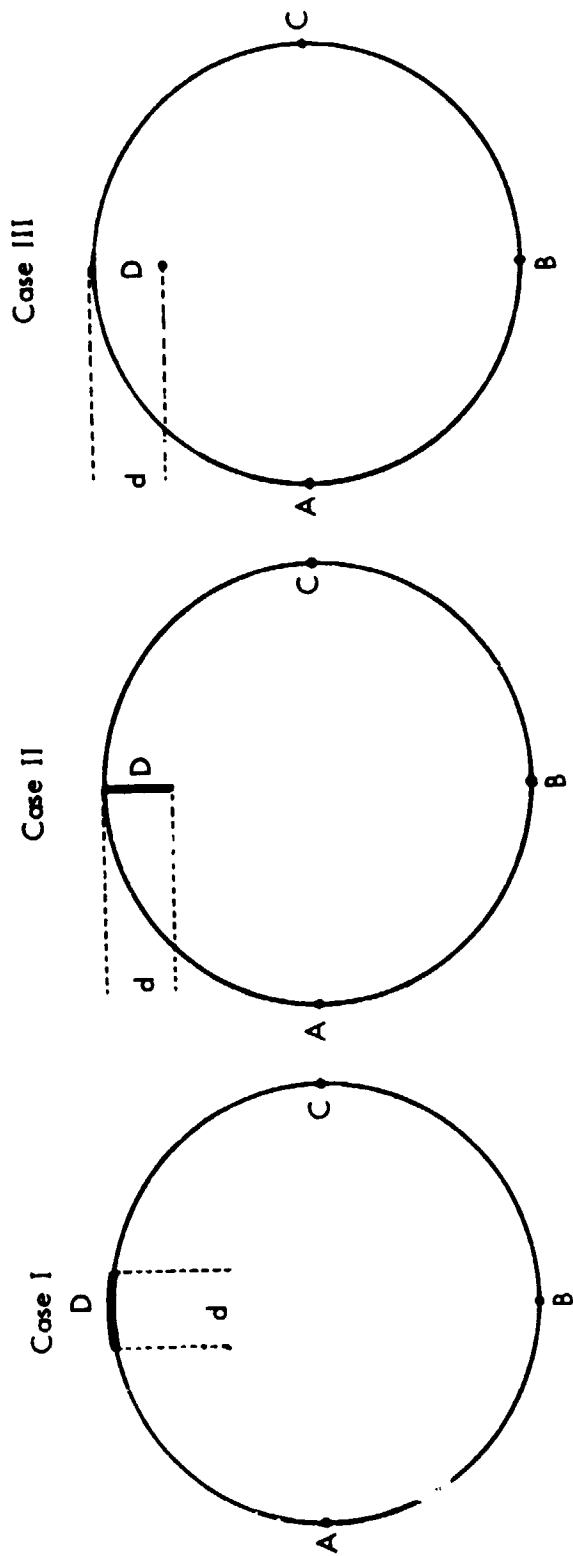
Fig. 3

II. One of the contacts is made in a direction perpendicular to the circumference and is of length "d".

III. One of the point contacts lies at a distance "d" from the circumference.

<u>Case I</u>. If D is the diameter of the sample and the values of $\frac{d}{D}$ and μB are small, the relation between $\frac{\Delta \rho}{\rho}$ and $\frac{\Delta \mu}{\mu}$, the relative errors introduced in resistivity and mobility, is given below:

$$\frac{\Delta \rho}{\rho} = -\frac{d^2}{16 D^2 \ln 2}$$

$$\frac{\Delta \mu_H}{\mu_H} = -\frac{2d}{\pi^2 D}$$

Taking a typical case of a contact diameter of 1.00 mm and sample slice diameter of 10 mm, the calculated relative errors are as follows:

$$\frac{\Delta \rho}{\rho} = -0.1\%$$

$$\frac{\Delta \mu_H}{\mu_H} = -2.0\%$$

<u>Case II</u>. In the second case, the error introduced will be as in the foregoing case, but with "d" twice as large.

$$\frac{\Delta \rho}{\rho} = -\frac{d^2}{4 D^2 \ln 2} = -0.3\%$$

$$\frac{\Delta \mu_H}{\mu_H} = -\frac{4d}{\pi^2 D} = -4\%$$

Case III. In the third case, the theoretical expressions and calculated errors are as follows:

$$\frac{\Delta \rho}{\rho} = -\frac{d^2}{2D^2 \ln 2} = -0.7\%$$

$$\frac{\Delta \mu_H}{\mu_H} = -\frac{2d}{\pi D} = -6\%$$

According to Van der Pauw, it can be shown that if more contacts have some of the above mentioned defects at the same time, the errors introduced to a first approximation will be additive. The above error factors can be incorporated as a correction factor.

TABLE VIII 120

PROPERTIES OF GaAs

Property	Description	Comments	References
Melting Point	$1238°C$	The phase diagram was obtained when vapor pressure was unknown. Possess appreciable vapor pressure at the mp.	1) H. Welker and H. Weiss, Solid State Phys., Vol 3, p.1, Academic Press, NY, (1956). 2) J. Vanden Boomgard, et al, Philips Res. Rept. 12, 127 (1958).
Density in g/cm^3	$5.3162 + 0.0002$ at $25°C^-$	Unannealed GaAs	3) L. R. Weisberg, et al, J. Appl. Phys, 34, 1002 (1963).
Crystal Structure	Zinc blende type cubic $a = 5.65315 + .0001$ Å at $25°C^-$		4) G.V. Ozolin'sh et al, Sov. Phys. Cryst, 7,691 (1963).
Space Group	$F\bar{4}3m$		5) Am. Inst. Phys. Handbook, Table 9b-1, (McGraw Hill Co., N.Y. 1957)
Energy Gap	1.53 ev at $0°K$ $1.49 - 1.52^a$ ev at $77°K$ $1.37 - 1.43$ ev at $300°K$	a) Values are uncertain	6) M.D. Sturge, Phys. Rev, 127, 768 (1962). 7) H. Piller, in Phys. of Semiconductors (Proc. 7th Intern. Conf) Academic Press, N.Y. 1964.
Average Effective Masses	0.07 – Electrons 0.12 – Light holes 0.68 – Heavy holes	Values given are ratios of the effective masses to the free electron mass.	8) Same as 6 and 7.
Spin – orbit Splitting Energy	0.35 ev		9) Same as ref. 6 and 7.
Index of Refraction	3.291 at 0.27 μ at room temperature		10) Semiconductors and Semimetals, Vol. 3, Academic Press, N.Y. (1967), p. 518.

Property	Description	Comments	References
Effective Charge	–0.51		11) Semiconductors and Semimetals, Vol I, Academic Press, N.Y. 1966, p. 13.
Electron Mobility cm^2/volt sec.	a) 8800 at room temp with total impurity concentration of $10^{15} cm^{-3}$ b) 55,000 at low temps. c) 110,000 at $56°K$ (vapor phase) with impurity contents near $6 \times 10^{14} cm^{-3}$ (ref 13)	Results (a) and (b) are for GaAs epitaxial layers. (ref. 12) By vapor phase technique. This material is much purer than any GaAs reported previously.	12) J. R. Knight, et al, Solid State Electron, 8, 178 (1965). 13) J. Whitaker, et al, Sol. State Comm, 4, 181, (1966).
Temperature Variation of Resistivity, Hall Constant and Mobility.	 J.R.Knight, et.al., Solid.State.Electron,8,178(1965)		14) Same as ref. 12.
Coefficienty of Linear Expan. $\alpha \times 10^6$ deg^{-1}	5.64 at ~370°K ~0.5 at 55°K	α becomes negative at a transition temp. $T_t = 55°K$.	15) S.I. Novikova, Sov. Phys. Sol. State, 3 129 (1961)

Property	Description	Comments	References
Thermal Conductivity watts/cm deg.	0.35 at $300°$ K ~30 at ~$10°$K 0.9 at $2°$K		16) M. G. Holland, Phys. Rev., <u>134</u>, A471 (1964)
Specific Heat at Constant Pressure	0.07640 cals/gm deg. at $298°$K		17) Semiconductors and Semimetals, Vol. II, Academic Press, N.Y., 1966, p. 52.
Characteristic Temperature $\theta_{el}(0)°$K	344	Calculated from Elastic Constants (given in next column)	18) P. M. Sutton, Phys. Rev. <u>99</u>, 1826 (1955). 19) Same as ref. 17, p. 56.
Elastic Constants (10^{11} dynes /cm^2)	$C_{11} = 11.88$ $C_{12} = 5.38$ $C_{44} = 5.98$ $T = 298°$K		20) Same as ref. 17, p. 56 21) T. B. Bateman, et al, J. Appl. Phys. <u>30</u>, 544, (1959).
Max heat treatment temp. (110) surface	$1000°$C		22) Same as ref. 17, p. 117.
Estimated Anneal temp (110) surface	$550°$C		23) Same as 22.
Ionicity	0.56		24) M. Hass. et al., J. Phys. Chem. Sol. <u>23</u>, 1099 (1962).
Paramagnetic Resonance Results			25) Ref. same as 17, p. 201.

Host lattice	Paramagnetic atom	Spin S	g-value	Fine structure constant $|a|$ (gauss)	Hyperfine interaction A (gauss)	Remarks
GaAs	Manganese	$\frac{5}{2}$	2.003	15.5	57	Fine structure not resolved
GaAs	Iron	$\frac{5}{2}$	2.046	374	—	Hyperfine structure not resolved
GaAs	Iron or defects	$\frac{5}{2}$	2.046	374	—	Spin density 10^2 times greater than iron density
GaAs	Nickel	$\frac{3}{2}$	2.106	—	—	One very broad line, about 130 G in half-width
GaAs	Zinc	$\frac{1}{2}$	8.1	—	—	Bound hole detected by uniaxial stress
GaAs	Cadmium	$\frac{1}{2}$	6.7	—	—	Bound hole detected by uniaxial stress
GaAs	Conduction elec.	$\frac{1}{2}$	0.52	—	—	About 100 G in half-width

Properties of GaAs

Property	Description	Comments	References
Etchants	5 5% NaOH Soln 1 30% H_2O_2	5 Min Removing material at a rate of 10 to 15 μ/min.	26) D. N. Nasledov, et al, Zh, Tekh. Fiz, 28, 779 (1958).
	2 HCl 1 HNO_3 2 H_2O	10 minutes Etching (111)	27) J. G. White, et al, J. Appl. Phys., 30, 946 (1959). 28) M. S. Abrahams, et al, eds., Property of Elemental and Compound Semiconduc- tors, p 225, Interscience Publishers, N.Y. 1960.
	1 HF 5 HNO_3 8 to 12% $AgNO_3$ Soln	Etching (111) and ($\bar{1}\bar{1}\bar{1}$). Ag inhibits attack on the normally fast etching ($1\bar{1}\bar{1}$).	29) J. L. Richards, et al, J. Appl. Phys, 31, 611 (1960).
	1 HF 3 HNO_3 2 H_2O	Chemical Polish	30) Same as ref. 29.
	1 HF 1 30% H_2O_2 1 H_2O	10 Min. Produces etch pits on (111)	31) J. L. Richards, J. Appl. Phys., 31, 600 (1960).
	1 HF 2 H_2O with 33% $Cr O_3$, 0.3% $AgNO_3$	10 Min. at 65°C Produces etch pits on (111), ($\bar{1}\bar{1}\bar{1}$), (110) and (100). Also re- veals dislocation lines	32) M. S. Abrahams, et al, J. Appl. Phys., 36, 2855, (1965).
	CH_3OH with 5 - 20% Br_2	Polishing	33) C. S. Fuller, et al, J. Electrochem. Soc. 109, 880 (1962).

References

1. Van der Pauw, L. J. Phillips Res. Rep. 13, 1, (1958).

2. J. Whitaker and D. E. Bolger, Solid State Commun. 4, 181 (1966).

3. C. M. Wolfe, G. E. Stillman and J. O. Dimmock, J. Appl. Phys. 41, 504 (1970).

4. C. Herring, J. Appl. Phys. 31, 1939 (1960).

5. L. R. Weisberg, J. Appl. Phys. 33, 1817 (1962).

6. C. M. Wolfe, G. E. Stillman and J. A. Rossi, J. Electro-Chem. Soc. 119, 250 (1972).

7. H. J. Van Daal, Phillips Res. Reports Supplement No. 3, (1965).

8. R. T. Bate, J. C. Bell and A. C. Beer, J. Appl. Phys. 32, 806 (1961).

9. H. Brooks, Advan. Electron. Phys. 7, 185 (1955).

10. J. C. Brice, R. E. Hunt, G. D. King and H. C. Wright, Sol. State Electronics 9, 853 (1966).

11. F. Hasegawa, J. Electrochem. Soc. 11, 930 (1972).

12. U. Zimmerli and A. Steinnmann, Solid State Commun. 5, 447 (1967).

I.C.5. GaAs EPITAXIAL LAYER SURFACE MORPHOLOGY

a. Introduction

Surface morphology will be used as a qualitative index to the perfection of GaAs substrates, films and crystallites. A rough grain-like or spongy surface would suggest polycrystallinity, while a loose film would suggest a nonepitaxial film. Lenie[1] suggests unaided viewing of the film against a dark background under a fluorescent light to identify such defects as scratches, pits, "orange peel" and pyramids. Microscopic examination will easily reveal scratches, voids, spikes, crowns, and dimples with measurements accurate to 1 micron.

b. SEM-Photomicrographs

The effectiveness of Scanning Electron Microscope photomicrographs for GaAs epitaxial film characterization is illustrated on Fig. 1 and Fig. 2. A film thickness of $20 \pm 1\ \mu$ is determined from the 140X photograph. The second photo shows a "blister" at 1600X which was the most noticeable defect of the surface of GaAs epi #1 as seen in Fig. 2.

c. GaAs Surface Study

Surface studies show that the GaAs seed faces (GaAs #10-1, #10-2 and #10-3) were rounded due to polishing such that the disk centers were about $10\ \mu$ higher than the edge. The minimum full scale tally surf deflection must be greater than $10\ \mu$ reducing instrument sensitivity by at least a factor of 10.

Recommendation - GaAs should be embedded in an epoxy. Then the epoxy and wafer could be ground and polished as one unit, thus keeping the surface flat.

If the GaAs wafers could be cut round, they could be fit flush into a polish-
ing holder having round holes. Both the GaAs and the holder would be polished to-
gether thus preventing preferential edge polishing.

d. GaAs Slicing

The technique of slicing GaAs (100) wafers from ingots of $\langle 100 \rangle$ growth direc-
tion has been mastered using a diamond lathe cutting wheel and a jig which holds the
crystal goniometer on the lathe in the same position as it sits on the X-ray beam. This
will alleviate our shortage of (100) crystals which deserve most attention in view of their
use in M-555.
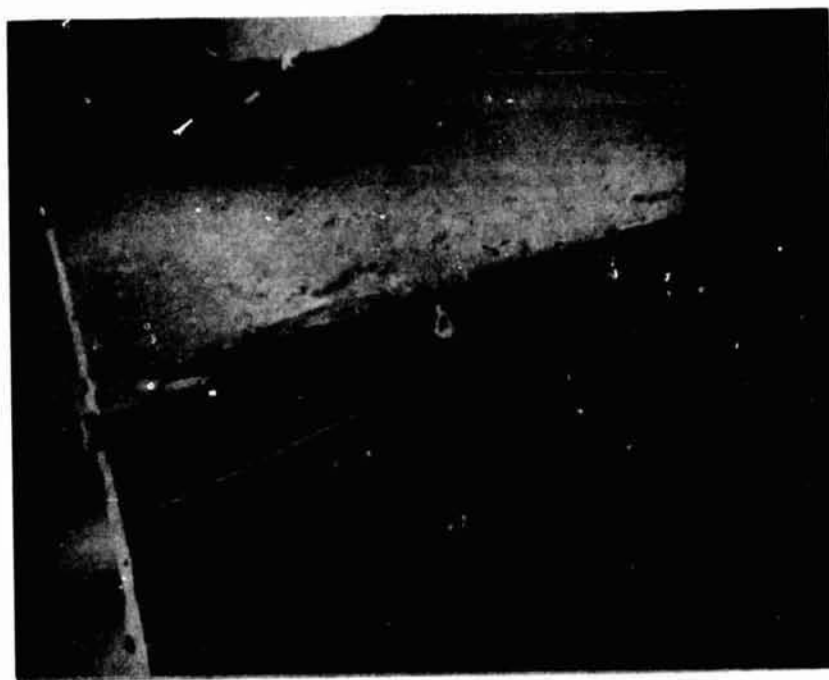
Fig. 1. Scanning Electron Microscope photomicrograph showing the exposed edge of GaAs Epi #1 which is used to calculate the epitaxial film thickness.
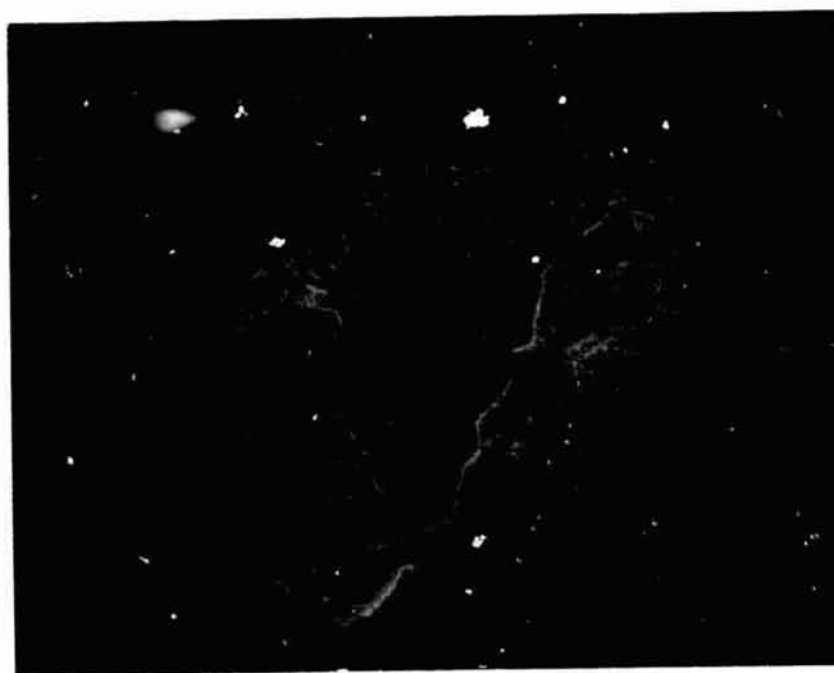
Fig. 2. Scanning Electron Microscope photomicrograph of GaAs Epi #1
epitaxial film surface showing a blister about 25 μm in size.
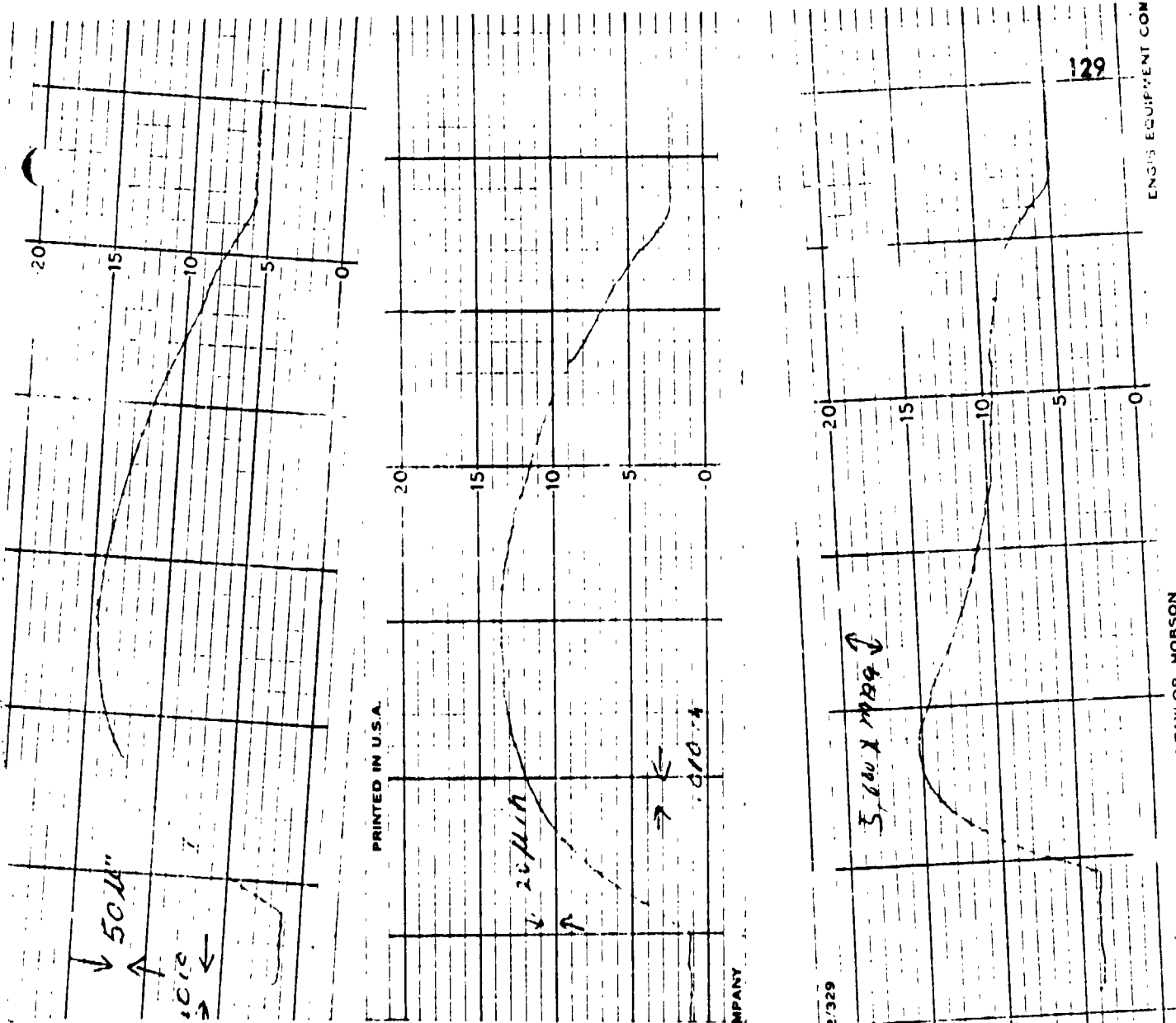
Fig. 3. Tally Surf scans of GaAs #10-1, #10-2 and 10-3 wafers. Note the rounded surface produced by polishing. The initial and final scans were produced before the scan began or after it had stopped so they should be ignored.
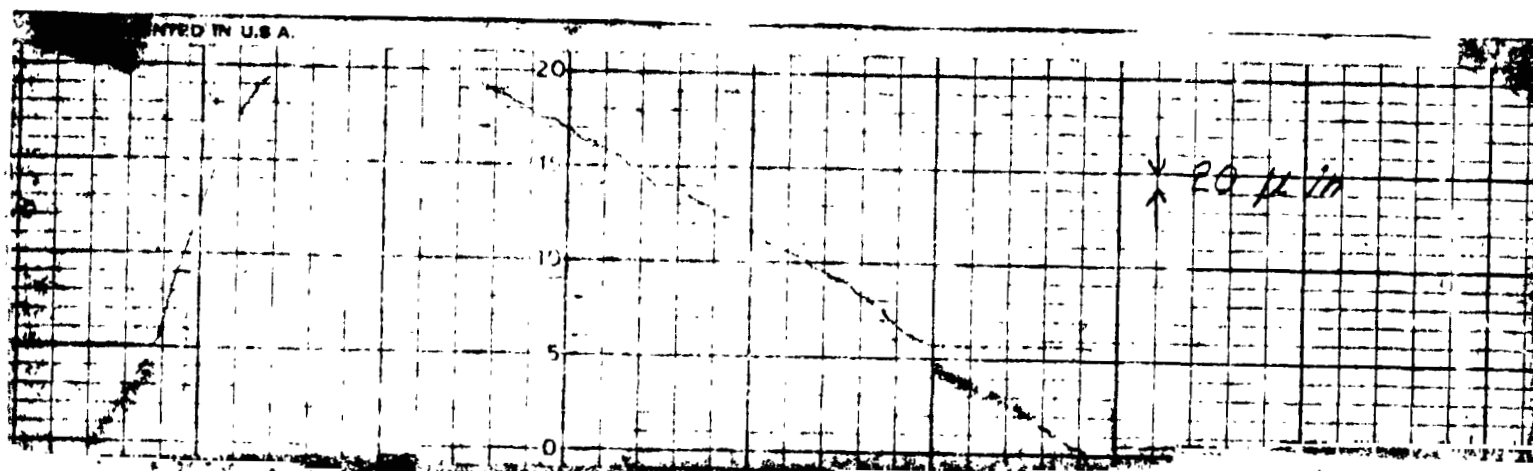
Fig. 4. GaAs #10-2 after chemical polishing. Note that the
surface contour is rougher than in Fig. 3 which was
made before chemical polishing. The chemical polish-
ing brings out scratches not seen visible before. Ob-
viously a flat surface would allow increased magnifica-
tion without clipping the top of the signal.

I. D. FLIGHT EXPERIMENT DEVELOPMENT AND FLIGHT EXPERIMENTS IN PROGRESS*

As outlined in a previous paragraph on Apollo Flyback Experiments (I.A.1),
near zero gravity in space environment (10^{-6} to 10^{-3} g are average values for an
orbiting space station) has a potential for producing single crystalling materials of
superior quality. Both, dopant homogeneity and structural quality is expected to be
improved with materials processed in space due to the lack of gravity driven convection.
(See I.A.1.)

Based upon the experiments on "containerless solidification of InBi and InSb"
and "diffusion and convection in a metallic melt" that were described in the section
on Apollo Flyback experiments, two similar experiments have been proposed for the
Skylab mission in 1973 and the ASTP mission in 1975:

1. Skylab Experiment "Growth of Spherical Crystals of InSb."

The purpose of this experiment is to study the feasibility of a new
technique developed by us for processing   containerless melts in space environment.
Since crucible contact is not only a possible source of contamination, but will neces-
sarily lead to thermal stresses due to different thermal expansion of crucible and sample
material, crucible contact has to be avoided if structurally good single crystals are
desired. Furthermore, if dopant homogeneity is of importance, the melt should stay
static during solidification; in particular no fluid motions should be induced by the
growth technique itself. Both of these conditions are met by our proposed experiment
(see I.A.1. and Experiment Implementation Plan).

The experiment was approved for Skylab in May 1972 by NASA Headquarters.
We are presently fabricating the flight hardware. A radiograph of a sample cartridge
is shown in Fig. 1.

---

*In charge: H. U. Walter
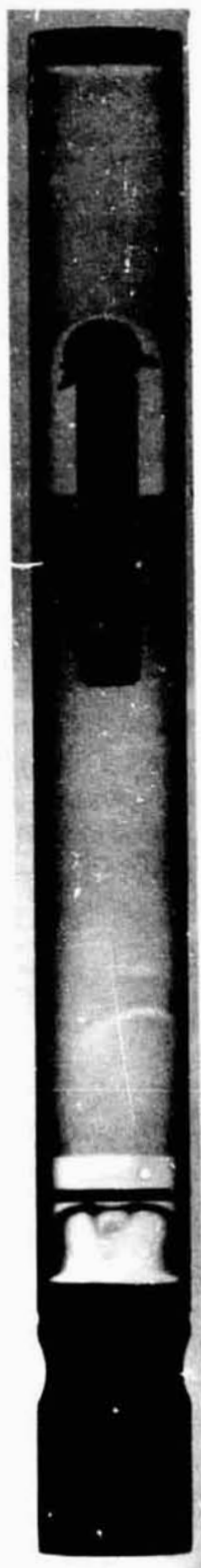
Fig. 1. Radiograph of sample cartridge for Skylab experiment M-560.

M560 3A

Since the approach used for Apollo flyback experiments (extension of melt through orifice and self-nucleation) was changed to melting back of cylindrical, single crystalline samples, high quality single crystals had to be produced. The required equipment was not available at UAH and we have designed and constructed the following equipment under this contract:

(1) High vacuum, high temperature furnace for alloying, casting, preparing ingots, etc.

(2) Horizontal boat arrangement (high vacuum, up to 1200°C).

(3) Czochralski system for growth of InSb (vacuum, up to 1200°C).

(4) UHV – Czochralski system.

(5) Several two and three zone Bridgman systems.

2. Convection and Diffusion in a Metallic Melt

This experiment was originally proposed as an Apollo flyback experiment. A more sophisticated version was submitted on October 24, 1972, for the ASTP mission in 1975. The concept of the experiment is as follows:

The basis of any future application of space environment for processing single crystals is quantitative knowledge of solidification kinetics as compared to solidification on earth and to the true, theoretical zero gravity case. Quantitative information can only be obtained if the parameters of the system before melting in space are known quantitatively and if the thermal parameters and thermal dynamics of the system during melting, soaking and solidfying are known as closely as possible. This leads to the following basic requirements for such an experiment:

(1) Geometry as simple as possible (cylindrical sample).

(2) Solid state diffusion negligible.

(3) Dopant distribution as defined as possible, which rules out remelting of doped single crystals, but makes casts (polycrystalline, small grain size) imperative. Stacking up of alternating slabs of casts with constant impurity level and casts of intrinsic material will provide this situation. The dopant concentration will follow a square function along the axis of the cylinder.

(4) A programmable furnace with actively and independently controlled hot and cold zones, such that the thermal history of a sample is known even without real-time monitoring of temperatures.

Melting and solidifying should preferably be short as compared to the soaking period where steady state conditions in terms of temperature are established. During soaking, dopant will diffuse into the initially undoped parts of the melt and, according to soak time and soak temperature, diffusion coefficient in the liquid and fluid motions, a dopant profile different from the initial square function will be established at the time where solidification is initiated. Dopants with distribution coefficient $k < 1$ and $k \approx 1$ will be used. An undoped seed crystal will be located at the cold end of the capsule.

As the solid-liquid interface travels along the cylindrical melt, dopant will be redistributed according to growth rate and distribution coefficient.

In the case of lacking convection, diffusion in the liquid will alter the square function of dopant concentration initially present to a distribution where the dopant concentration decays exponentially and symmetrically towards both undoped slabs on either side (neglecting differences in temperature in the two areas due to the

temperature gradient along the cartridge during soaking, an assumption that can

reasonably be made at low gradients and small spacing). Solidification will then,

in the case of $k = 1$, preserve this profile; in the case of $k < 1$, it will alter the symmet-

rical profile to an asymmetrical distribution, where the asymmetry is due to segregation

effects only.

If there is residual convection in the melt, dopant will not only be redis-

tributed by diffusion and segregation effects, but also by fluid transport. Provided that

solidification rates are kept constant and the temperature gradients are kept steep

enough to avoid constitutional supercooling, any random oscillation in dopant con-

centration can be attributed to fluid flow.

In order to verify that these conditions of growth were kept up during solidi-

fication, a control cartridge of identical geometry with seed and only one cast of con-

stant dopant level will be processed. Assuming that a furnace similar to the multipur-

pose electric furnace that is being used in the MS program of Skylab in 1973 will be

available, three cartridges can be processed simultaneously. One of the three will be

the above-mentioned control cartridge. A copper liner extending to about one third of

the length of the capsule from both hot and cold ends of the cartridge will generate

three gradient regions with kinks where the copper sleeves end. After melting and

soaking, the temperature of both of the controlled zones would be lowered, for

example, by synchronously and linearly reducing the reference voltages of the controllers

thus providing constant solidification rates within isogradient regions. As the inter-

face travels into a different gradient region, the solidification rate would alter and

an inhomogeneity in dopant concentration would mark this event. Correlation of

additional markings in the control sample with markings found in the two other samples would prove either presence of convection if no correlation could be made, or a variation in growth rate due to electrical and thermal instabilities if correlation could be made.

Since both diffusion and self-diffusion constants in the liquid and also segregation coefficients for the proposed systems are known, dopant profiles can be computed assuming a lack of fluid motion.

Comparison of the computed plots with dopant dist-ibution found in the samples that were melted, soaked and resolidified in space will provide quantitative information on eventually present residual convection. In the case where disturbances of the dopant profiles by fluid flow are minor and the general pattern observed is in agreement (eventually after computer averaging) with the general shape of the computed plots, diffusion coefficients of the different dopants in the melt and values of segregation coefficients can be refined. This is of basic value since any of these parameters are now being determined with a large inherent error due to interfering convection processes.

Similarly, segregation coefficients are determined under conditions where complete mixing can be assumed. Values for k given by various authors scatter considerably. The distribution coefficient of selenium in indium antimonide, for example, is given by various authors as 0.17, 0.5 and 0.35.

Matching of the computed plots for dopant distribution with the observed distributions by a computer iteration process where k and D are variables (starting out with available values for k and D) will yield refined values for k and D. The major

condition to be met would be a symmetrical dopant profile before solidification starts, asymmetry of the profile has to be caused by segregation only.

The experiment will provide the basic information required to conceive further scientific and production-type experimentation on solidification. It will prove whether and to what extent doping can sense disturbances caused by residual convection, information that is essential for further investigations and applications. It will also provide basic information on solidification kinetics and solidification parameters that should prove helpful for both space processing and ground based experimentation.

II. ADVERSE EFFECTS OF GRAVITY ON WHISKERS

A. INTRODUCTION AND BACKGROUND

The purpose of this investigation is to determine whether or not whisker growth is significantly improved in an earth orbit. This is a continuation of an earlier study[1] of manufacturing in space. The scope is limited to whiskers to assure a complete and intensive investigation.

Whiskers are high strength, filamentary single crystals. They are of interest mainly because of their high tensile strength which approaches the theoretical limiting strength of a material. Bulk crystals tensile strengths are from two to three orders of magnitude below the predicted theoretical value. As the cross section area of successive whiskers becomes smaller, in the neighborhood of $1 \mu^2$, the tensile strength increases by about a factor of 100, being roughly inversely proportional to the diameter.

So far, technology has been unable to fully utilize the high strength whiskers. This is partly because no rapid mass production method of growing good quality whiskers is available in an earth environment. Whiskers now available are either too short, have multiple branches, or are too scarce to be used in the reinforcement of high strength composites. In a zero-gravity space environment, whiskers should grow longer, thinner, and, thus, stronger.

Whiskers used to strengthen composites should have a high aspect ratio. The aspect ratio is the ratio of whisker length to thickness (or diameter). The long, thin whiskers have more surface area per unit whisker tension; thus, they would not pull free from the plastic matrix when the composite is under tension.

Conceivably, a gravitational field could affect the atomic whisker growth mechanism by vapor deposition growth which involves the gaseous states. In the vapor

deposition process,[3] a source material is slowly vaporized in the hot portion of the furnace and as the vapor moves to the cool region, it becomes supersaturated and condenses metal atoms to form a solid which often grows in whisker form. This is done in an inert atmosphere as seen in Fig. 1. The diffusion should be very slow; however, in a temperature gradient, nonuniform convection currents are set up which add to the diffusion in transporting the atoms to the lattice. These circulating currents (due to gravity) are probably unstable, thus producing an excess of supercooling which could result in massive nucleation which produces polycrystals instead of a single crystal growth. The convection is due to warm and cool gas having a different density in the presence of a gravitational field. The absence of convection at zero gravity should allow diffusion to produce a more uniform vapor for better crystal growth.

An experiment was conducted to test indirectly the above hypothesis. If 1-g produces an adverse effect on whisker growth, then 2-g should produce an even more adverse effect, etc. By applying several g's of acceleration to the whiskers during the growth by vapor deposition, and by comparing this growth to 1-g growth, one may then predict some effects of 0-g.

B. EXPERIMENTAL RESULTS OF CADMIUM WHISKER GROWTH BY VAPOR DEPOSITION FROM "g" to 20 "g" ACCELERATION IN A CENTRIFUGE

Cadmium whiskers and small crystals were grown in a centrifuge[1] for the purpose of determining the effect of increased "g" forces on crystal growth. Two growth tubes were used, and each crystal was grown for about five hours at 1, 5, 10, and 20 "g's".

The crystals were grown in the conventional manner (see Fig. 1) with a typical temperature gradient so as to prevent artificial exaggeration of the effect of gravity. The
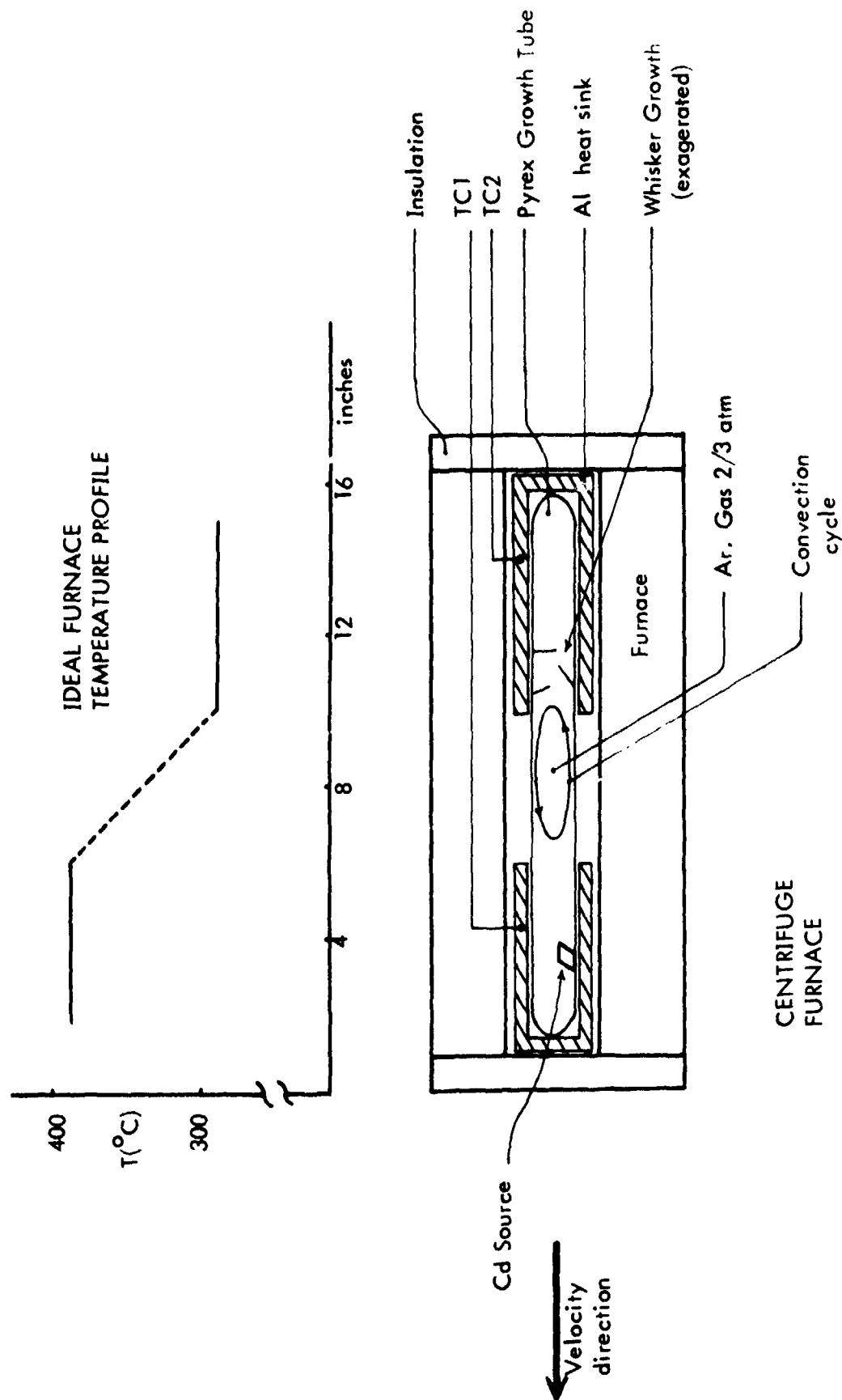
Fig. 1. A tubular whisker growth furnace adapted for rotation on a 1 meter long centrifuge arm. The insulation and the heavy aluminum sleeves were needed to maintain a constant temperature field in spite of the 20 M/sec furnace velocity through air.
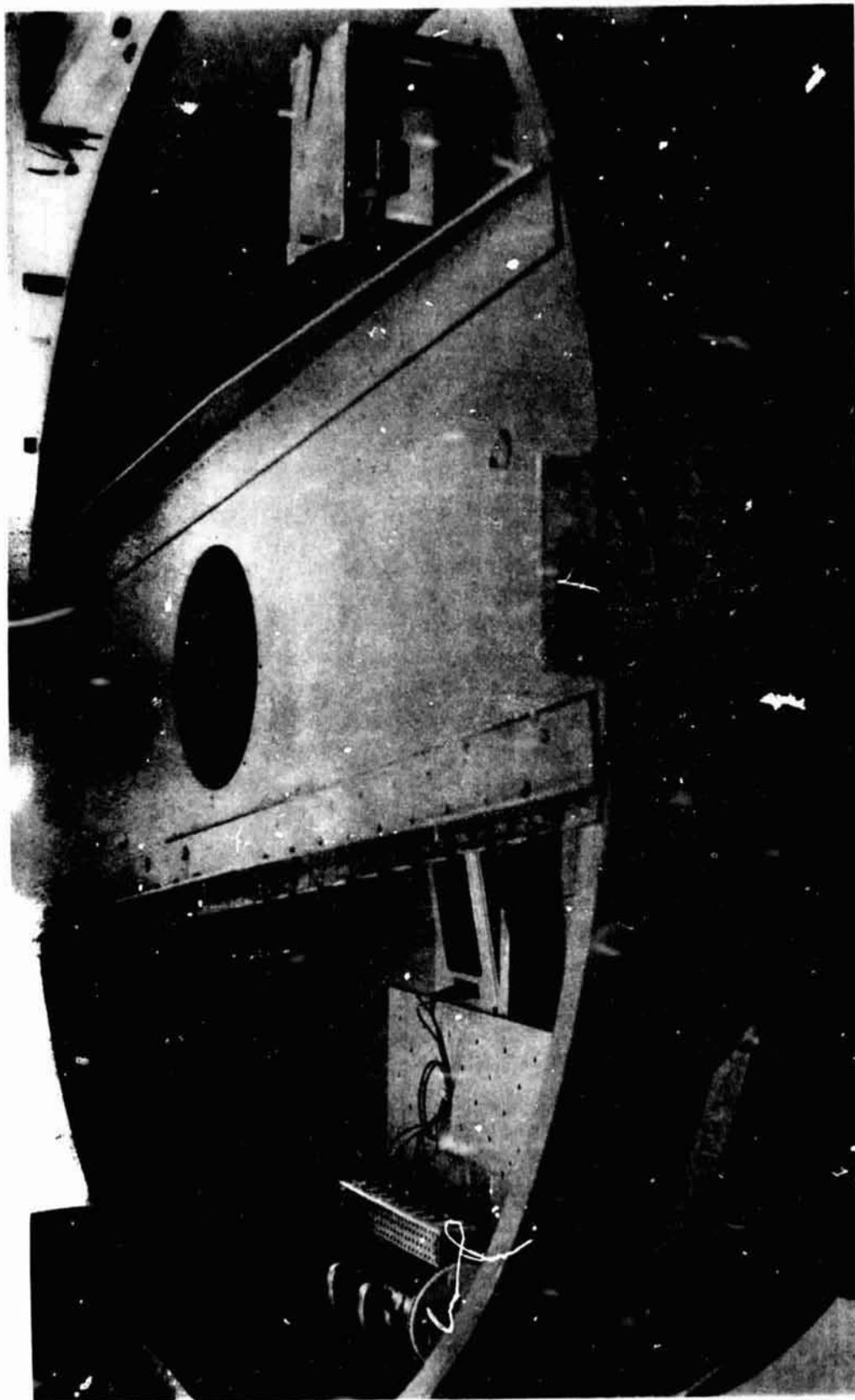
Fig. 2. Furnace mounted on centrifuge arm. Counter balance cylinder could be moved both up and out to minimize vibrational acceleration to below .005 g.

Pyrex tube, 2.2 cm ID by 40 cm long, containing about 2 gm of 99.999% pure cadmium in an atmosphere of (initially) 99.9999% pure argon at a pressure of about two-thirds of an atmosphere. The tube was placed inside a Marshall furnace with a 6 in. cold zone, maintained at approximately 290°C, and a 6 in. hot zone, maintained at approximately 390°C. The two zones were separated by a 4 in. stainless steel divider. The furnace was mounted on a centrifuge arm as shown in Fig. 2. The furnace had only negligible vibrations of about 0.002 "g" in the radial direction, 0.01 "g" in the tangential direction, and 0.003 "g" vertically as measured with a Statham instrument accelerometer.

In measuring the pure effect of increased gravity, all other parameters such as argon pressure, Pyrex surface condition, Cd source mass, and trace impurities must be held fixed. This may be done by reverse distillation of the Cd growth back to its original side of the tube, thus allowing reuse of the same tube without changing the above parameters. The drawback, of course, is that the whiskers must be evaluated and photographed before reverse distillation, leaving no permanent growth for later study.

Due to different heat transfer rates of the various centrifuge furnace velocities through air, extra care was needed. For example, at 20 g the furnace velocity is 20 m/sec and if this had caused preferential cooling on one end of the furnace so as to alter the temperature gradient, our results would have been rendered worthless. Thus, each half of the furnace contained a heavy aluminum cylinder 2-1/2" OD by 1" ID by 6" long to maintain near isothermal conditions on each half of the growth tube. In addition, two independent temperature regulators were necessary to hold the temperature of each half

Fig 3. The amount of vapor transported along growth tube as a function of the centrifuge acceleration. This shows the strong effect of convection.

143
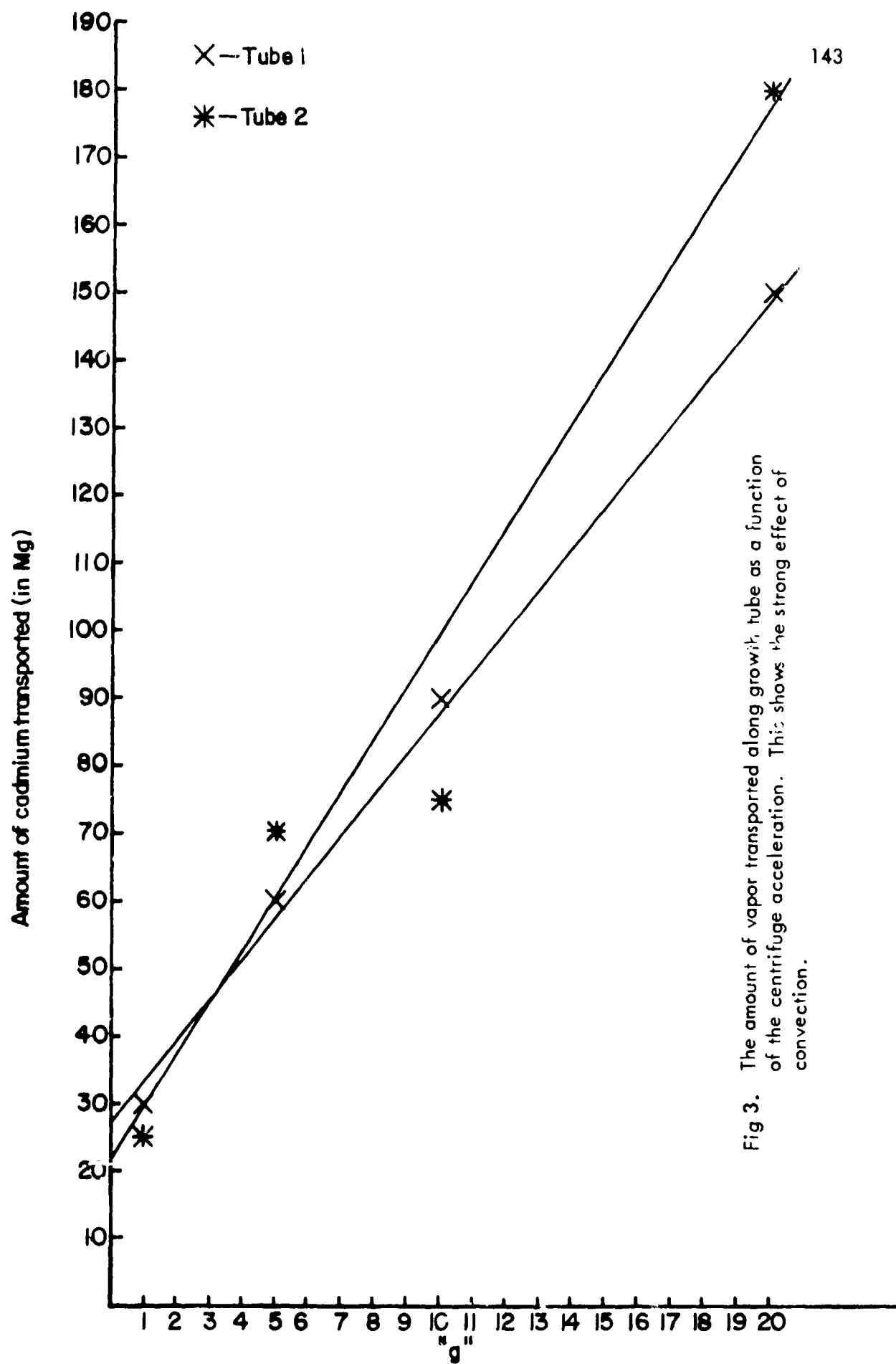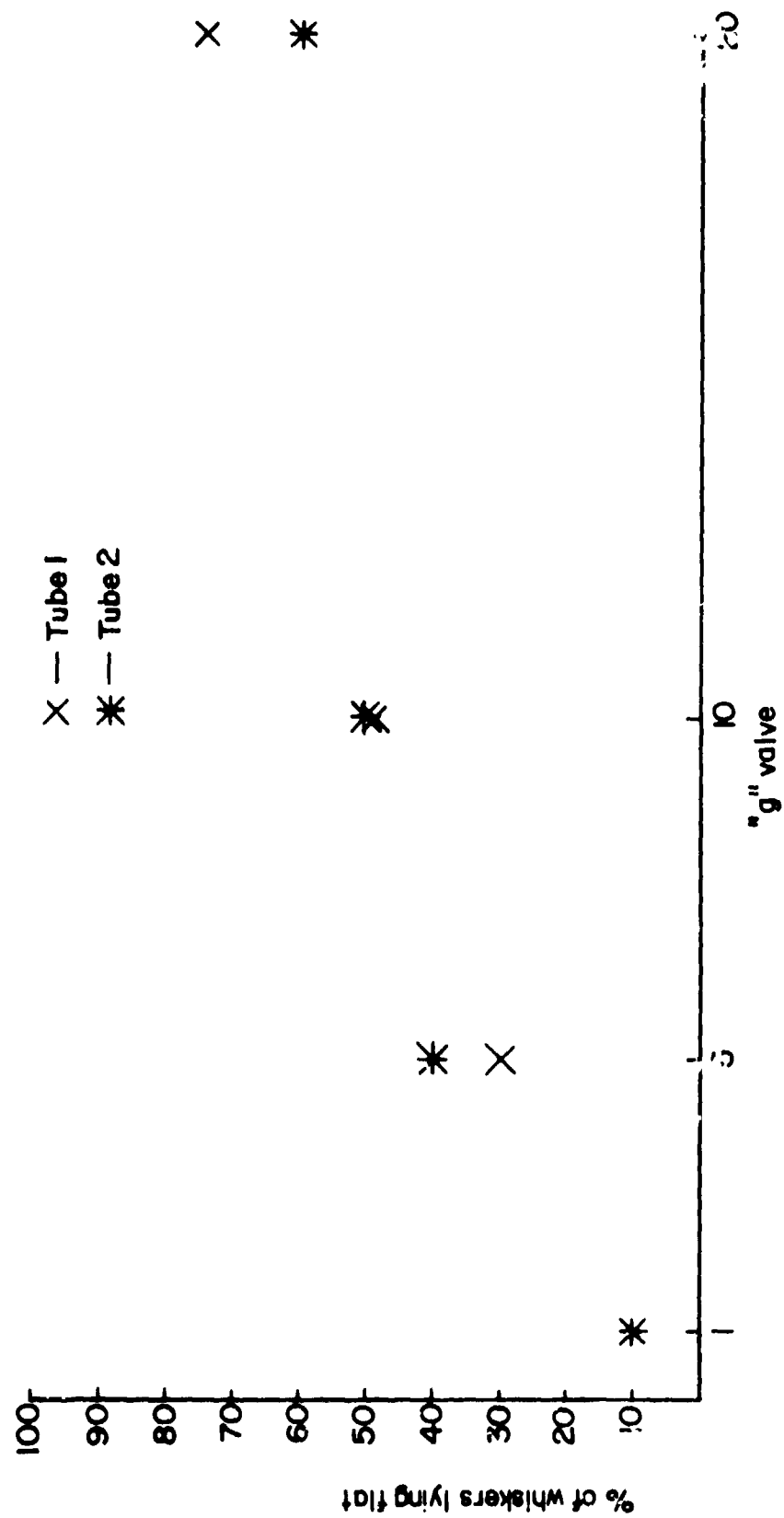
Fig 4. The percentage of whiskers lying flat increased greatly with in-
creased acceleration.

Table I

"g" Value	Time Grown	*Amt. of Cd Transported	% of Platelets	% of Whiskers	% of Dots	% of Whiskers Lying Flat	Length / Thickenss. Maximum
TUBE 1							
1	5:05	30 Mg	60	30	10	10	530
5	5:05	60 Mg	30	30	40	30	1300
10	5:10	90 Mg	9	1	90	50	300
20	4:55	150 Mg	30	20	50	75	600
TUBE 2							
1	5:05	25 Mg	75	20	5	10	400
5	5:05	70 Mg	40	30	30	40	375
10	5:10	75 Mg	40	40	20	50	1300
20	4:50	180 Mg	60	20	20	60	750

* Estimate

of the furnace constant at the various rotation speeds used. A dual pen recorder monitored the temperature of each half of the furnace and revealed, upon starting the centrifuge, a transient 15° temperature oscillation which decayed away after a few cycles (about 15 minutes). The effect of this transient was judged to be negligible considering that the total growth time was five hours.

As shown in Fig. 3, the amount of transported material increased linearly with the increasing "g" force. The percentage of whiskers lying flat increased from 10% for both tubes at 1 "g" to 75% and 60% for tube 1 and tube 2, respectively, at 20 "g's" each as seen in the graph in Fig. 4.

It should be noted in Table 1 that the two tubes sometimes behaved very differently. Apparently the argon pressure and the amount of cadmium in the tube have a very large effect on the tube's growth, so much so that we used the same tube by reverse distillation for a complete series of experiments.

The graph in Fig. 3 strongly and clearly demonstrates the effect of increased gravity on the quantity of transported material for crystal growth. Such an effect had been predicted theroretically but to my knowledge had not had experimental conforma-tion. The material transport increased about a factor of 10 with increasing gravity indi-cating that gravitational effects should not be neglected in similar situations involving a fluid in a temperature gradient.

The graph in Fig. 4 clearly confirms the detrimental effect of gravity on growing whiskers. With increasing "g" values, five times more whiskers fall onto the substrate, where growth is inhibited or distorted. The falling is either a direct result of gravity or is due to fluid drag from convection which is further discussed in Section II.C.

This clearly points toward a zero-gravity environment as being ideal for whisker crystal growth. This (1 to 20 g) experiment must be labeled as crude since most of the observational data were taken on the most visible (larger) whiskers and while the high aspect ratio (long, thin) whiskers are the most useful, but also the most susceptible to gravity bending and entanglement with other whiskers and the substrate. Later experiments should incorporate rectangular (instead of cylindrical) growth tubes for better microscope focusing on the important smaller whiskers.

C. GRAVITATIONALLY INDUCED CONVECTIVE FLUID DRAG FORCE IS SOMETIMES 1000X GREATER THAN THE DIRECT GRAVITY FORCE ON A WHISKER

In studying the gravitational effect on whisker growth, it is important to be able to account for other forces which may be equally as important as gravity. For example, if whiskers are grown in earth orbit, we surely want to keep the random vibration acceleration less than 1 g. We also know it would be useless to do an experiment in orbit if the fluid drag force on the whiskers is of the order of 1 g. With this in mind, we will do some calculations to determine the force on a whisker due to air motion.

For simplicity, a uniform fluid flow was assumed without considering the zero velocity boundary layer at the wall which would shield a whisker lying almost flat against a substrate.

B. E. Lamb[4] derives on the following equation for the force on a long, thin cylinder which includes the gas viscosity. This equation has been verified experimentally by Wieselsberger (Phys. Zeitschr. 1921, p. 321).

$$\frac{F}{L} = \frac{4\pi\mu V}{\frac{1}{2} - \gamma - \log\frac{Va}{4\nu}} \tag{1}$$

where F/L is the fluid force per unit length on the cylinder.

V = fluid velocity

a = rod radius

γ = Euler constant = 0.577

ν = Kinematic air viscosity = $160 \times 10^{-8} \, ft^2/sec$

μ = Air viscosity = $0.362 \times 10^{-6} \, lbs - sec/ft^2$ (at one atmosphere pressure)

for a whisker of 1 μ diameter if V is about 1 cm/sec

$$\frac{F}{L} = 1.6 \times 10^{-7} \, gr \times V \tag{2}$$

if V = 1 cm/sec, then the force is twice the force of gravity (for tin).

In order to compare gravitational forces to fluid forces, we have plotted the graph shown in Fig. 5. Since the fluid (air) drag depends both on velocity and whisker diameter, we have plotted effective gravitational force (that is, whisker force divided by mass of the whisker) as a function of air velocity. Each curve represents a whisker of different diameter. As the whisker diameter becomes smaller, the fluid forces become much more significant than the direct gravity force. The near linearity results from the log term in Equ. 1 being relatively constant.

Conclusion: From the graph we see that even the expected 1 cm/sec velocity associated with convection will cause a force 300 times stronger than the direct gravitational forces if the whisker's diameter is 0.1 μ.

Thus, in summary, gravity may adversely affect whiskers not only by a directly

bending force,[1] and by convective disturbance of the supersaturation ratio and the

growth process, but now we see that the gravity-driven convection will also cause a

destructive fluid drag force which may be several orders of magnitude longer than

direct gravity forces. This zero-convective drag makes zero-g even more enticing

for whisker growth. These fluid and direct-g forces are destructive in the sense that

they might: (a) break the growing whisker from the substrate at its weakest point,

the nucleation point, (b) bend the whisker so that the tip touches the substrate, stopping

growth, and (c) bend two whiskers so that they touch, grow and "weld" together.

Long Ultrathin Whiskers (A New Frontier)

A whole new domain of scientific advancement could result from growth of an

ultrathin ($\sim$ 10 Å), but long (1 mm) whisker which could carry a current. Such a

whisker would (a) serve to check one dimensional solid state theories, (b) serve to

measure the surface scattering of electrons, (c) have (according to theory) a super-

conducting transition temperature due to an increased density of states, (d) exhibit an

order of magnitude greater superconducting fluctuation effects which would help to

settle questions on the basic theory of superconductivity, and (e) be wound for a

small memory storage coil with 160 turns and a 1 μ diameter.

By extrapolating the graph in Fig. 5 one finds that an air velocity of only 1 cm/sec

exerts a force 100,000 times greater than the direct force of gravity on a 10 Å diameter

whisker. Such a fluid force due to convection could be responsible for the absence of

10 Å whiskers in the literature. Repeating the whisker growth experiments in zero

gravity would greatly increase the chances of finding such 10 Å whiskers.

The problem of "in orbit" detection and diameter measurement of these invisible fibers could be handled electronically by use of a high impedance electrode would be shorted by the growing whisker. Each time a whisker shorts an electrode the current could be increased until the whisker melts at $I = I_{max}$. This forms both a record of the number of whiskers and of their diameters. Since each detected whisker is melted the electrode would be automatically reenergized for detection of the next whisker.

D. EVIDENCE FOR POSSIBLE GRAVITATIONAL EFFECT ON WHISKER ORIENTA-TION

The following is a quote from the thesis of Mr. Charles Lee Watlington, entitled "The Effect of Boundary Scattering on the Superconducting Transition Temperature of Tin Whiskers," Clemson University, 1970.

> "It appears possible to select a whisker of a given (crystallographic) orientation. Selecting whiskers which stood straight on the growing surface usually resulted in either a ⟨001⟩ or a ⟨100⟩ orientation. On the other hand, selecting whiskers which were elastically bent by gravity, almost all ⟨001⟩ whiskers were obtained. This did not hold for very small whiskers which would not stand by themselves in any case."

Several possible explanations are offered here:

1. ⟨101⟩ whiskers may be ribbon shaped and thus bend easier in one direction.

2. The elasticity tensor for tin may be such that bending in the ⟨101⟩ direction is easiest.

3. Gravity may directly affect the whisker orientation, i.e., strain at the whisker base due to gravity may make ⟨101⟩ growth preferable to other orienta-tions.

FROM HYDRODYNAMIC EQUATION
FOR AIR DRAG ON A LONG THIN CYLINDRICAL
ROD AS A FUNCTION OF AIR VELOCITY AND THE
AND ROD DIAMETER
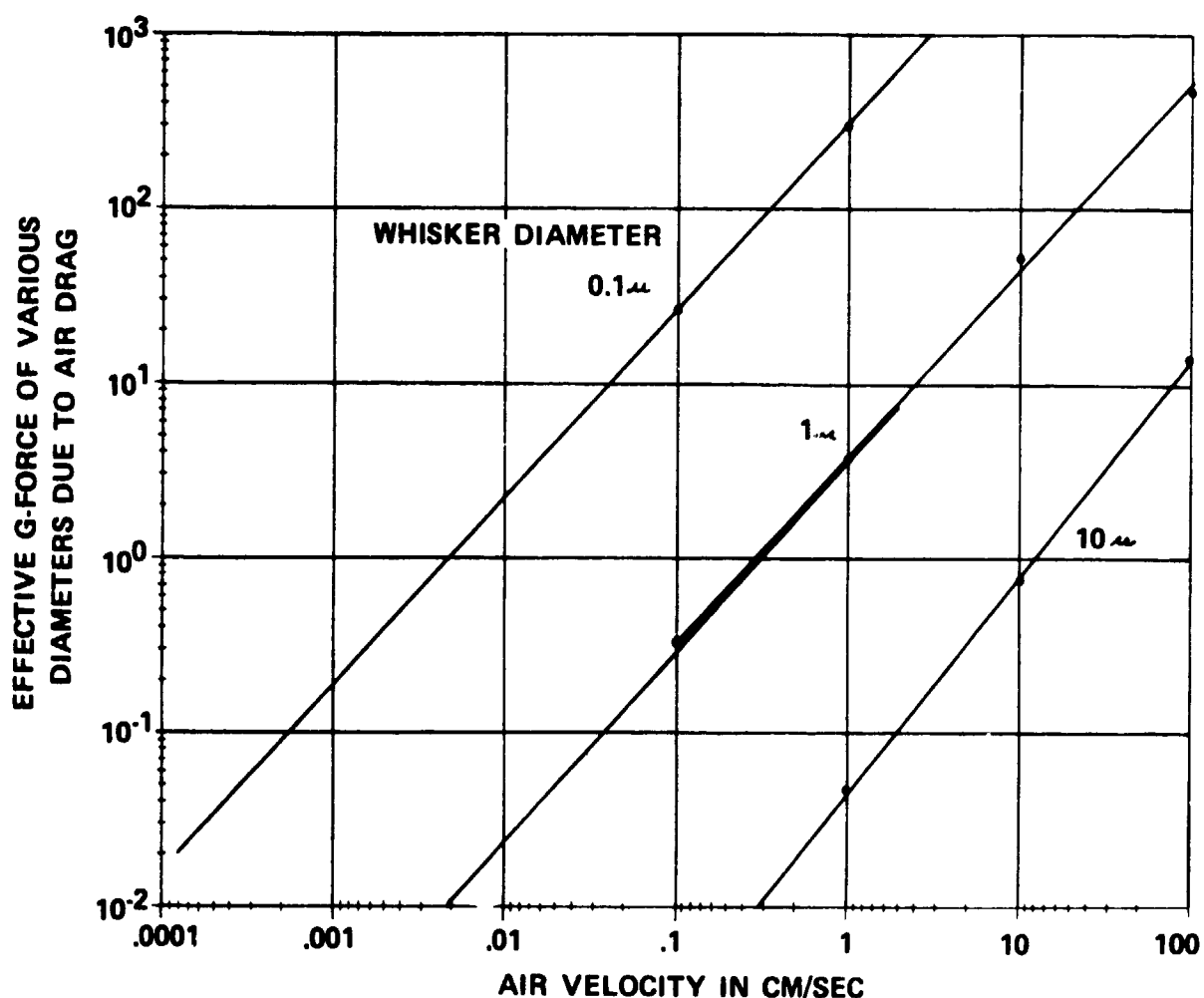
Fig. 5. This curve shows the relative magnitude of hydrodynamic drag forces to
gravitational forces on long thin rods (whiskers). This effective force
is plotted as a function of air velocity for various diameter whiskers.
Note that at 10 cm/sec the drag force on a .1μ diameter whisker is
several thousand times the gravitational force.

.E. ZERO GRAVITY MAY PRODUCE WHISKERS BY EXOTHERMIC CHEMICAL
REACTION WHICH WOULD NOT GROW IN ONE-G

It is within the realm of possibility that convective flow induced by gravity
could have an adverse effect on whisker growth by chemical reaction. Consider the
following situation: The two gases are being heated together H_2 + MCl to form HCl
and whiskers of the metal M. M could be any metal, copper for example. Suppose
this reaction is exothermic and the reaction rate increases with temperature. Heat
is generated at the growing whisker tip which increases the temperature and thus, the
reaction rate. The situation then is highly unstable, like lighting a match in a room
filled with oxygen and hydrogen. At the hot whisker tip, convective currents flow
to replenish the supply of MCl near the whisker as pictured in Fig. 6. This could
result in an oversaturation which could result in polycrystal instead of single crystal
growth.

Whisker growth requires a slow, well-regulated reaction and the above reaction
has no self-regulating features in a g field. However, in zero gravity, the hot
whisker tip would generate no convection and then the reaction could proceed
no faster than the MCl could diffuse through the H_2 gas. This regulation may
allow whisker growth in a zero g environment which would otherwise be impossible.
As convection stops, its cooling effect is reduced and the whisker tip may be ex-
pected to heat, increasing the reaction rate. However, the reactant density re-
duction should slow the reaction in spite of the higher temperature whisker tip. The
candle flame is extinguished as "g" approaches zero for the same reason.

WHISKER GROWTH BY CHEM. REACTION

$2 CuF + H_2 = 2Cu - 2HF + Heat$
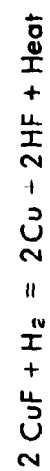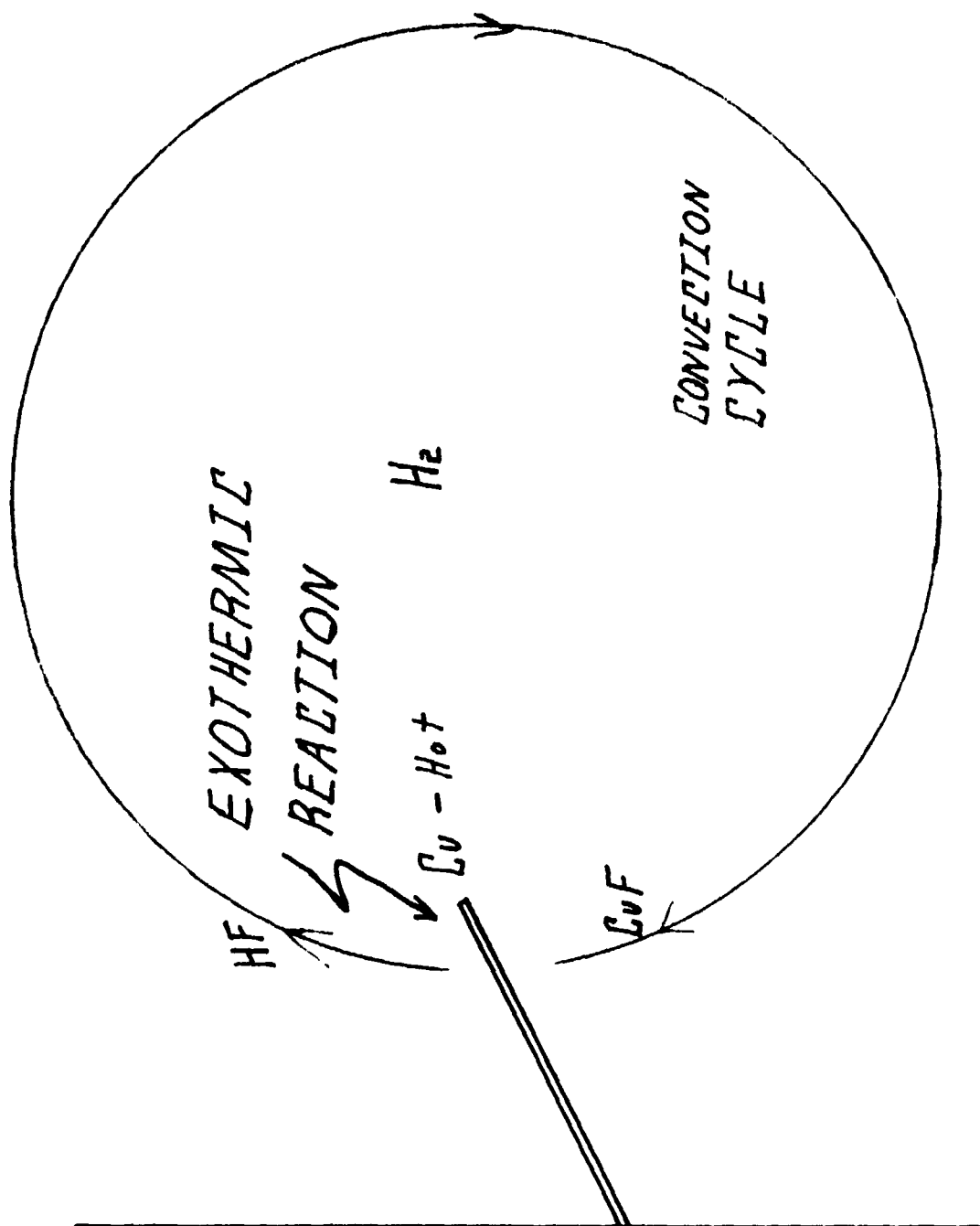
Fig. 6. The above reaction is probably unstable since it produces heat which
further increases the reaction rate by producing convection cycles.

In searching through literature, some experimental evidence has been uncovered which lends support. Consider this reaction:

$$2MCl + H_2 + Energy = 2M + 2HCl.$$

If the energy supplied is positive, the reaction is endothermic; if energy is negative, the reaction is exothermic. According to Brenner,[6] whiskers grow by this reaction if chlorides, bromides, or iodides are used; however, whiskers do not grow if the fluoride is used. It is very interesting to note that all the reactions are endothermic except the fluoride. This may be only a coincidence; however, it does directly support our hypothesis that whisker growth is suppressed in an exothermic chemical reaction, possibly due to convection.

A suggestion then would be to attempt whisker growth from the reaction

$$H_2 + 2CuF = 2Cu + 2HF$$
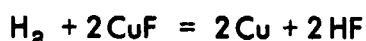
in a zero gravity environment.

If such a whisker would grow in zero gravity but not in one gravity, then a whole new class of exothermic whisker growth reactions would probably become possible.

One may argue against the above statement by saying that all whisker growth by the pure vapor deposition process (no chemical reaction) is grown by an exothermic process. But vapor growth rate is automatically lowered and self-regulated as the whisker becomes too hot; whereas in a chemical reaction, the growth rate increases with temperature and is unregulated. Therefore, we need only be concerned with exothermic chemical reaction interfering with whisker growth.

References (Part II)

1. Interim Report #1, NASA Contract No. NAS8-24612, June 1970.

2. A. P. Levitt, Whisker Technology, Wiley-Interscience, N.Y. (1970).

3. T. Garbor and J. M. Blocher, J. Appl. Phys. $\underline{40}$, 2696 (1970).

4. B. E. Lamb, Hydrodynamics, Dover, N.Y. (1945).

5. S. S. Brenner, Acta. Met. $\underline{4}$, 62 (1956).

III. DISCOVERY OF A NEW TYPE VACUUM GAUGE USING BROWNIAN MOTION IN ZERO GRAVITY

This investigation into Brownian motion in zero gravity at low pressures was prompted by the realization that our existing high-vacuum measurement techniques are not as accurate nor as simple as one would wish. Often times, it is necessary to break into and thereby contaminate a sealed container in order to measure the pressure inside. This procedure always results in a great disturbance and contamination of the gas. Our calculations and ideas are aimed at relieving this inadequacy by providing a built-in pressure gauge for any sealed container, and employing only the principles of Brownian motion as the apparatus by which we measure the pressure. This procedure would certainly reduce the cost and disturbance of a hot gauge.

The idea most basic to our calculations was that the behavior of a Brownian particle is similar to that of an ideal gas molecule. At a lower pressure, it would be assumed that the particle experienced fewer collisions. With this in mind, we first turned to Einstein's equation.[1]

$$\overline{S^a} = \frac{2 k T_t}{f} \tag{1}$$

Where $\overline{S^a}$ is the average of the square of the distance traveled, k is Boltzman's constant, T is temperature and t is time. The parameter f, given by $F_d = f V_p$, is a drag, due to the Doppler-type collisions of molecules on a Brownian particle. F_d is the drag force, and V_f is the particle velocity. Using an elemental microscopic approach to the momentum changes experienced by the particle due to the number of elastic collisions per unit time, and substituting in the ideal gas equation, we find the drag to be

$$f = \frac{2}{3} d^2 \, n \sqrt{M_m kT} \tag{2}$$

where d^2 is the cross-sectional area of the particle, n is the number of molecules per unit volume, and M_m is the mass of the gas molecule. Substitution into the Einstein equation predicts the Brownian (average diffusion distance) to be

$$\overline{S^2} = \frac{3 \sqrt{\dfrac{kT}{M_m}}}{d^2 n} \, t . \tag{3}$$

Using $PV = nkT$, the equation becomes

$$\overline{S^2} = \frac{3 \, t \, (kT)^{\frac{3}{2}}}{P d^2 (M_m)^{\frac{1}{2}}} \tag{4}$$

But this equation is based on the assumption that $t \gg \dfrac{M_m}{f}$, which is quite difficult to achieve. However, Uhlenbeck and Orenstein[2] had derived the general form of this equation, which is

$$\overline{S^2} \approx \frac{2mkT}{f^2} \left(\frac{ft}{m} - 1 + e^{-\frac{ft}{m}} \right), \tag{5}$$

which we substituted into to obtain

$$\overline{S^2} = \frac{9 \rho (kT)^2}{2 d P^2 M_m} \left[\frac{2 \, Pt (M_m)^{\frac{1}{2}}}{3 \rho d (kT)^{\frac{1}{2}}} - 1 + e^{\frac{-2Pt (M_m)^{\frac{1}{2}}}{3 \rho d (kT)^{\frac{1}{2}}}} \right] \tag{6}$$

where

ρ = density of the Brownian particle.

We gave some optimum values to some of the parameters – $T = 300^\circ K$, $\rho = .1 \, g/cm^3$,

M_m = Atomic mass of X_e, and d ranged from 10^{-6} to 10^{-3}, with $t = .1, 1,$ and 10 sec. Pressure was graduated in decades from 100 to 10^{-8} torr. All these values were treated as constants in plotting the Figs. 1, 2, and 3. Figs. 1, 2, and 3 are calculator-driven X-Y recorder plots of equation (6) of rms Brownian particle displacement as a function of gas pressure.

The flat portion on the upper left of the graphs represents the region where the distance traveled per unit time is constant at any lower pressure, and the particle travels as if it were virtually free of collisions. The sloping part of the graph represents the only range of useful information in pressure determination. Please neglect the small slope changes around 10^{-8} to 10^{-7} torr; they were due to the calculator's limited range. The curves should all be flat below 10^{-6} torr.

Equation 2 begins to fail with rising pressure as the mean free path of the molecule approaches the particle diameter (d). This region is shown by dashed lines in the graphs in Figs. 1, 2 and 3. However, at even higher pressures (Stokes law holds and S becomes independent of pressure) the curve again becomes flat and the gauge useless as depicted by the dashed line in the d = 10^{-3} cm curve on Fig. 2.

The maximum useful range extends from 10^{-5} to 10 torr under the ideal conditions. The heavy X_e gas was used to enhance the effect since the gauge is less sensitive to lighter elements such as hydrogen.

The best curves are with d = 10^{-6} cm, but the particle velocity is fairly large for optical microscope detection so d = 10^{-3} could be used with some reduction of useful pressure range.

Measuring the diffusion distance (S) at the end of each second would be experimentally easy. One could set up a movie camera to photograph the position of the particle at 1 second intervals. From 11 photos 10 values of $\overline{S^2}$ could be measured and plugged into Fig. 2 to determine the pressure.

How much spread should be observed in the above 10 numbers? Three of the numbers will be (on average) greater than the standard deviation. The standard deviation is also equal to $\sqrt{\overline{S^2}}$, according to Uhlenbeck and Ornstein's Eq. 7. In other words, if only one value of $\sqrt{\overline{S^2}}$ were measured, there would be a one-third chance of having an error greater than a factor of 2 in the resulting pressure. The probable error of the mean would be greatly reduced as more data are averaged together.

The question is how many observations of $(\overline{S^2})^{\frac{1}{2}}$ would be needed to generate a reasonable accuracy in the pressure. From statistical sampling theory, a theorem (P. G. Hoel, Introduction to Mathematical Statistics)[a] states that:

> If x is normally distributed with mean μ and standard deviation σ and a random sample of size n is drawn, then the sample mean $\bar{x}$ will be normally distributed with mean μ and standard deviation $\dfrac{\sigma}{n^{\frac{1}{2}}}$

This means that if 100 values of $(S^2)^{\frac{1}{2}}$ are measured, that there will be a one-third probability of having an error greater than 10%. If only 10 measurements are made, there will be a one-third probability of having an error greater than 30%. If this method were used for calibration purposes, a large number of measurements would be needed. However, many times, knowing only the order of magnitude of the pressure is necessary.

In which case, two or three readings would be sufficient. Most vacuum gauges have a limit of accuracy, but the accuracy of this method may be improved by taking more data rather than buying a new gauge. Of course, this method is no more accurate than the data and parameters which go into the pressure equation.

Improvements in technology could further enhance the effectiveness of the BMVG. For example, if the particle density could be reduced by a factor of 1000 by using hollow bubbles, the gauge range could be extended several orders of magnitude. By using an optical particle tracking the gauge range could also be extended by several orders of magnitude.

By counteracting gravity with electrostatic or magnetic suspension the gauge could be used in a 1-g field.

In conclusion, the zero gravity Brownian motion vacuum gauge offers a new approach to the old problem of measuring pressure. As with other vacuum gauges its range covers, at best, up to five orders of magnitude pressure variation. Since only one-man month of effort has been expended on this gauge, it is felt that we have only "scratched the surface" as far as refinement of the gauge goes. However, our purpose here is only to identify (and not to refine) possible zero gravity experiments.

Actually this Brownian movement vacuum gauge (BMVG) will be classified as a friction gauge along with the rotating cylinder and vibrating reed gauges. They all monitor viscosity which is pressure dependent as described in a good review article by H. W. Darwin.[4]

DISTANCE TRAVELED BY A
BROWNIAN PARTICLE
vs.
PRESSURE OF GAS (Xe).
(Log Scale)

t = .1 sec.

d = 10⁵

d = 10⁷

d = 10³

d = 10⁻²

Fig. 1.
d is in cm

PRESSURE (Torr)

161

DISTANCE TRAVELED BY A
BROWNIAN PARTICLE
vs.
PRESSURE OF GAS (Xe).
(Log Scale)

t = 1 sec.

d = 10⁵

d = 10⁰

d = 10⁰

Fig. 2.
d is in cm

d = 10⁻²

$\sqrt{\overline{S^2}}$ (cm.)

PRESSURE (Torr)

162

Fig. 3.
d is in cm

DISTANCE TRAVELED BY A
BROWNIAN PARTICLE
vs.
PRESSURE OF GAS (Xe).
(Log Scale)

t = 10 sec.

163
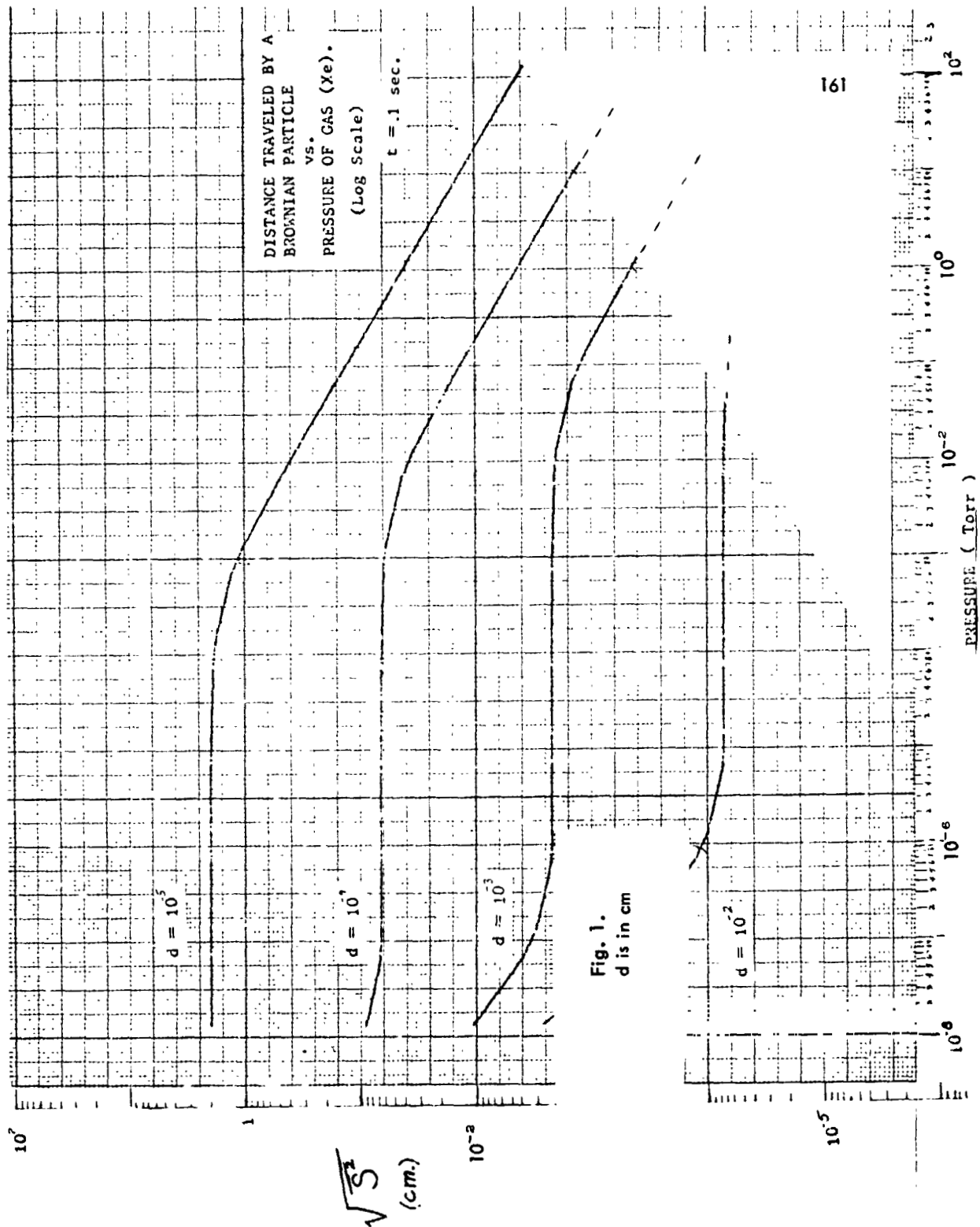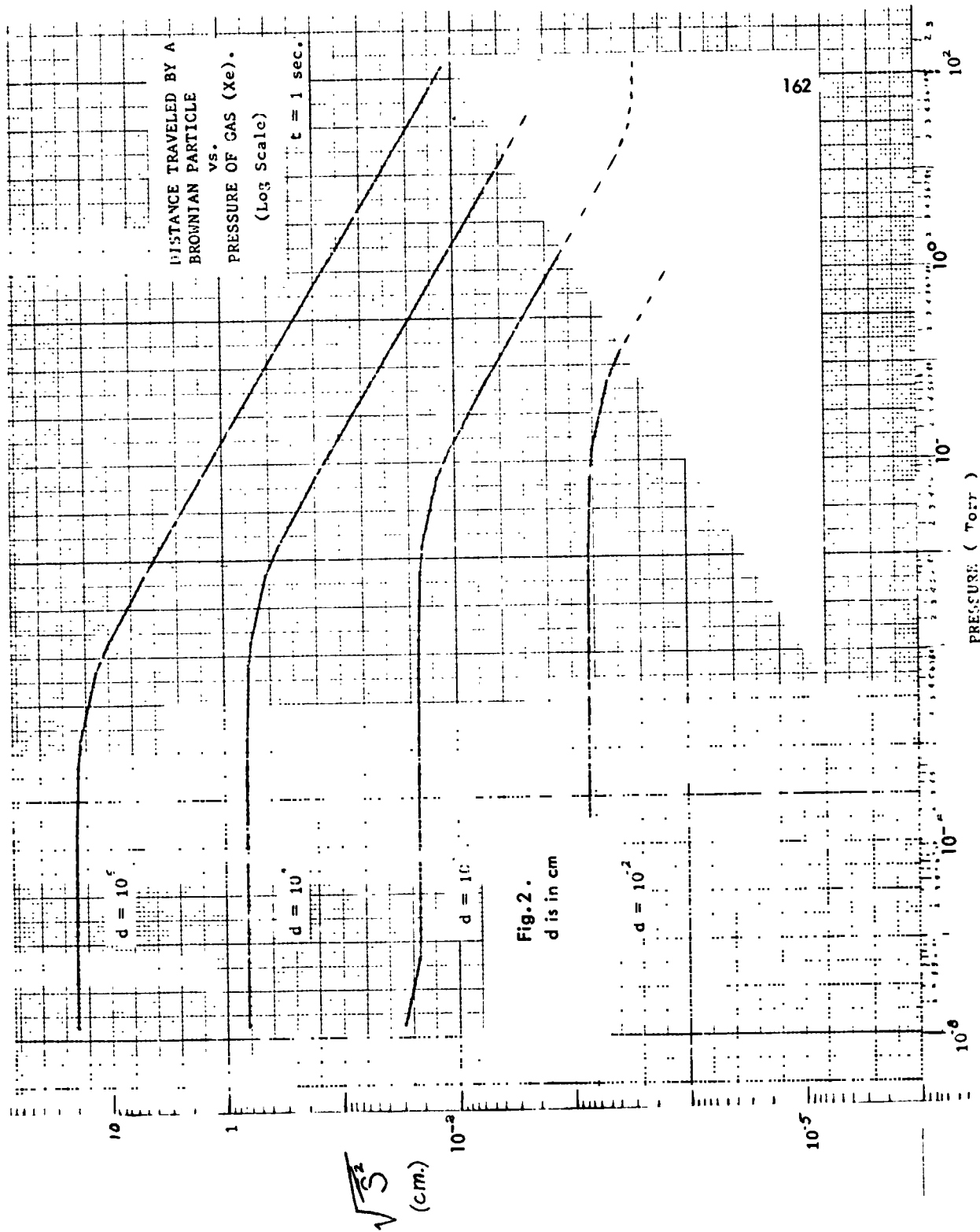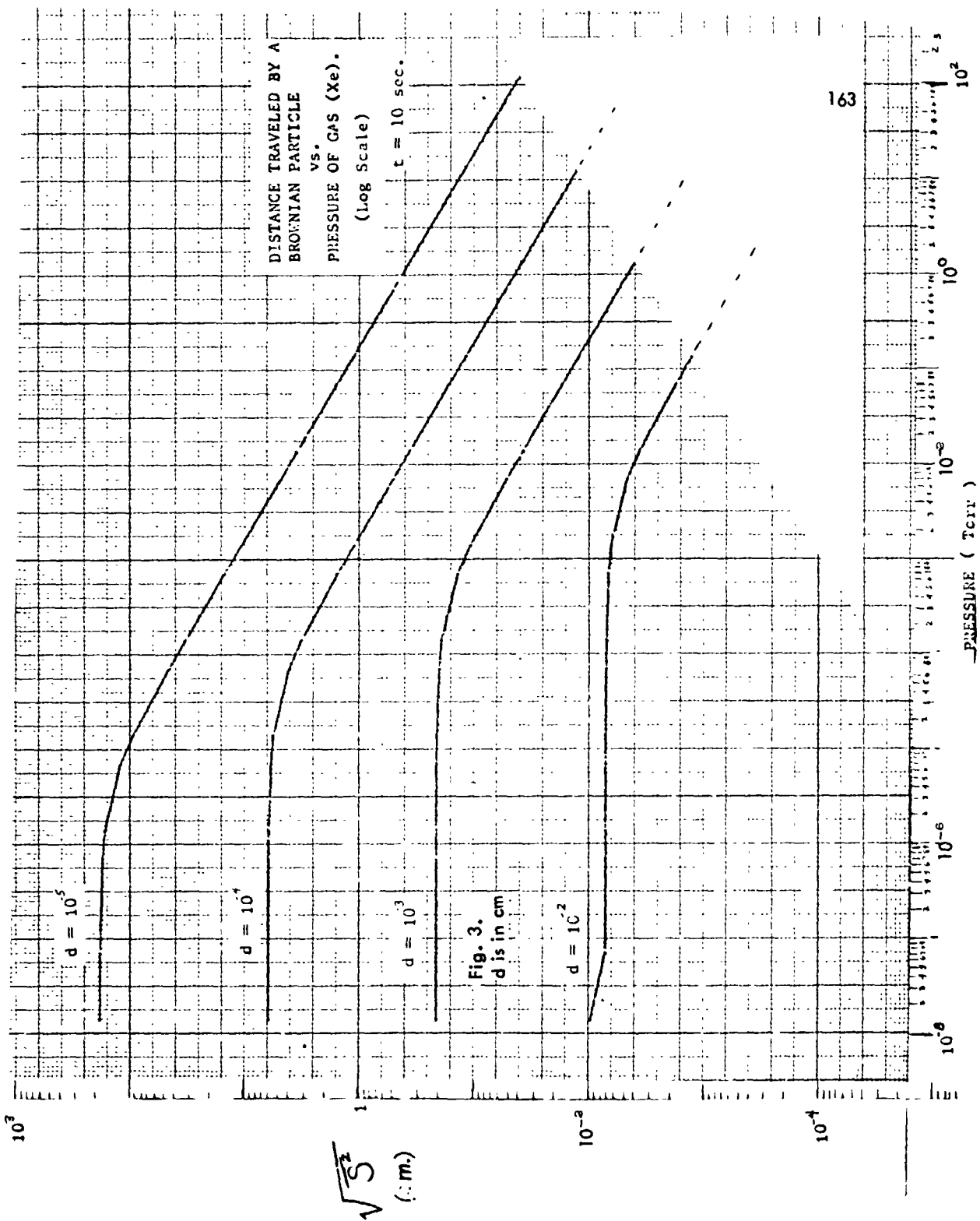
Although literature has been searched under the Brownian Movement heading, searching the field of aerosol diffusion should be more fruitful and current. For example, the paper on "Theory of Drag on Neutral or Charged Spheroid Aerosol Particles"[5] should prove quite useful for further work in this area.

James Gordon III, a student lab assistant, generated Figs. 1, 2, and 3 on a Hewlett Packard Model 9100-B calculator.

References (Part III)

1. A. Einstein, "Investigation of the Theory of Brownian Movement," Dutton, N.Y.

2. G. E. Uhlenbeck and L. S. Omstein, Phys. Rev., 36 (11930) 823.

3. P. G. Hoel, Introduction to Mathematical Statistics, 2nd Ed., 1954 Wiley.

4. H. W. Darwin, Vacuum, V. 15, No. 3, p. 99.

5. B. U. Anms, A. P. Malinauskas, and E. A. Mason, Aerosol Science, V. 3, p. 55.

IV.I.   FINAL TECHNICAL REPORT FOR

                  PART D OF CONTRACT NAS8-26793

Subject: High Frequency Characterization (HFC) of GaAs

Period Covered: March thru September 1972

Professional Staff: J. G. Castle, Jr., Professor of Physics, UAH and
                                        Principal Investigator

                    R. R. Lattanzi, Research Engineer, UAH

                    P. T. Huang, Graduate Student, UAH

Contents of Report on HFC:

PART IV: HIGH FREQUENCY CHARACTERIZATION OF GaAs

A. <u>ABSTRACT</u>

The potential role of high frequencies in characterizing the uniformity of thin layers at the surface of semiconductor crystals without the use of electrical contacts is emphasized. Progress is reported in the development of techniques satisfactory for high frequency measurements of two parameters, surface resistance and surface Hall coefficient, of GaAs crystals similar to those crystals to be used in M-555 Flight Experiment. A non-resonant reflectance bridge operated at 35 GHz yielded values of GaAs resistivity in the undisturbed surface layer (circa 100 μ m thick) that were averages over only a few square millimeters of the GaAs surface and were reproducible to within approximately 5%; when greater precision in the surface map is needed, microwave bridge and cavity techniques are available for adaptation. For the surface Hall coefficient at the same frequency (and, therefore to the same depth) several bimodal cavities were designed. One cavity was constructed of brass, preliminary tests of which show 27 db isolation between the two modes at zero external magnetic field, and indicate thereby that successful surface Hall measurements should be attained after tuning controls are added.

B. SCOPE

The scope was chosen to answer the need of NASA/MSFC Space Sciences Laboratory for means by which to characterize the electrical properties of resistivity and Hall coefficient in the surface regions of semiconducting crystals to be grown in flight experiments but without attaching electrical contacts to the semiconductor. Satisfactory characterization of a flat semiconductor surface requires mapping the uniformity of the resistivity and Hall coefficient without electrical contacts. A precision of 5 to 10% is expected to be sufficient for evaluating the effects of microgravity on the planned growth of GaAs epitaxial layers and the GaAs self-nucleated crystals expected in M555 Flight Experiment. Commercial high frequency techniques are not available but state-of-the-art laboratory microwave techniques are expected to be sufficient in answering this need for high frequency characterization (HFC). Therefore, the goals of this seven month study of HFC were:

Aim 1: to demonstrate the precision available in and to begin the study of the reliability of contactless surface resistance measurements of flat undoped GaAs surfaces at 35 GHz at room temperature. The aim was to map the surface with a resolution of a few square millimeters. The choice of 35 GHz was dictated by the desire to sample the thickness expected of the GaAs epilayers on M555.

Aim 2: to demonstrate the feasibility of adapting the microwave rotation measurements reported at lower microwave frequencies to the service of mapping surface Hall coefficient of the same GaAs surfaces without the need for contacts.

Aim 3: To consult with the SSL staff on their crystal growth program and to begin the use of HFC in their program on GaAs growth and surface preparation.

C. THEORETICAL BACKGROUND

A. Surface Resistance of GaAs

The relaxation time τ of the principal carriers is very short in n-type un-doped GaAs. Therefore, the products of τ with the angular frequency and with the cyclotron frequency of these GaAs carriers are both much smaller than 1. So the complex tensor conductivity is approximately the DC conductivity σ_0 and the high frequency skin depth $\frac{1}{\beta}$ will be effectively the classical skin depth δ. So,

$$\frac{1}{\beta} \approx \delta_0 = c/(2\pi\omega\sigma_0)^{\frac{1}{2}}$$

Typical values of δ_0 are 100 μm at 35 GHz in GaAs. If the quality of the GaAs epilayers can be markedly improved to the extent of longer relaxation times for the carriers, then deviations from this classical relation would be expected. But then several other interesting characterization measurements would become feasible, and should lead to valuable quality mapping of such features as carrier mass and electronic scattering time itself.

B. Surface Hall Effect in GaAs at High Frequency

Consider the contactless measurement of the high frequency Hall coefficient for the surface region of a flat GaAs sample in a square, bimodal TE112 cavity, resonant at 35 GHz. The pattern of microwave current induced in the surface of the square end wall of the cavity is parallel lines as shown in the figure.

current

H field
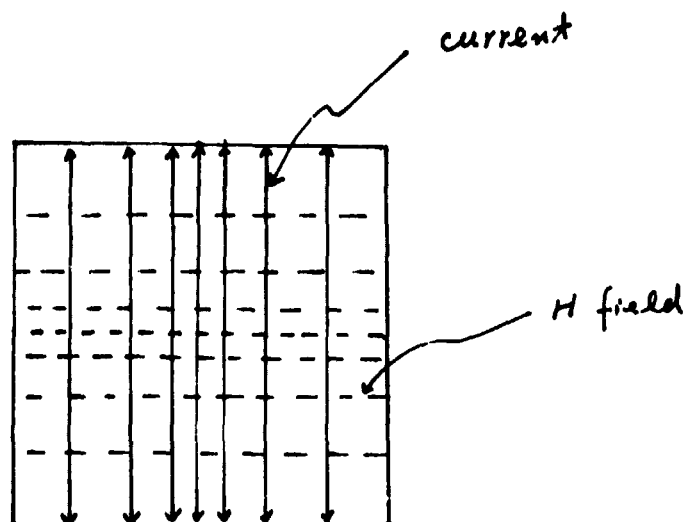
If we make a hole whose area is about 10% of the area of the cavity bottom at its center, and a flat GaAs sample is mounted over the hole with adequate choke joints but without diffused electrical contacts, then the rf induced current J_x flows across the exposed surface of the GaAs sample. When we switch on a steady magnetic field perpendicular to the GaAs surface, the surface current is deflected by the Hall angle, generating a transverse "Hall current" which transfers stored energy to the orthogonal cavity mode.

Under the condition that the mean free path of the carriers, ℓ, is much less than the skin depth δ Maxwell's equations and the equations of motion of the carriers on the Drude-Zener model gives the following quantities:

1. Tensor conductivity,

$$(\sigma_{xx})_{real} = \frac{\sigma_0}{\langle \tau \rangle} \left\langle \frac{\tau(1 + (\omega\tau)^2 + (\omega_c\tau)^2}{[1 - (\omega\tau)^2 + (\omega_c\tau)^2]^2 + 4(\omega\tau)^2} \right\rangle$$

$$(\sigma_{xx})_{imag} = \frac{\sigma_0}{\langle \tau \rangle} \left\langle \frac{\tau^2(1 + (\omega\tau)^2 - (\omega_c\tau)^2}{(1 - (\omega\tau)^2 + (\omega_c\tau)^2)^2 + 4(\omega\tau)^2} \right\rangle$$

2. Surface resistance,

$$R_s = \frac{\beta(\sigma_{xx})_{real} - \alpha(\sigma_{xx})_{imag}}{(\sigma_{xx})^2_{real}}$$

3. Surface Hall coefficient $\gamma_s = \beta R_H$.

where $\alpha + i\beta$ is the propagation constant of the 35 GHz wave into the GaAs surface.
More details are given in Appendix VIII.

Consider the following example as being typical of the GaAs crystals to be used in
the M555 Flight experiment. For n-type undoped GaAs at room temperature, the
scattering time of the electrons τ is about 10^{-14} second; $\omega\tau \approx 3(10^{-3}) << 1$
for 35 GHz. Furthermore, $\omega_c\tau \sim 3(10^{-2})$ for $B_z = 10^4$ Gauss. So we calculate
that $(\sigma_{xx})_{real} = \sigma_0$, the DC conductivity, that $(\sigma_{xx})_{imag} \sim 0$.
Therefore, undoped GaAs can be analyzed as a good conductor. For $\rho \sim 0.5\,\Omega$ cm,
we calculate the skin depth to be $\delta = 1/\beta \approx 150\,\mu m$, and $R_s \sim 7\Omega$. For $\mu_{Hall} \approx 3000$
$cm^2/volt$ sec, we then expect the high frequency Hall effect to give

$$Y_s = \beta R_H \sim 2(10^5)\ cm/volt\ sec.$$

D. RATIONALE AND APPROACH TAKEN

Effective characterization for NASA's early flight samples implies being able to detect rather small inhomogeneities in the surface regions of the semiconductor crystal without contamination from diffused electrical contacts and without damage from high pressure mechanical contacts. These features were taken as design constraints on the microwave techniques being developed. In view of the urgency of obtaining some electrical data on the surface characteristics of GaAs seed crystals before the fall of 1972, we chose to take only one approach out of the many possible for accomplishing each of the two major high frequency characterization procedures cited above, namely surface resistance and surface Hall effect.

The initial frequency of 35 GHz was chosen so that the skin depth in the GaAs seed crystals, based on R.B. Lal's preliminary data on boule G3-77, was comparable to the thickness of growth (of some 100 μm) expected onM555 Flight Experiment. Once the reflectance technique is established at 35 GHz, measurements at lower frequencies for probing deeper into the GaAs should be readily adapted. Techniques at higher frequencies will be expensive to implement, but may well be worth while in characterizing the surface resistance of M555 samples.

Contacts were avoided by designing thin choke coupling configurations. Mechanical pressure on the GaAs surface was to be minimized by interposing thin dielectric films between the metal microwave coupler and the GaAs surface to be mapped. Mapping was then to be accomplished by repositioning the GaAs slab over the opening of the metal coupler and repeating the microwave measurement.

The size of the opening in each metal microwave coupler corresponds to the

resolution element of the map and was chosen initially to be 3.5 x 7 mm for surface

resistance mapping and 4.2 mm diameter for Hall effect. Resolution elements as

small as one mm can readily be obtained for surface resistance at 35 GHz.

Inhomogereities of the high frequency (surface) electrical properties as small

as 10% should be observable. The basis for calculating resistivity from non-resonant

surface reflectance data, as shown in Appendix IX, indicates that 0.5% reproducibility

in the r.f. power readings corresponds to 5% uncertainty in each calculated resistivity

value for a surface of the typical (G3-77) seed crystal.

The precision of the s   e Hall coefficient similarly depends on the absolute

value of the surface resistivity. Detecting inhomogeneities in surface R_H as small as

10% with a coupler comprised of a 35 GHz bimodal cavity of normal metal walls will

require isolation between the two modes of at least 50 db.

E   RESULTS

1. Surface Resistance from Microwave Reflectance Measurements

A 35 GHz reflectance test bench has been designed and assembled from com-

ponents borrowed from the Physical Sciences Laboratory, USA MICOM. It has been

calibrated and operated to measure the microwave powe. reflected from a flat surface

of a sample of GaAs mounted at the end of a specially designed microwave coupler.

Sample contact with the coupler face is electrically insensitive to pressure.

In order to determine the value of the incident and reflected microwave power at the

coupler-sample interface, microwave power measurements have been made after successive

substitutions of the GaAs samples and an aluminum foil standard sample. Thus, a reflected

power is referred to a reference plane established at the coupler-sample in.erface , and

thereby corrects for losses and reflections in the transmission line between the sample and the power detecting element. Reproducibility of about ± 0.5% has been obtained for power reflectance measurements with a corresponding uncertainty of about ± 5.0% for values of resistivity in the neighborhood of 0.5 ohm-cm such as for repeated maps of the G3-77 seed crystal samples.

In conclusion, the non-resonant reflectance measurement gives the desired 5% precision in the surface resistivity averaged over a resolution element of approximately 20 square millimeters. The reproducibility is obtained without the use of diffused electrical contacts or high pressure mechanical contact. It appears to be only a matter of machining to obtain similar precision in surface resistance with resolution elements as small as one mm high.

It should be noted that dependence of 35 GHz surface resistance on orientation of the GaAs crystal can be readily examined with the present waveguide termination technique. The microwave currents induced in the GaAs flat are unidirectional over the full resolution element and successive rotations are accommodated as readily as successive translations. Initial rotational maps showed no angular variation at room temperature as large as 10%; none was expected.

2. Volume Resistivity at Low Ratio Frequencies

A logical extension of the analysis (indicated in Section II above) to the case of skin depth comparable to the sample dimensions was employed to test the feasibility of measuring bulk resistivity and bulk Hall effect without contacts. Very preliminary results at 3 MHz on GaAs slabs, such as from boule G3-77 where $\delta(3MHz) \sim 10$ mm, were obtained from coil loading. Observations of the Q change

of a copper coil when loaded by each of a variety of GaAs samples indicate that the rf losses due to bulk conduction in the undoped GaAs crystals available can be measured with considerable precision (good reproducibility). Calculation of the mean bulk resistivity will, of course, require reasonable control over sample geometry and coil configuration.

A test of the rotational (Hall) effects of a strong DC magnetic field on coil loading was run and a small but definite Q change was observed at 10 kilogauss. Therefore, it appears possible to design a crossed coil system for the appropriate sample geometry to get some measure of the bulk Hall effect in the seed and source crystals prior to the M555 Flight Experiments without diffusing electrical contacts.

In conclusion, the technique of coil loading by GaAs crystals having a regular shape appears to be a feasible way of measuring an average bulk resistivity and an average bulk Hall effect without diffusing electrical contacts. It is recommended that the development of this technique be considered for bulk characterization of the GaAs seed and source crystals to be used in M555 Flight Experiment.

3. Surface Hall Effect at 35 GHz

As noted in the rationale above, the approach was to use a flat GaAs surface as part of the wall surface of a bimodal cavity and aim at transferring 35 GHz energy from one mode into the other by means of the Hall effect on the surface currents in the GaAs. Design calculations for several bimodal cavities were performed which would permit some 10 to 20 mm^2 area of the GaAs surface to be effectively a part of the cavity wall without diffused electrical contacts or undue

mechanical pressure. One cavity was machined out of the best brass available; preservation of four fold symmetry was attempted in order to minimize the direct coupling between the two modes. Several trials were needed to obtain useful coupling through the four waveguide irises. With iris coupling adjusted for optimum transmission through cavity mode 1, the direct coupling through the orthogonal mode was found to be 27 db. The measured cavity Q with the GaAs surface as part of one wall agrees with theory. From the DC values of the Hall coefficient for Ga As at room temperature as measured by R. B. Lal, the coupling between modes due to the GaAs Hall effect in this cavity is expected to be about 40 db. Therefore, before obtaining surface Hall data with this cavity, tuning controls will have to be added.

An alternate bimodal cavity has been designed in which the Hall coupling for a GaAs end wall is increased about one order of magnitude. If the machining tolerances attained for the first bimodal cavity can be maintained in the construction of this alternate cavity, precision of better than 20% in the surface Hall coefficient of GaAs can be expected at room temperature for each resolution element of some 4 mm across and approximately 100 microns deep.

In conclusion, the preliminary tests of a bimodal cavity method for mapping the surface Hall effect at 35 GHz are favorable. The machining tolerances attainable by John Medlin and his staff are sufficiently small to require only rather modest tuning of the cavity modes in order to get the desired precision for mapping the Hall coefficient over the skin depth of some 100 μ m on flat GaAs surfaces without diffused electrical contacts or undue mechanical pressure.

F.   SUMMARY OF PROGRESS ON HIGH FREQUENCY CHARACTERIZATION

The results reported above meet the stated aims for this first seven month period of adapting microwave measurement techniques reported in the literature to the job of characterizing the surface layers, circa 100 μm deep, of the semi-conducting crystals to be used and grown on M555 flight experiments. In parti-cular, the surface resistance at 35 GHz has been shown to give contactless mapping of resistivity within 100 μm of the GaAs surface to within ± 5% without contacts. Furthermore, the initial cavity designs and tests indicate reasonable precision in surface Hall coefficient should be attainable with this technique. Even the contact-less measurement of the bulk resistivity of GaAs by coil loading in the MF to VHF ranges appears to be feasible from the very preliminary tests reported here.

Acknowledgements

The reported progress on surface resistance would not have been possible without the loan of microwave equipment from the Physical Sciences Directorate of USA MICOM. The precision of the UAH machine shop under the supervision of Mr. John Medlin is the basis for optimism about characterizing the Hall mobility in the surface of NASA's semiconducting flight samples.

BIBLIOGRAPHY

(useful for High Frequency Characterization of GaAs)

1. GaAs Properties

   Glover, G. H., High Field Microwave Permittivity of Electrons in Bulk GaAs, Journal of Applied Physics, Vol. 42, No. 13, Dec. 1971.

   Stillman, G. E. et al, Hall Coefficient Factor for Polar Mode Scattering in n-type GaAs, J. Phys. Chem. Solids, Vol. 31, pp 1199-1204, Pergamon Press 1970.

   Inoue, M. et al, Microwave Measurement of the Velocity-Field Characteristics in n-Type Gallium Arsenide, Japanese Journal of Applied Physics, Vol. 10, No. 10, Oct. 1971.

   Kaneda, S. and Abe, M., Microwave Anisotropy and Frequency Dependence of Hot Electron in n-Type GaAs, Japanese Journal of Applied Physics, Vol. 10, No. 10, Oct. 1971.

   Wolfe, C. M. et al, Ionized Impurity Density in n-Type GaAs, Journal of Applied Physics, Vol. 41, No. 2, Feb. 1970.

   Ehrenreich, H., Band Structure and Electron Transport of GaAs, Physical Review, Vol. 120, No. 6, Dec. 1960.

   Kang, C. S. and Greene, P. E., Preparation and Properties of High-Purity Epitaxial GaAs Grown from Ga Solution, Applied Physics Letters, Vol. 11, No. 5, Sept. 1967.

   Whitaker, J. and Bolger, D. C., Shallow Donor Levels and High Mobility in Epitaxial Gallium Arsenide, Solid State Communications, Vol. 4, pp 181-184, Pergamon Press, 1966.

2. Microwave Measurements of Semiconductor

   Jacobs, H. et al, "New Microwave Techniques in the Measurement of Semi-conductor Phenomena," I.R.E. International Convention Record, 1962.

   Lindmayer, J. and Kutsko, M., "Reflection of Microwaves from Semiconductors," Solid State Electronics, Vol. 6, pp 377-381, Pergamon Press, 1963.

   Brice, J. C. and Moore, P, Contactless Resistivity Meter for Semiconductors, Journal of Scientific Instruments, Vol. 38, July 1961.

   Donovan, G., "The Hall Effect in Metals at High Frequencies," Proc. Phys. Soc. A, 68, 1026 (1955).

2. Microwave Measurements of Semiconductor (Contd)

Hambleton, G. E. and Gartner, W. W., Microwave Hall Effect in Germanium and Silicon at 20 kmc/s, J. Phys. Chem. Solids, Vol. 8, pp 329-332, Pergamon Press 1959.

Galt, J. K. et al, Cyclotron Absorption in Metallic Bismuth and its Alloys, Physical Review, Vol. 114, No. 6, June 1959.

Dresselhous, G. et al, Cyclotron Resonance of Electrons and Holes in Silicon and Germanium Crystals, Physical Review, Vol. 98, No. 2, April 1955.

Price, W. L. V., Extension of van der Pauw's Theorem for Measuring Specific Resistivity in Discs of Arbitrary Shape to Anisotropic Media, J. Phys. D: Appl. Phys., Vol. 5, 1972.

Banbury, P. C. et al, On the Theory of the Isothermal Hall Effect in Semiconductors, Proc. Phys. Soc LXVI, 8-A.

Donovan, B. and March, N. H., High Frequency Conductivity in Semiconductors, Proc. Phys. Soc. A, 69, 528 (1956).

Donovan, B., The Magneto-Resistance Effect in Metals at High Frequencies, Proc. Phys. Soc. A, 67, 305 (1954).

Shockley, W., "Cyclotron Resonances, Magnetoresistance, and Brillouin Zones in Semiconductors," Physical Review, Vol. 90, 1953.

Smith, R. A.,"Semiconductors," Cambridge University Press, 1959

3. Microwave Rotation Experiments

Portis, A. M. and Teaney, D., "Microwave Faraday Rotation: Design and Analysis of a Bimodal Cavity," Journal of Applied Physics, Vol. 29, No. 12, Dec. 1951.

Portis, A. M., "Microwave Faraday Rotation: Measurement of the Conductivity Tensor," J. Phys. Chem. Solids, Vol. 8, 326-329, Pergamon Press, 1959.

4. Microwave Design

Bethe, H. A., "Lumped Constants for Small Irises," Radiation Laboratory Report 43-22, March 24, 1943.

Kinzer, J. P. and Wilson, I. G., "End Plate and Side Wall Currents in Circular Cylinder Cavity Resonator," Bell System Technical Journal, July 1946.

4. Microwave Design (Contd)

Wilson, I. G. et al, "High Q Resonant Cavities for Microwave Testing," Bell System Technical Journal, July 1946.

Harvey, S. F., Microwave Engineering, Academic Press, 1963.

Waldrom, R. A., Theory of Guided Electromagnetic Waves, Van Nostrand Reinhold Co., 1969.

Montgomery, C. G., "Technique of Microwave Measurements," MIT Radiation Laboratory Series, Vol. 11, McGraw-Hill, 1947.

APPENDIX I

CHARACTERIZATION PLAN FOR APOLLO 14
TECHNICAL DEMONSTRATIONS NO. 15,
No. 16, No. 17, and No. 18

T. C. Bannister

R. B. Lal

H. U. Walter

Space Sciences Laboratory

University of Alabama, Huntsville

ABSTRACT

A characterization plan for solidification experiments during Apollo
14 fly back from the moon is presented. The plan describes an evaluation
procedure for each of the four considered experiments according to the
specific objectives of each experiment.

I. Introduction

The concept of materials characterization has been clarified in 1967 by a committee of the Materials Advisory Board of the National Research Council *(Ref. 1), which defines that characterization describes those features of composition and structure (including defects) of a material that are significant for a particular preparation, study of properties, or use, and suffice for the reproduction of the material.

Single crystals of various substances have gained increasing practical importance, often for scientific investigations, but primarily for technical and industrial applications. These crystals are mostly grown from the melt. The chemical and structural quality of these crystals, which in turn determines very strongly the physical properties of the crystalline materials, is mainly restricted by fluid motions during the solidification process. The main driving force is gravity and it is therefore expected to improve the quality of the crystals by producing the crystals under reduced gravity conditions in space. The first solidification experiments in space will hopefully be done during the Apollo 14 flyback from the moon. The proposed plan has been prepared with the intention of evaluating the returned samples in such a manner as to obtain a maximum amount of information. The relative quality of the materials grown in space (0-gravity) may be judged by comparison with materials grown under the same conditions on earth.

*(Ref. 1)
  Characterization of Materials: Nat. Acad. Sci. Nat. Acad. Engg., NRD, Rept, No. MAB-229-M, Washington, D.C. (1967)

II. Receiving, Opening and Distribution of Samples

At the meeting held January 19, 1971 at the ME Laboratory, it was decided that the samples will be received, opened and distributed to the investigators by ME Laboratory under the supervision of Mr. Paul Schuerer and Mr. Bill Aldrich . A log of each sample and the administrative paper work will also be maintained and handled by ME Laboratory.

Prior to opening of the sample tubes, X-ray photographs of the whole tube should be taken. The opening of the sample tubes should be done in such a manner that no appreciable heat is developed and no mechanical strains, for example, due to vibrations, shocks and spinning, are involved. In addition, contamination of the samples should be avoided. Handling of samples with plastic gloves in a clean area seems to be sufficient.

III.   Characterization Plan

The four solidification experiments considered in this plan have been designed to obtain information about the influence of reduced gravity on the solidification process of metallic melts. Since each experiment has specific objectives, a specific evaluation plan for each experiment is needed.

III. A.   Specimen No. 15

Indium Bismuth Controlled Eutectic Solidification

The objective, significance and application of this experiment have been summarized in the objective plan as follows:

Objective:

This experiment is directed toward obtaining preliminary information from which the effects of zero gravity on the control of eutectic formation in a directionally solidified metal alloy can be assessed.

Significance:

This experiment will provide information in support of hardware development for approved Skylab composite casting experiments. A first orde assessment of the criticality of controlling the rate at which the solidification front travels through the melt can be made.

Application:

This experiment, using a low melting point metal alloy which can be flown aboard Apollo 14, will provide supporting information for the development of similar composites of higher temperature systems. These composites such as the AlCu eutectic being planned for Skylab have potential application in structural members which exhibit controlled anisotropic properties and in the field of power transmission where the directionally solidified phase may perform as a superconductor.

Characterization Plan for Specimen No. 15

The following characterization plan has been worked out with strong emphasis on the evaluation of the relative crystallographic and geometric orientation and the size of the simultaneously solidified phases. In addition to this, information regarding crystal perfection can be obtained.

The plan includes the following:

a)   Non-destructive testing without cutting the whole crystal

b)   Parallel tests after cutting the sample.

a)   Non-destructive tests

The test will be performed in the numeric order as described below.

1.   X-ray transmission microscopy of the whole sample in the tube before opening will reveal the shape, and superficial irregularities (cracks, etc.) of the sample.

2.   Techniques to open the sample tube with minimum danger of generating mechanical strains, plastic deformation, scratches, increased temperature and inducing contamination have to be considered.

3.   All samples should be weighed. Also the sample should be described phenomenologically. Each sample should be photographed together with a measuring scale to give an idea of the size, shape, etc. of the sample. Step No. 1 can be repeated if no X-ray damage is known.

4.   Electropolishing of the sample should be done. The whole sample is then etched or possibly anodized in order to reveal grain boundaries.

5.   Dislocation density may be determined by etching and optical microscopy.

6. Mapping of grain boundaries and determination of crystallographic orientation of the grains by the Laue back deflection technique are very important and must be done.

7. Electrical resistivity of the whole crystal will be measured by two point probe method at room temperature. Electrical contacts may be made by cold welding of pure indium contacts to the sample.

8. Single crystal X-ray diffraction measurements may be made to reveal lattice parameters,etc.

9. Electron microprobe analysis or scanning microscopy may be done on the whole sample, if possible, which will reveal the chemical homogeneity of particular grains.

b) Investigations which will need cutting of the sample:

At this stage the sample can be cut. The number and shape of the pieces depends on the final decision which investigations will be performed. The best technique for cutting is the one which involves minimum strains, damage and contamination and should be used. Mechanical cutting is not desirable, acid cutting or electrochemical cutting should be strongly considered. Three pieces of the crystal (one from each end and one from the center) should be kept aside for reference. The following investigations can be performed simultaneously.

1. Electron microprobe analysis, electron scanning microscopy, and electron microscopy

2. Electrical resistivity and Hall effect measurements

3. Superconductivity

4. Optical microscopy - (phase contrast,etc.)

5. NMR

6. Dislocation density by etch pit technique

7. Optical reflection measurements.

8. Spark source mass spectrometry for impurities.

III. B. <u>Specimen No. 16</u>

<u>Indium Bismuth Remelt Experiment</u>

The objective, significance and application of this experiment
have been summarized in the objective plan as follows

<u>Objective</u>:

The proposed experiment is designed to allow the direct
comparison of solidification characteristics prevailing under laboratory
conditions and under zero gravity. The approach provides a unique means for
determining directly (on a compound partially formed on earth and partially
in space) the effect of gravity on homogeneity of impurities (striations
and coring), nature and concentration of defects, solid-liquid interface
phenomena, and growth characteristics.

<u>Significance</u>

The experiment will provide preliminary information on zero-g
solidification phenomena which will aid in the development of hardware for
Skylab experiments.

<u>Application</u>:

The proposed experiment should provide useful information
(using a low melting metal) which will allow improvements in hardware now
under development for growing improved semiconductor crystals. High
quality semiconductor crystals have a wide range of commercial applications
in the electronics industry.

<u>Characterization Plan for Specimen No. 16</u>

For this experiment it is of particular importance to trace the position
up to which the material has been melted and resolidified in space. This
can be done by an iteration technique with resistivity measurements.

The plan includes the following:

a) Non-destructive testing without cutting the whole crystal

b) Parallel tests after cutting the sample.

a) Non-destructive tests

The test will be performed in the numeric order as described below.

1. X-ray transmission microscopy of the whole sample in the tube before opening will reveal the shape and superficial irregularities (cracks, etc.) of the sample.

2. Techniques to open the sample tube tube with minimum danger of generating mechanical strains, plastic deformation, scratches, increased temperature and inducing contamination have to be considered.

3. All samples should be weighed. Also the sample should be described phenomenologically. Each sample should be photographed together with a measuring scale to give an idea of the size, shape, etc. of the sample. Step No. 1 can be repeated if no X-ray damage is known.

4. Electropolishing of the sample should be done. The whole sample is then etched or possibly anodized in order to reveal grain boundaries.

5. By conductivity measurements followed by dislocation density measurements, electron microprobe analysis, etc., the position up to which the material has been melted and resolidified in space has to be determined.

6. Dislocation density may be determined by etching and optical microscopy.

7. Mapping of grain boundaries and determination of crystallographic orientation of the grains by the Laue back deflection technique are very important and must be done.

8. X-ray diffraction studies to reveal the crystalline perfection, lattice parameters, etc., may be made.

9. Electron microprobe analysis or scanning microscopy may be done on the whole sample, if possible, which will reveal the chemical homogeneity of particular grains.

b) <u>Investigations which will need cutting of the sample:</u>

At this stage the sample can be cut. The cutting has to be done along the axis, and it is therefore not reasonable to make more than 3 slices(o.d. of the sample is only 0.249"). The best technique for cutting is the one which involves minimum strains, damage and contamination and should be used. Mechanical cutting is not desirable; acid cutting or electrochemical cutting should be strongly considered. Three pieces of the crystal (one from each end and one from the center) should be kept aside for reference. The following investigations should be done with each of the three slices.

1. Electron microprobe analysis, electron scanning microscopy, and electron microscopy

2. Electrical resistivity and Hall effect measurements

3. Superconductivity

4. Optical microscopy - (phase contrast, etc.)

5. Dislocation density by etch pit technique

6. Optical reflection measurements

III. C.   Specimen No. 17

Indium Bismuth Solidification Demonstration (Point-Nucleation)

The objective, significance and application of this experiment have been summarized in the objective plan as follows:

Objective:

The objective of this demonstration is to study the solidification of an intermetallic compound in space. The crystallization of the InBi will begin at a point and then continue down the rod as determined by the heating and cooling plan.

Significance:

The presence of gravity induced thermal convection in the liquid melt causes irregularities in the solidification of crystalline material. Eliminating thermal convection at the solid-liquid interface should result in a more uniform and perfect crystalline structure.

Application:

The crystal growth experiments that have been proposed for processing in space are predominantly based on the possible advantages of solidification in a convection-free environment. The controlled solidification of InBi may show the magnitude of the possible improvement.

Characterization plan for Specimen No. 17

This sample is most likely to be single crystalline. Particular emphasis should therefore be put on the evaluation of crystalline and chemical perfection in comparison to structural and chemical homogeneity of samples grown under the same conditions on earth.

The plan includes the following:

a) Non-destructive testing without cutting the whole crystal

b) Parallel tests after cutting the sample.

a) **Non-destructive tests**

The test will be performed in the numeric order as described below.

1. X-ray transmission microscopy of the whole sample in the tube before opening will reveal the shape, and superficial irregularities (cracks, etc.) of the sample.

2. Techniques to open the sample tube tube with minimum danger of generating mechanical strains, plastic deformation, scratches, increased temperature and inducing contamination have to be considered.

3. All samples should be weighed. Also the sample should be described phenomenologically. Each sample should be photographed together with a measuring scale to give an idea of the size, shape, etc. of the sample. Step No. 1 can be repeated if no X-ray damage is known.

4. Electropolishing of the sample should be done. The whole sample is then etched or possibly anodized in order to reveal grain boundaries.

5. By conductivity measurements followed by dislocation density measurements, electron microprobe analysis, etc., the position up to which the material has been melted and resolidified in space has to be determined.

6. Dislocation density may be determined by etching and optical microscopy.

7. Mapping of grain boundaries and determination of crystallographic orientation of the grains by the Laue back deflection technique are very important and must be done.

8. X-ray diffraction studies to reveal the crystalline perfection, lattice parameters, etc., have to be made.

9. Electron microprobe analysis may be done on the whole sample, if possible, which will reveal the chemical homogeneity of particular grains.

b) Investigations which will need cutting of the sample:

At this stage the sample can be cut. The best technique for cutting is the one which involves minimum strains, damage and contamination and should be used. Mechanical cutting is not desirable, acid cutting or electrochemical cutting should be strongly considered. Three pieces of the crystal (one from each end and one from the center) should be kept aside for reference. The following investigations should be done:

1. Electron microprobe analysis , electron scanning microscopy, and electron microscopy

2. Electrical resistivity and Hall effect measurements

3. Superconductivity

4. Optical microscopy - (phase contrast, etc.)

5. Dislocation density by etch pit technique

6. Optical reflection measurements

III. D. Specimen No. 18

Sphere Casting Demonstration

The objective, significance and application of this experiment have been summarized in the objective plan as follows:

Objective:

The objective of this demonstration will be to solidify a suspended metal melt in the weightlessness of space. The experiment will provide the first information ever obtained on containerless processing in zero gravity.

Significance:

a. The melt is static during the process of solidification. After the spherical melt is formed, there are no further motions of the liquid or solid material. Therefore, structural and chemical properties should be more homogenous.

b. The melt is point suspended containerless and, therefore, contamination, induced stresses and heterogenous nucleation are minimized.

c. Information will be obtained on homogenous and heterogeneous nucleation, grain size and distribution and other solidification phenomena.

Application

Since the spherical shape of the casting will be determined primarily by the surface energy of the melt, this demonstration will be the first example of the containerless processing required by many proposed space materials experiments. Measurements made on the sphericity and surface finish will provide information on experiments such as the spherical casting experiment part of M512.

Characterization Plan for Specimen No. 18

The sphericity and the topographical surface characteristics need to be investigated first. Homogeneous and surface nucleation and also the directional growth of the two eutectical phases should be studied intensively. The latter could inform about the general shape of the isotherms in the static melt during solidification.

The plan includes the following:

a)   Non-destructive testing without cutting the whole crystal

b)   Parallel tests after cutting the sample.

a)   **Non-destructive tests**

The test will be performed in the numeric order as described below.

1.   X-ray transmission microscopy of the whole sample in the tube before opening will reveal the shape and superficial irregularities (cracks, etc.) of the sample.

2.   Techniques to open the sample tube with minimum danger of generating mechanical strains, plastic deformation, scratches, increased temperature and inducing contamination have to be considered. Particular care should be given to the opening procedure if the sample has been found not to be ruptured from the capillary by the X-ray transmission photograph.

3.   All samples should be weighed. Also the sample should be described phenomenologically. Each sample should be photographed together with a measuring scale to give an idea of the size, shape, etc. of the sample. Step No. 1 can be repeated.

4. Sphericity studies by photographic techniques, followed by

5. Direct mechanical measuring techniques should be done.

6. Smoothness of the surface by techniques which have to be strongly related to the quality of the surfaces should be performed. It the surfaces are perfect, interferometric techniques should be used.

7. After the sphericity and topography studies are completed, optical studies on phase distributions at the surface can be performed. Actual mapping will not be possible because of the relative large number and complicated shape of arrays of different phases which are expected. Therefore some representative areas may be described more closely, otherwise a general description seems to be sufficient.

b) <u>Investigations which will need cutting of the sample</u>:

At this stage the sample can be cut. The best technique for cutting is the one which involves minimum strains, damage and contamination and should be used. Mechanical cutting is not desirable, acid cutting or electrochemical cutting should be strongly considered. The following investigations can be performed simultaneously.

1. Electron microprobe analysis, electron scanning microscopy, and electron microscopy

2. Electrical resistivity measurements, which might bring some information about average phase alignment

3. Optical microscopy to study phase alignment (texture)

IV.   Conclusions

During the writing of this report, a number of problems and questions have arisen. Some of them are listed below:

1.   Which electrolytes   current densities, cathode material etc., should be best used for electropolishing?

2.   Which etchants should be used for etching and dislocation density studies?

3.   Is anodizing possible and how?

4.   How to make electrical contacts for conducting measurements.

5.   What about radiation damage by X-rays?

6.   Sample preparation for electron microprobe analysis.

7.   How to properly cut the samples.

These and other questions have to be answered before touching and possibly damaging the irreplaceable Apollo 14 samples!

APPENDIX II

A. GaAs CHARACTERIZATION PLAN

DESIGNED TO MEASURE THE EFFECT OF MICROGRAVITY

ON GaAs SOLUTION GROWTH

Expected Effect of Microgravity on GaAs Crystal Growth from Ga Solution

A. Although UAH did not propose or design the M-555 experiment, in order to characterize 0-g effects, we must make some projection of the expected results. The six projected effects of Zero-g are only qualitative since the exact magnitude of some of the parameters is not in the literature..

    1. Reduced convection should reduce the GaAs mass transport to the growth area so that either

        (a) the crystals grow at a slower rate, or

        (b) fewer crystals are grown

    2. A slight increase in temperature gradient should result from the lower effective conductivity of stationary Ga due to a reduced convection.

    3. Microcrystallites of GaAs will remain in Ga suspension and not float to the surface. Therefore, the chances of them bumping into and sticking to the film are increased in a microgravity environment. However, without convection the chances of a micron size crystallite being swept into the seed are also reduced.

Both microscopy and X-ray topography will be used to identify evidence for micro-crystal deposition on the substrate.

    4. Lack of convection should give rise to increased geometric effects which could cause a spatial variation of the GaAs film thickness, e.g., a greater amount of GaAs would diffuse to the edge of the substrate disc than to the center. Careful film thickness measurements, of course, will check this experimentally.

    5. Convection at one-g tends to mix the not rich GaAs in Ga solution into the cooler end of the growth tube. The solution then finds itself supersaturated at the

lower temperature so it condensed into nucleating additional new grains causing polycrystalline growth. At zero-g we expect smaller temperature and concentration gradients (due to lack of convection) which should produce a steady unperturbed growth of crystals and epitaxial layers. This increased perfection should extend to the atomic scale increasing the electrons mobility and increasing the lattice perfection. Such zero-g improvements should be readily detected by our proposed characterization measurements.

6. In zero gravity without convection a larger difference in dopant impurity concentration should exist between the GaAs source and seed. Without convection the impurity transport depends only on its diffusion rate through the Ga and some dopants may travel faster and some slower than the GaAs. Since a silicon dopant is being considered, this effect may be readily detected.

7. Assuming some inert gases were left in the ampoule, bubbles would be more likely to remain in the liquid Ga in zero gravity. If a bubble resides on the GaAs seed, then, of course, no epitaxial film would grow on that spot, resulting in a void on the film. Evidence of such voids will be sought during microscopic examination.

If the surface tension of Ga decreases with temperature as is the case with most liquids, then the bubbles would move toward the hot end of the ampoule away from the seed.

I. GaAs Morphology - Characterization

Introduction

Surface morphology will be used as a qualitative index to the perfection of GaAs substrates, films and crystallites. A rough grain-like or spongy surface would suggest polycrystallinity, while a loose film would suggest a nonepitaxial film. Lenie suggests unaided viewing of the film against a dark background under a flourescent light to identify such defects as scratches, pits, "orange peel" and pyramids. Microscopic examination will easily reveal scratches, voids, spikes, crowns, and dimples with measurements accurate to 1 micron.

A. Interferometry

Smaller surface variations will be detected by using Fizeau Interferometry. This technique utilizes a 1/2 silvered mirror just above and almost parallel to the film, monochromatic illumination produces parallel interference fringes if the film is flat, any derivation from flatness by $\lambda/4$ will cause a jog of 1/2 fringe distance in the otherwise parallel fringe pattern. In other words, using sodium light ($\lambda = .589\ \mu$) each fringe shift represents a film surface depression (or rise) of $.29\mu$. If fringes are shifted by 10 spaces, then the irregularity depth is $2.9\ \mu$. A series of fringe photographs (about 20) will map the whole surface. The fringes are like elevation contours or terraces on a field map. Utilization of optical interference is possible only if the surface is nearly flat and mirror-like. This technique is best suited to the highly polished substrate and can be used for a high quality epitaxial film.

In optical microscopy, the light source is highly important. The illumination should be metallurgical type that is highly collimated parallel to the optical axis of the

objective lens. Any region of the epitaxial film which is not flat will reflect its light away from the optical axis causing that region to appear dark. A calibrated tilting stage may be used to both bring the misaligned region into alignment and to measure the misorientation angle.

B. Reflectogram

The related reflectogram method could give qualitative pictures of the film surface. A parallel light beam is allowed to strike the epitaxial film at an angle of 45°, the reflected beam then photographed on a fine textured white screen. If the film is mirror-like, a uniform round spot is observed; however, a low quality epitaxial film would result in nonspecular reflections producing a broader spot. Beam stops insure that no portion of the beam strikes the sample edge, otherwise additional broadening would result.

C. Scanning Electron Microscope

The scanning electron microscope (SEM) can be used to study the specimen's morphology. Its advantages are:

1. A larger depth of field and greater magnification by an order of magnitude.

2. The specimen may be an active part of an electrical circuit and the circuit parameters may be displayed on a screen in phase with the electron beam sweep. This technique has been used to map the P-N junction.

3. A qualitative contrast mode may be used to map the location of different elements on the surface.

4. The nonscanning electron microscope will not be used here since it produces only a shadow of a specimen which gives little or no information on surface morphology.

D. Detection of Epitaxial Film Surface Defects

C. E. Hallas and E. J. Fatzner (IBM)[2] have reported the following surface defects observed by microscope on (111) silicon epitaxial wafers: orientation flat terracing, crescents and fishtails, snowballs, mounds and cloudy surfaces. The probable cause of each of these defects is given, but the above nomenclature is not completely standard. Photographs of the defects are shown so they may be readily recognized and it is emphasized that no etching is required, thus this observation is nondestructive.

C. A. Lenie's[1] article, "Characterization of Film Defects in Silicone Epitaxial Wafers," describes defects such as the substrate scratch, after scratch, pit, void, pyramid, orange peel, dimple, crown, edge ledge and haze.

Apparently stacking faults could be observed under a phase contrast microscope (Leitz Wetflar Light-Wave Surface Tester' without etching and with a metallurgical microscope after etching!

II. Electrical Properties

Electrical Characterization

The resistivity of semiconductors is a basic material parameter whose measurement is required for determining the sign, density and interaction of charge carriers with the host crystal lattice and with impurities.

The measurement of electrical parameters in epitaxial films is aggravated by a number of difficulties. These include surface roughness and thickness variation, also microscopic chemical inhomogeneities, impurity fluctuations and space charge effects, which pose a formidable barrier in the way of the quantitative characterization of resistivity and other parameters.

To characterize the epitaxial layer of GaAs and other small self nucleated crystallites, the following two types of electrical measurements are proposed:

a. High frequency electrical characterization

b. D.C. electrical characterization

The above two methods are described in detail in separate sections. It is to be emphasized that the results of each different technique will be useful in double checking the results and giving greater confidence on the results.

A. D. C. Electrical Charazterization

In the case of semiconductors, as in GaAs, the number of charge carriers, as well as the mobilities, depend upon temperature and also on the presence of defects and impurities. In such a case the most common measurement made of the properties of a semiconducting solid is the electrical conductivity. In the case of n-type of material, the expression reduces to,

$$\sigma = ne\mu_n$$

where σ (the reciprocal of resistivity) is the conductivity, e is the electronic charge and μ_n drift mobility of electrons. Since σ can be measured experimentally, we can determine the majority carriers, if the drift mobility can be determined.

In order to determine the type, concentration and mobility of charge carriers, the measurements made on the resistivity of the film must be supplemented by galvano-magnetic measurements made over a wide temperature range. A determination of R_H, the Hall coefficient, of the film as a function of temperature is of particular interest.

In the proposed work we have decided to use the technique developed by Van der Pauw,[1] for the determination of resistivity and Hall coefficient in GaAs films and crystallites.

Van der Pauw method requires plane parallel samples of arbitrary shape with four small ohmic contacts on the circumference. A current is passed between two adjacent contacts while potential differences between the other two are measured By cyclic permutation two independent pseudo-resistances R_1 and R_2 are obtained as voltage current ratios. It has been shown by Van der Pauw that between R_1 and R_2, the resistivity ρ and the thickness of the platelet d, the following relation exists.

$$\rho = \left\{ \frac{\pi d}{2 \ell n_2} \right\} \left\{ R_1 + R_2 \right\} \ f\left(\frac{R_1}{R_2} \right) \tag{1}$$

The function $f\left(\frac{R_1}{R_2} \right)$ is given by Van der Pauw and only depends on the ratic $\frac{R_1}{R_2}$ and is given a graphical form (the maximum error in the curve is $\sim 2\%$).

The Hall constant R_H will be determined by using the same contacts by

passing the current in the nonadjacent contacts. The change in voltage is measured across the other contacts when a magnetic field is applied perpendicular to the sample.

The Hall coefficient R_H is given by

$$R_H = \frac{d}{B} \wedge R_3$$

where B is the magnetic induction and $\wedge R_3$ the change in resistance R_3 with magnetic field and d is the thickness of the sample. Also, n, the carrier concentration, can be calculated from

$$R_H = \frac{1}{ne}$$

where e is the electronic charge. The mobility μ_H can also be calculated from the expression

$$\mu_H = \frac{R_H}{\rho}$$

From the temperature variation of resistivity and Hall coefficient, the total ionized impurity concentration $N_D + N_A$ and N_A, and N_D can be calculated using the method of Wolfe, et al.[a]

The experimental setup to do the above measurements down to $4.2^{\circ}K$ is available at UAH.

The following parameters will be used to evaluate the overall role of space environment on the growth of GaAs epitaxial films and self-nucleated crystals.

1. The overall carrier concentration and mobility of the sample.

2. Type of film grown, n or p-type.

3. Homogeneity of the sample.

4. Mobility

The quantities mentioned in items 1 and 2 earlier can be determined by the method described earlier. The homogeneity of the sample (item 3) can be studied by studying the temperature variation of the ratio of the two resistances R_1 and R_2 occurring in Van der Pauw's equation and also by studying the resistances between different combination of contacts on the sample. The ratio $\frac{R_1}{R_2}$ which appears in equation (1) depends only on the geometry of the sample and the contacts. This means that it should be independent of temperature. Nevertheless, when $\frac{R_1}{R_2}$ for a sample is found to change with temperature, the sample must be inhomogeneous, the resistivity of different parts of the sample having different temperature dependencies. These phenomena were found in many samples studied at UAH. Although a change of $\frac{R_1}{R_2}$ with temperature indicates that the sample is not homogeneous, it is emphasized that constancy of $\frac{R_1}{R_2}$ does not necessarily mean that the sample is homogeneous. It may still be composed of homogeneous layers of different composition parallel to the plane of the sample, or it may be composed of parts with different resistivities having the same temperature variation.

Especially now in the present plan of having Si-doped seed and undoped film and, in the other case, undoped seed and Si-doped film, the technique of four probes [3] with points on the opposite side of the film will be worth trying. This method of four probes with t o probes on the other side of the wafer has been successfully used by Schumann and Hallenbeck,[3] for the epitaxial layer of n or n^+ in the case of silicon.

In the case of growth of epitaxial layer n or n^+ type GaAs, a method of three-point probe developed by Brownson [4] will be tried on some practice samples.

In all the three cases of growth, (a) undoped film on n-type substrate, (b) undoped film on heavily Si-doped n^+ substrate and (c) Si-doped film on undoped substrate, the overall change of resistivity, mobility and carrier concentration as compared to the values measured on the seed sample will be able to show the difference of growth in space environment. In the case (a) changes of $\pm$ 20% may be detected by resistivity measurements while in cases (b and c) even if the resistivity remains the same it is expected that values of mobility, carrier concentration and the total ionized impurity density may significantly change to give meaningful results.

In the case of crystallites, if they are not spongy, measurements can be made for resistivity and Hall effect after polishing and lapping down to a flat surface. If the crystallites can be picked up at different places along the entire length of the growth tube, measurements can be more meaningful.

C. Static Magnetic Susceptibility Measurements on Self-Nucleated GaAs Crystallites

Measurement of magnetic susceptibility is another way to get information about the band structure and the impurity contents in semiconductors . The magnetic susceptibility χ can be divided into three parts.

1. That of the free carriers (electrons and holes), χ_c.

2. That of the electrons in the valence band and in the atomic cores, χ_ℓ.

3. That of charge carriers bound to impurities, χ_{imp}.

The magnetic properties of imperfect crystals are in general different from those of perfect crystals. Electrons and holes give rise to both a diamagnetic and a paramagnetic contribution. Atomic imperfections give rise to paramagnetic contribution if they contain electrons in unpaired state, and to diamagnetism in the opposite case. The effects are usually small but can be separated by studying the temperature variation of susceptibility. If the pure crystal is diamagnetic, as in the case of GaAs, the effect of imperfections and paramagnetic impurities can be studied by studying their temperature variation.

Static susceptibility at room temperature and at lower temperatures can be accurately measured with the existing equipment at SSL/MSFC. The number of paramagnetic centers/cm^3 can be calculated for different crystallites which will give information regarding impurity concentrations on different crystallites within the length of the growth tube.

II. B. HFC Elements of GaAs Characterization Plan

1. Microwave Surface Resistance on Large Flat Surfaces

The surface resistance of flat samples of GaAs can be measured from microwave power reflectance from the sample which has a shallow skin depth at 35 GHz. Thus the resistivity of the epilayer can be mapped in area increments of $3.5 \times \sim 4$ mm. Reproducibility of measurements better than $\pm 1\%$ has been obtained. The value of resistivity can be calculated to within $\pm 10\%$. No contacts are attached to the sample.

2. Microwave Surface Resistance on Small Crystallites

The surface resistance of small crystallites with surface areas of approximately 1 mm^2 can be measured by mounting the crystallite inside a waveguide or cavity. Losses associated with crystallite surface currents are measured which are a function of sample resistivity. An absolute accuracy of $\pm 10\%$ is expected for resistivity. No contacts are attached to the sample.

3. Microwave Hall Effect on Large Flat Surfaces

The measurement of Hall effect on large flat surfaces requires the use of a cavity with degenerate, orthogonal modes. Surface currents on the sample are caused to rotate upon application of an external magnetic field resulting in the excitation of the orthogonal mode in the cavity. For a coupling β of approximately 20 db, it is expected by previous calculations that the Hall coefficient can be obtained with an accuracy of $\pm 10\%$. Mapping of the large flat surface can be done in small area increments with an absolute accuracy expected of $\pm 50\%$. No contacts are attached to the sample.

4. Microwave Hall Effect on Small Crystallites

The Hall coefficient average for each crystallite with a total surface area of 1 mm^2 can be obtained with the use of a microwave cavity. An absolute accuracy of $\pm$ 50% is expected. No contacts are attached to the sample.

5. Electron Spin Resonance on Large Flat Surfaces

Electron spin resonance (ESR) is useful for nondestructive identification of paramagnetic impurities and paramagnetic defects in high resistivity semiconductors. The utility of ESR in medium resistivity semiconductors depends in detail on the strength of surface currents on the sample. ESR has been observed for some of the deep traps such as iron in GaAs. Investigation will be required for shallow impurities in GaAs. Low temperatures will probably be required. A resolution of 10^{11} centers/mm^2 in 100 μ m surface layer can be obtained. An absolute accuracy for mapping paramagnetic defect and impurity concentrations of $\pm$ 30% is expected. No contacts are attached to the sample.

6. Electron Spin Resonance on Small Crystallites

The total paramagnetic impurity and defect concentrations are expected to be determined to within an absolute accuracy of $\pm$ 30%. No contacts are attached to the sample.

III. STRUCTURAL PERFECTION OF GaAs SUBSTRATE, EPITAXIAL FILM AND SELF-NUCLEATED CRYSTALLITES

Improvements of the quality of space grown epitaxial layers of GaAs in terms of structural perfection are expected and were implied as one of the major objectives of the M 555 experiment. Studying the structural properties of the space grown film with respect to the quality of films grown in the laboratory should, therefore, be one of the major task..

However, prior to growing films in the laboratory and even more so in space, characterization of the structural quality of the substrate has to be done. Since growing of a layer of only a few hundred microns thickness will not allow defects that are present in the substrate to grow out, one can generally expect that defects will be projected into the epilayer to a very high extent. Selection of acceptable substrate material with no two-dimensional defects and low dislocation density is, therefore, extremely important.

Provided that self-nucleated crystals can be recovered, preferably at the original site of growth in the ampoule, one should be able to elucidate a variety of aspects on diffusion and growth kinetics by analyzing the dopant distribution in the crystallites. Structural perfection should also be studied, but eventually at a lower key.

In the following is a short outline on techniques to study structural defects in the expected range; there is, however, a wide variety of approaches (more than 30 X-ray techniques were reported) and only a few of the most suitable and efficient techniques are considered. These techniques will, on the other hand, cover the spectrum of defects to be expected completely. Each of the techniques

recommended can be applied with slight modification for each substrate, film

and crystallite.

(1) Determination of Dislocation Density by Etch Pit Counts

GaAs was subject to a large number of investigations concerning the determina-

tion of dislocation density by etch pit counts. About 30 references are available to

us. Preferential etching of GaAs is, therefore, a well established technique and will

not present major obstacles. Etching of (100) planes is somewhat difficult since the

pits can usually not be discriminated from the background as well as for example on

(111) or ($\overline{111}$) planes. A melt of KOH was found most suitable by us, . It involves,

however, heat treatment to about 300°C for ex. 20 Min. On the other hand, a

series of alternative etchants are available and the problems encountered should be

nominal only.

(2) Berg-Barrett Method

This technique was conceived to study the mosaic structure, coherent and in-

coherent grain boundaries, and local strains and inclusions. It is a nondestructive

technique since it is operated in back reflection; both substrate quality and overall

film quality can, therefore, be investigated. The basic approach is as follows.

A line source aligned in a plane normal to the crystal surface under study is used.

The crystal is set in a position satisfying the Bragg equation for a specific wave-

length of a characteristic spectrum. In the case of an "ideal"crystal, only those

beams are diffracted which are traveling strictly parallel to a specific direction

of the incident beam. Since the beam is also divergent in the vertical direction,

e.ch point of the linear focal spot gives a vertical diffraction line. In consequence,

a representation of an area of the crystal is obtained on the film. Imperfect crystals

produce inhomogeneous reflections due to the different orientations of the mosaic

blocks. A second X-ray technique that will enable one to look at imperfections

on a smaller scale, namely at single dislocations is the

(3) Lang Technique

This technique is suitable for detecting single dislocations in the bulk of a

crystal. A slit-collimated, monochromatic beam, preferably hard radiation from

a point focus tube is used and the reflected beam that is transmitted through the

crystal is photographed. According to the absorption coefficients for X-rays,

specimen thickness has to be small enough for the sample to be transparent to the

radiation. With sample and film held stationary, a section topograph is obtained.

Mounting the crystal and film on a carriage and moving back and forth during ex-

posure with a constant-velocity translation mechanism, large crystal slabs can be

probed entirely. Both survey of distribution of imperfections and registration of single

dislocations are thus obtained. Since the mass absorption coefficients for Ga (e.g.

for Mo K_α: 60.1) and As (for Mo K_α: 69.7) are relatively high and so are the

atomic weights (Ga: 69.72 and As: 74.922), the mass absorption coefficient $\bar{\mu}^*$

of GaAs is approximately 65 cm^2/g. According to the equation

$$I = I_0 \cdot e^{-\bar{\mu}^* \rho x}$$

and a density ρ of 5.316 g/cm^3 for GaAs samples for transmission will have to

be less than 100, better less than 20 microns thick, otherwise extreme exposure

times will be required. The technique has to be considered semidestructive and

is not applicable for characterization of the substrate prior to growth. The technique is,

however, extremely valuable for studying the film itself, besides detecting

dislocations from 1 to $10^4/cm^2$, strain fields resulting from growth phenomena, plastic deformation or diffusion processes, small angular displacements such as low angle boundaries, inclusions and magnetic domain walls can be made visible. Complete specimens up to several inches square can be probed.

The samples prepared for Lang topography could consequently - after thinning by chemical means - be used for

Transmission Electron Microscopy

Preferably a 150 - 200 KV machine should be used. Information on stacking faults and identification of screw and step dislocations could be produced . For the general purpose of determination of substrate orientation Laue back reflection will be used, orientation of the substrates within $\pm 0.5^c$ is of importance .

IV. Chemical Imperfection

Semiconductor electrical proper˙es are extremely sensitive to chemical im-

purity doping even in the ppm range. The semiconductor would be an insulator at

lower temperatures without some impurities (dopants) which contribute electrical

charge carriers. Ideally, therefore, one would like to know the exact quantity of

each elemental impurit⁄ at least to one part per billion (ppb).

A. Emission Spectroscopy

almost
However, this is/impossible in practice and even using "Emission Spectroscopy"

on GaAs only a few metals are detectable in the ppb range and most are detectable only

in ppm or higher, and nonmetals go undetected as shown in Table I. Table I applies

only to 0.2 gm GaAs sample using a split burn technique.

B. Mass Spectroscopy of GaAs

In a GaAs lattice a mass spectrometer analysis has a sensitivity 100 times

greater than that of an emission spectrometer for most impurities and it also detects

the nonmetals as shown in Table II. The mass spectroscopy results are considered

accurate to a factor of 3. Note, however, that for silicon the emission is still more

sensitive than the mass spectrograph.

C. Electron Beam Scanning

In a scanning electron microscope (SEM) the electron beam "splashes" off

electrons at a rate proportional to the atomic number of the sample. Thus, by measur-

ing this electron current on different spots on the sample, different elements can be

detected qualitatively. In the scanning mode, a surface composition map is generated.

This may be useful for detecting Ga inclusions or residue from the gold electrodes used

in the Copeland probe.

Table 5-1. Sensitivity Levels for GaAs, in ppm Atomic, Using the Emission Spectrographic Split-burn Technique†

Period	IA	IIA	IIIP	IVB	VB	VIB	VIIB	VIII	VIII	VIII	IB	IIB	IIIA	IVA	VA	VIA	VIIA	0
1	H																	He
2	Li 0.1	Be 0.08											B 335	C	N	O	F	Ne
3	Na 0.15	Mg 0.0015											Al 0.05	Si 0.025	P 1.2	S	Cl	A
4	K 2.0	Ca 0.9	Sc 2.0	Ti 0.03	V 70	Cr 0.02	Mn 0.015	Fe 0.007	Co 0.03	Ni 0.12	Cu 0.0006	Zn 3.6	Ga	Ge 0.1	As	Se 90	Br	Kr
5	Rb 0.8	Sr 0.4	Y 0.4	Zr 40	Nb 40	Mo 0.08	Tc	Ru 0.7	Rh 0.8	Pd 0.7	Ag 0.0004	Cd 20	In 0.06	Sn 0.3	Sb 0.3	Te 6.0	I	Xe
6	Cs 270	Ba 0.5	La 0.25	Hf	Ta 40	W 80	Re	Os 40	Ir 185	Pt 2	Au 0.002	Hg 0.2	Tl 18	Pb 0.007	Bi 0.2	Po	At	Rn
7	Fr	Ra	Ac															

6	Ce 100	Pr 225	Nd 250	Pm	Sm 480	Eu 2.5	Gd 230	Tb 225	Dy 135	Ho 220	Er 2.0	Tm	Yb 0.2	Lu
7	Th	Pa	U											

†Adapted from Kane.[20]

Chart taken from P. F. Kane and G. B. Larrabee, "Characterization of Semiconductor Materials," McGraw-Hill (1970).

108

TABLE I

Table 5-9. Sensitivity Levels for GaAs, in ppm Atomic, Using the Solids Mass Spectrograph†

	IA	IIA	IIIB	IVB	VB	VIB	VIIB	VIII	VIII	VIII	IB	IIB	IIIA	IVA	VA	VIA	VIIA	
1	H																	He
2	Li 0.003	Be 0.002											B 0.003	C 5.0	N 0.2	O 1.0	F 0.006	Ne
3	Na	Mg	10										Al 0.002	Si 0.1	P 0.002	S 0.05	Cl 0.01	A
4	K 0.062	Ca 0.004	Sc 0.01	Ti 0.03	V 0.002	Cr 0.02	Mn 0.005	Fe 0.03	Co 0.005	Ni 0.01	Cu 0.1	Zn 0.1	Ga	Ge 1.0	As	Se 0.5	Br 0.5	Kr
5	Rb 0.4	Sr 0.3	Y 0.2	Zr 0.5	Nb 0.2	Mo 0.06	Tc	Ru 0.06	Rh 0.1	Pd 0.007	Ag 0.004	Cd 0.01	In 0.01	Sn 0.006	Sb 0.004	Te 0.01	I 0.002	Xe
6	Cs 0.002	Ba .0.04	La 0.02	Hf 0.01	Tr 0.2	W 0.007	Re 0.003	Os 0.005	Ir 0.003	Pt 0.006	Au 0.002	Hg 0.005	Tl 0.003	Pb 0.004	Bi 0.002	Po	At	Rn
7	Fr	Ra	Ac															

	Ce	Pr	Nd	Pm	Sm	Eu	Gd	Tb	Dy	Ho	Er	Tm	Yb	Lu
6	1.0	0.06	0.02		0.008	0.004	0.02	0.002	0.02	0.002	0.006	0.002	0.006	0.002
	Th	Pa	U											
7	0.002	0.002												

†Adapted from Kane.[30]

Chart taken from P. F. Kane and G. B. Larrabee, "Characterization of Semiconductor Materials," McGraw-Hill (1970).

114

TABLE II

D. Electron Microprobe (EM) Impurity Characterization

The electron-probe microanalysis offers far less impurity sensitivity, only 300 to 1000 ppm than the mass or emission spectrometer, however, it does have three distinct advantages in that (1) it is nondestructive, (2) it probes about 2 μ m into the semiconductor surface and (3) an area of as small as 100 μ^2 may be probed at one time allowing mapping of impurity concentration.

Since the E.M. is nondestructive, it can be used repeatedly checking for GaAs surface contamination. For example, the total impurities are identified by a mass spectrometer. The surface impurities may be subtracted to detect the actual bulk impurities.

Mr. E. C. McKannan (S.E. ASTN-MM) has generously agreed by phone to place any equipment and technician needed in the GaAs characterization plan at our disposal for performing electron microprobe analysis on the GaAs samples.

UAH, SSL, and Westinghouse personnel met 7/24/72 to consider which characterization tasks were best suited to each lab. The results of that agreement are shown on the next page.

The characterization tasks of M-555 were assigned as follows in the
SSL-UAH-Westinghouse meeting 7/24/72.

Technique	Lab
Optical Microscopy	UAH, WH & SSL
Scanning E. Microscopy	UAH & SSL
Taly Surf	WH
A.C. Resistivity	UAH
A.C. Hall	UAH
X-ray Diffraction	UAH, WH & SSL
X-ray Topography	UAH/SSL
Photo Luminescence	SSL
ESR	UAH
Electron Microprobe Analysis	Astronautics (or T.I.)
Copeland Probe	WH
Angle Lap	WH
D.C. Resistance	UAH
D.C. Hall Effect	UAH
Etch Pit Density	UAH & WH
Slice Crystal	WH
Emission Spectroscopy	SSL (or T.I.)
Lang Topography	UAH

Non-destructive (brace spanning from Optical Microscopy through Electron Microprobe Analysis)

APPENDIX III

SATURDAY MORNING AT 8:30   SESSION JC   ROOM 106

(E. P. STILLWELL, presiding)

Thermal and Elastic Properties. Electron Transport in Non-metals

Invited Paper

JC1. Crystal Field Investigation by Neutron Inelastic Scattering. HERBERT A. MOOK, Oak Ridge National Laboratory. (30 min.)

JC3. Evidence for Large Anisotropy in the Thermal Expansion Coefficients of InBi.* J. H. DAVIS and R. B. LAL, Univ. Ala. In Huntsville and B. E. POWELL, West Ga. College--The resistance, R, of polycrystalline InBi doubled irreversibly upon cycling from 295 to 77 to 295°K and was independent of cooling rate. Microscopic observations on polished surfaces showed widening of grain boundaries, slight grain tilts from the polished plane, and fine cracks which could account for the increase in R. Up to 20% of the excess resistance could be removed by annealing for about 6 hours at 50°C. The large magnitude of these effects may be due to the strong cleavability of InBi in the (001) plane. These effects were not observed in single crystals of InBi, suggesting that anisotropic thermal expansion in each grain, similar to that reported by Boas and Honeycomb[1] for noncubic metals, is responsible.

* Work supported by NASA contract.

[1] W. Boas and R. W. K. Honeycomb, Proc. Roy. Soc. A286, 57 (1946).

APPENDIX IV

bulletin

OF THE AMERICAN PHYSICAL SOCIETY

APRIL 1972

1972 SPRING MEETING IN WASHINGTON, D.C.
24 – 27 APRIL 1972

EL 14 Electrical Resistivity of InBi Single Crystals. R. B. LAL, H. U. WALTER, and J H. DAVIS, The Univ. of Ala. in Huntsville.--Single crystals of InBi of different crystalline perfection were grown by the Czochralski and Bridgman methods by varying the growth conditions. $\rho_{\parallel}$ and $\rho_{\perp}$ for oriented samples were studied from $300°K$ to $2.5°K$. The variation of $\rho_{\parallel}$ and $\rho_{\perp}$ with temperature indicates the metallic character of InBi, with residual resistivity at or above $8°K$. The crystals had residual resistivity ratios between 250 and 50 depending on the crystal quality and growth conditions. Our temperature variation of $\rho_{\perp}$ contradicts the results of Hashimoto[1] whose $\rho_{\perp}$ decreased by two orders of magnitude as the temperature changed from 2 to $4°K$. His low resistivity and low melting point (103 C instead of $110°C$) suggest the presence of some In_2Bi phase which superconducts at $5.6°K$. By fitting our resistivity data to the Gruneisen equation, a value of resistance characteristic temperature (θ_R) has been found to be $130°K \pm 10°K$.

Work supported by NASA contract.
[1] K. Hashimoto, J. Phys. Soc. Japan, 12, 1423 (1957).

EL 15 Electronic Properties of Vanadium Nitrides. F. J. KAAN, Univ. of Penn. and H. K. MacCkONE, Rensselaer Polytechnic Institute.--The magnetic susceptibi-

( )

APPENDIX V

Growth of In₂Bi Whiskers*

J. R. Huckle, J. H. Davis, and R. B. Lal
The University of Alabama in Huntsville, Huntsville, Alabama 35807
(Received 1 June 1971; in final form 26 July 1971)

The first compound whisker grown by squeeze technique (In_2Bi) is reported. Rotating crystal x-ray analysis and melting-point measurements confirmed that the whiskers were In_2Bi. The whisker axis coincided with the (001) direction for all four whiskers. A scanning electron microscope photograph indicates that the whiskers have diameters of a few μ and a morphology similar to tin whiskers.

The first compound whisker grown by the "squeeze technique"[1] (In_2Bi) is reported herein. Sines[2] used this technique to produce whiskers of soft low-melting-point metals and alloys.

The In_2Bi compound was prepared by mixing with an accuracy of 0.1% the required ratio of 99.99%-pure In into molten 99.99%-pure Bi and then allowing the compound to solidify in a graphite split mold. The melting point of the compound formed was found to be 89 °C as expected. Using the squeeze technique, whiskers grew from between the interfaces of a stack of cold-rolled steel washers (12.7 mm i.d., 15.9 mm o.d., and 0.25 mm thick) which were compressed on a 12.7-mm ($\frac{1}{2}$-in.) bolt. One side of each washer was coated with a film about 1 μ thick by evaporation of In_2Bi at a pressure of 10^{-5} Torr at a rate of about 1 g in 15 min.

The film was evidently not deposited homogeneously, since Bi was found to evaporate from hot In_2Bi about 4% in excess of the expected stoichiometric ratio. This conclusion was drawn from the phase diagram,[3,4] using the fact that when evaporation was

FIG. 1. Scanning electron microscope photograph of the tip (after breaking) of an In$_2$Bi whisker.

stopped with half the In$_2$Bi evaporated the liquidus melting point of the remaining material was found to be 85 °C, instead of 89 °C as expected for compound In$_2$Bi. It is not surprising that the residue was In rich, since In has about 1% of the vapor pressure of Bi at 800 °C.

Whiskers were observed after 24-h growth at room temperature and some grew to a length of 1 mm in 6 weeks. Most of the whiskers, like tin whiskers,[1] appeared to be several μ thick, fluted, straight, and elastic to at least 1% strain in bending.

Since there was some doubt as to the whisker composition, four of the whiskers were examined by x-ray diffraction using a Nonius 75.3-mm-diam rotating crystal camera. Independent spots |(300) (110) (220) (410) (101) (102) (112) (202) (212) (302) (312)| on the rotating pattern were analyzed to determine the interplanar spacings. Makarov[5] reported from powder x-ray diffraction measurements that In$_2$Bi possesses a hexagonal structure with $a = 5.496$ Å and $c = 6.579$ Å. The spacings were found to fit the hexagonal structure reported by Makarov[5] with a

root-mean-square error of only 0.8% and a maximum error of 1.30%. The whisker axis was always found to be in the (001) direction.

According to Giessen et al.,[4] the In$_2$Bi phase exists from 30 to 33 at.% Bi. Although the whisker melting point was measured at 89 ± 1 °C, this, as well as the x-ray data, only confirms a predominance of In$_2$Bi and does not rule out the possibility of the presence in smaller quantities of other phases such as In$_5$Bi$_3$.

A scanning electron microscope photograph (Fig. 1) of the end of an In$_2$Bi whisker shows an elliptical ($a/b = 2$) heavily fluted cross section. This is not surprising, since a similar morphology has been observed for tin[6-8] and indium[9] whiskers. This further supports the idea that the growth recrystallization site[10] and not the material causes this morphology.

Further work on electrical properties of the whiskers is in progress and will be reported later.

*Work supported by a NASA contract.

[1] R.M. Fisher, L.S. Darken, and G.K. Caroll, Acta Met. 2, 368 (1954).

[2] G. Sines, J. Phys. Soc. Japan 15, 1199 (1960).

[3] E.A. Peretti and S.C. Carapella, Trans. Am. Soc. Metals 41, 947 (1949).

[4] B.C. Giessen, M. Morris, and N.J. Grant, Trans. AIME 239, 883 (1967).

[5] E.S. Makarov, Sov. Phys. Crystallogr. 3, 3 (1958).

[6] S.M. Arnold, Technical Proceedings of the 43rd Annual Convention of the American Electroplaters Society, 1956, p. 26 (unpublished).

[7] E.E. Thomas, Acta Met. 4, 94 (1956).

[8] D.E. Bradley, J. Frank, and P.E. Rush, Proc. Phys. Soc. (London) B70, 889 (1957).

[9] J.H. Davis and P.S. Bisenius (unpublished).

[10] W.C. Ellis, D.F. Gibbons, and R.G. Treuting, Growth and Perfection of Crystals, edited by R.H. Doremus et al. (Wiley, New York, 1958), p. 103.

APPENDIX VI

THE EFFECT OF THERMAL CYCLING ON THE RESISTANCE AND MORPHOLOGY OF InBi SINGLE CRYSTALS AND POLYCRYSTALS*

R. B. LAL and J. H. DAVIS

The University of Alabama in Huntsville, Huntsville, Ala. 35807 (U.S.A.)

and

B. I. POWELL

West Georgia College, Carrollton, Ga. 30117 (U.S.A.)

(Received January 19th, 1972)

SUMMARY

The resistivity of single crystals of InBi has been measured at 295 K, 77 K and again after warming at 295 K. There was no evidence of hysteresis or morphology change. The apparent resistivity of polycrystals decreases with temperature but has an irreversible increase over the original room temperature value when warmed back to 295 K. Accompanying the increase of resistance with thermal cycling is the appearance of cracks on the surface of the sample, which may be explained by assuming that InBi has a large anisotropy in thermal expansion coefficients.

INTRODUCTION

The structure and some physical properties of InBi have been reported in the literature. From X-ray crystallographic analysis Binnie[1] found the intermetallic compound InBi to be tetragonal. According to the phase diagram reported by Giessen et al.[2], the melting point of InBi is 109.5°C. The temperature dependence of the resistivity of single crystals of InBi has been measured from 350 to 100 K by Asanabe[3] and from 10 to 2 K by Hashimoto[4] who found that Mathiessen's rule did not hold.

This paper gives the results of the measurement of the electrical resistance of InBi single crystals and polycrystals at 295 and 77 K. Because the room temperature value of the apparent resistivity of polycrystals was about twice as high after immersion in liquid nitrogen, the samples were annealed to study the excess resistance. Finally, the effects of thermal cycling on the surface morphology of polycrystals are reported.

SAMPLES

Single crystals of InBi were grown by the Czochralski method at The University of Alabama in Huntsville by Dr. U. Roy. High purity (99.999%) indium and bismuth were used. The single crystals were cleaved along the (001) plane and a sample having

368   R. B. LAL, J. H. DAVIS, B. E. POWELL

a rectangular cross section was cut from the cleaved crystal. The sample dimensions
(typically 2 × 4 × 10 mm) were measured with a traveling microscope. Laue X-ray
patterns confirmed the four-fold symmetry normal to the cleavage plane.

The polycrystalline samples were solidified from the above high-purity molten
InBi in a cylindrical, 6.4 mm diam. split graphite mold. Sample dimensions were
measured with a traveling microscope. The melting point of one of the polycrystals
was checked and found to be 109 ± 1°C, as expected. This eliminates the possibility
that the presence of heterogeneous[5] phases, such as In or Bi, caused the results found
in thermal cycling.

PROCEDURE

The resistance was measured by a two-point probe method, i.e., we measured
the voltage drop across the sample between two potential probes while we determined
the current by measuring the potential drop across a standard Leeds and Northrup
0.1 ohm resistor. The polycrystalline sample holder had copper electrical pressure
contacts for current and voltage. The current contacts on the single crystal sample
were made using a low melting solder (m.p. 95°C) and the potential contacts were
made with silver conducting paint. All the contacts were found to be ohmic throughout
the entire range of the temperature studied. A Hewlett Packard data acquisition
system with a 1 μV resolution was used to print out time of measurement and also
voltages from the sample, the standard resistor, the copper–constantan thermocouple
and the germanium resistor. The low-temperature resistance was measured using a
glass cryostat.

RESULTS OF SINGLE CRYSTALS

The results of measurements of the resistivity (ρ) at room temperature and at
the temperature of liquid nitrogen are shown in Table I. There was no indication of
hysteresis. The ratio of ρ_{295}/ρ_{77} is 5 and $\rho_{295}/\rho_{4.2}$ is 34. These results are in agree-
ment with the results of Hashimoto[4] and Asanabe[3].

RESULTS FOR POLYCRYSTALLINE SAMPLES

The results of resistance measurements on polycrystalline InBi samples at
room temperature and the temperature of liquid nitrogen are shown in Table I. The

TABLE I

RESISTANCE RATIOS OF INDIUM BISMUTH SAMPLES

Sample	$\dfrac{\rho'_{77}}{\rho_{295}}$	$\dfrac{\rho'_{295}}{\rho_{295}}$
Single crystal 1	0.20	1.0
InBi polycrystal 2	0.47	1.8
3	0.55	2.0
4		2.3
5	0.69	2.2

Fig. 2. The same InBi surface after seven thermal cycles to $77\ K$.

Their X-ray examination of samples, for which the surface layers had been etched away to remove slip lines, indicated that the deformation occurred throughout the specimen. Epprecht[5] has studied the behavior of heterogeneous alloys by thermal treatment and has found deformations when the thermal expansion coefficients of the components were considerably different. Likhachev[9] has studied the problem of stresses generated in crystals theoretically in terms of the temperature variation, the elastic constants, and the differences of thermal expansion constants.

The present results for polycrystals of InBi are attributed to an anisotropy in the thermal expansion and the good cleavability in the (001) plane. The deformation resulting from the temperature change produced the irreversible change of the resistivity and morphology. The observation that there were no changes of the resistivity or morphology of single crystals of InBi is compatible with this analysis because a single crystal would not have surrounding grains on which to exert stress.

Obviously any experimentalist contemplating using polycrystalline InBi at low temperature should consider using single crystal samples or take into account the effects of stress on his results. Polycrystalline InBi appears unreliable upon cooling to cryogenic temperatures, structurally or as an electrical solder.

ACKNOWLEDGEMENT

REFERENCES

1 W. P. Binnie, *Acta Cryst.*, 9 (1956) 686.
2 B. C. Giessen, M. Morris and N. J. Grant, *Trans. AIME*, 239 (1967) 883.
3 S. Asanabe, *Mem. Fac. Sci., Kyusyu. Univ.*, Ser. B. 2 (1956) 82.
4 K. Hashimoto, *J. Phys. Soc. Japan*, 12 (1957) 1423.
5 W. Epprecht, *Z. Metallk.*, 59 (1968) 1.
6 W. Boas and R. W. K. Honeycombe, *Proc. Roy. Soc. (London)*, A186 (1946) 57.
7 W. Boas and R. W. K. Honeycombe, *Proc. Roy. Soc. (London)*, A188 (1947) 427.
8 R. W. K. Horeycombe, *Plastic Deformation in Metals*, St. Martins Press., New York, 1968.
9 V. A. Likhachev, *Sov. Phys. Solid State*, 3 (1961) 1330.

APPENDIX VII

Growth and Morphology of InBi Whisker Crystals.

J. R. Huckle, J. H. Davis, R. B. Lal and

D. P. Nicholas.   Journal of Crystal Growth,

(1972), p. 43-44

GROWTH AND MORPHOLOGY OF InBi WHISKER CRYSTALS*

J. R. HUCKLE, J. H. DAVIS and R. B. LAL

The University of Alabama in Huntsville, Huntsville, Alabama 35807, U.S.A.

and

D. P. NICOLAS

Marshall Space Flight Center, Alabama 35812, U.S.A.

The growth of whiskers of compound InBi by the "squeeze technique" is reported. Rotating crystal X-ray analysis and melting point measurements confirmed that the whiskers were InBi. The whisker axis coincided with the ⟨101⟩ direction for all three whiskers. Scanning electron microscope photographs indicate that the whiskers share the irregular cross section and ribbonlike morphology of other "squeeze-grown" metal whiskers.

The intermetallic compound InBi had gained considerable interest because of its low melting point (109.5 °C) as compared to other compounds of the III-V series, and also because of the National Aeronautics and Space Administration's (NASA) interest in solidifying this compound in one of the Apollo flyback missions.

Bulk single crystals have been grown by Bridgman[1], Czochralski and soft-mold techniques[2,3]. This article describes the growth of InBi whiskers by the "squeeze technique"[4], which has been used earlier to grow whiskers of soft, low melting-point metals[4], alloys[5], and the compound In_2Bi[6].

The starting material for the InBi whiskers was a cast sample of InBi compound solidified in a graphite split mold from 5 N purity molten indium and bismuth. The mp of the compound so formed was found to be 109.5 °C, as expected from the phase diagram[7]. Then the "squeeze technique" was employed which consisted of vacuum evaporating InBi to form a 1 μm thick film on cold-rolled steel washers (12.7 mm i.d., 15.9 mm o.d., and 25 mm thick) which were then compressed between regular washers by a nut on a 12.7 mm ($\frac{1}{2}$ in.) bolt. InBi whiskers were observed at the washer interface after two or three weeks growth at room temperature. Some whiskers grew (relatively slowly) to a length of 1 mm in eight weeks.

Both growth and evaporation of InBi could have been non-stoichiometric, leaving the phase (crystal

structure) of the whiskers in doubt. Finding the whiskers to have the expected mp of InBi suggested, but did not confirm, that the whiskers were InBi. Therefore, three of the whiskers were examined by X-ray diffraction using a Nonius 57.3 mm diameter rotating crystal camera. Exposure times of up to 150 hr were required using Cu-Kα X-rays at 35 kV and 15 mA. On all three whiskers, eighteen independent spots on the rotation patterns were analyzed to determine the interplanar

TABLE 1

Interplanar spacings in InBi whisker

d_x from X-ray (Å)	d_c calculated (Å)	Error (%)	h	k	l	*Layer Line No.
3.45	3.453	0.1	1	0	1	0
2.85	2.841	0.3	1	1	1	0
2.50	2.500	.0	0	2	0	0
2.02	2.025	0.2	1	2	1	0
1.73	1.726	0.2	2	0	2	0
1.63	1.632	0.1	2	1	2	0
1.50	1.501	0.1	1	3	1	0
3.46	3.453	0.2	0	1	1	1
3.44	3.453	0.4	0	1	1	1
2.86	2.841	0.7	1	1	1	2
2.84	2.841	.0	1	1	1	2
2.50	2.500	.0	2	0	0	2
2.38	2.387	0.3	0	0	2	2
2.16	2.154	0.3	0	1	2	2
2.16	2.154	0.3	0	1	2	2
1.77	1.768	0.1	2	2	0	2
1.77	1.768	0.1	2	2	0	2
1.49	1.501	0.7	1	3	1	2

* The rotation axis coincided with the long whisker axis which was 101.

Fig. 1 A scanning electron microscope photograph of the tip of an InBi whisker. The bend at the tip is the result of an attempt to cleave the whisker. Note "celery stick" appearance which reveals no indication of crystal symmetry.

Fig. 2. A different view of fig. 1.

spacings. Table 1 gives the values of measured interplanar spacings (dx) and also the calculated spacing (dc) using the lattice constants reported by Binnie[8]). Binnie reported that InBi crystals possess a tetragonal structure with $a = 5.000$ Å and $c = 4.733$ Å. Our spacings were found to fit the reported structure with a rms error of only 0.3% and a maximum error of 0.7%, suggesting again that the whiskers are predominately, if not totally, InBi. Each whisker axis lay in the $\langle 101 \rangle$ direction. This is not surprising since the $\langle 101 \rangle$ direction is the expected direction of easy slip and growth for a fcc metal and InBi structure is nearly fcc.

Figs. 1 and 2 are scanning electron microscope views of an InBi whisker. Note the highly irregular, unsymmetrical, ribbon-like cross section. As with other "squeeze-grown" whiskers[9]), the cross sections varied from whisker to whisker but did not change appreciably along the length. The whiskers were straight, fluted and elastic to about 1% strain in bending. Their similarity to other "squeeze-grown" whiskers further supports the theory[10]) that the whisker material has less influence on morphology than other factors such as the nucleation grain or the growth site.

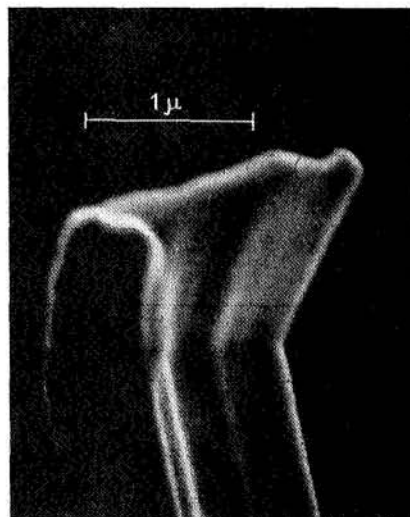The figures show no evidence of our attempt to induce stress cleavage on the usual (001) plane. The stress probably did cause the bend ($\sim 20°$). This bend was not a growth kink, but evidently was stress-induced since the bending is greater on the thinner side of the whisker.

According to the phase diagrams of Giessen et al.[7]) and Peretti and Carapella[11]), InBi is more compound-like in that it had no detectable stoichiometric deviation, whereas In_2Bi is more alloy-like in that its composition range covers 3 at%. Therefore, this note offers even stronger evidence that compound whiskers may be grown by the "squeeze technique"

References

1) Y Shapira, S. J. Williamson and S. Fischler, Phys. Rev. **144** (1966) 715.
2) U. Roy, being submitted to J. Crystal Growth.
3) H. U. Walter, being submitted to J. Crystal Growth.
4) R. M. Fisher, L. S. Darken and K. G. Carroll, Acta Met. **2** (1957) 368.
5) G. Sines, J. Phys. Soc. Japan **15** (1960) 1199.
6) J. R. Huckle, J H. Davis and R. B. Lal, Appl. Phys. Letters **19** (1971) 220.
7) B. C. Giessen, M. Morris and N. J. Grant, Trans. AIME **239** (1967) 883.
8) W P. Binnie, Acta Cryst. **9** (1956) 686.
9) D. E. Bradley, J. Frank and P. E. Rush, Proc. Phys. Soc. (London) B70 (1957) 889.
10) W C. Ellis, D. F. Gibbons and R. G. Treuting, *Growth and Perfection of Crystals*, Eds. R. H. Doremus et al. (Wiley, New York, 1958) p. 103.
11) E. A. Peretti and S. C. Carapella, Trans. ASM **41** (1949) 947
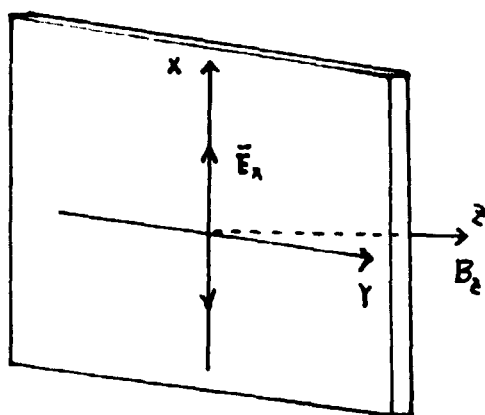
APPENDIX VIII

Surface Hall Coefficient

Fig (1)
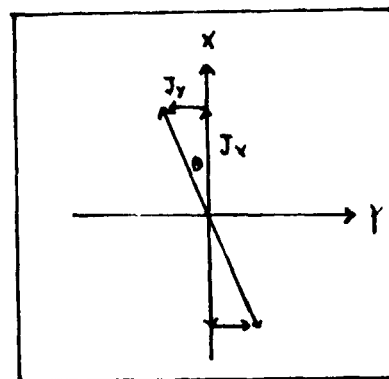
Suppose just inside the surface ($z = 0$) of the semiconducting portion of the wall of a microwave cavity, we have an alternating electric field

$$\overline{E}_x = (\, E_{ox} e^{-i\omega t}, \quad 0, \quad 0 \,)$$

and a magnetic field

$$\overline{B} = (\, 0, \quad B_{oy} e^{-i\omega t}, \quad B_z \,)$$

acting on an isotropic medium as Figure (1) where $B_{oy} \ll B_z$. Then the equation of motion of free carriers can be written with reasonable accuracy as

$$\left(\frac{d}{dt} + \frac{1}{\tau} \right) \begin{pmatrix} m^* & 0 \\ 0 & m^* \end{pmatrix} \begin{pmatrix} v_x \\ v_y \end{pmatrix} = \begin{pmatrix} e E_x + \frac{e}{c} v_y B_z, & 0 \\ 0, & -\frac{e}{c} v_x B_z \end{pmatrix}$$

where τ = isotropic relaxation time, m^* = effective mass of carriers on a spherical

Fermi surface, and B_{oy} has been neglected.

Solving for V_x and V_y, one can obtain

$$V_x = \left(\frac{e\tau}{m^*}\right) \frac{1 - i\omega\tau}{\left[(1-i\omega\tau)^2 + (\omega_c\tau)^2\right]} E_{ox} e^{-i\omega t}$$

$$= \left(\frac{e\tau}{m^*}\right) \frac{\left[1 + (\omega\tau)^2 + (\omega_c\tau)^2\right] + i\omega\tau\left[1 + (\omega\tau)^2 - (\omega_c\tau)^2\right]}{\left[1 - (\omega\tau)^2 + (\omega_c\tau)^2\right]^2 + 4(\omega\tau)^2} E_{ox} e^{-i\omega t}$$

where $\qquad \omega_c = \dfrac{e B_z}{c\, m^*} \qquad$, the cyclotron frequency.

The velocity must be averaged over the allowed values of energy and one

obtains

$$\langle V_x \rangle = \frac{e}{m^*} \left\{ \left\langle \frac{\tau\left[1 + (\omega\tau)^2 + (\omega_c\tau)^2\right]}{\left[1 - (\omega\tau)^2 + (\omega_c\tau)^2\right]^2 + 4(\omega\tau)^2} \right\rangle \right.$$

$$\left. + i\omega \left\langle \frac{\tau^2\left[1 + (\omega\tau)^2 - (\omega_c\tau)^2\right]}{\left[1 - (\omega\tau)^2 + (\omega_c\tau)^2\right]^2 + 4(\omega\tau)^2} \right\rangle \right\} E_{ox} e^{-i\omega t}$$

Therefore, the x - component current is

$$J_x \equiv ne \langle V_x \rangle$$

$$= \frac{\sigma_o}{\langle \tau \rangle} \left\{ \left\langle \frac{\tau\left[1 + (\omega\tau)^2 + (\omega_c\tau)^2\right]}{\left[1 - (\omega\tau)^2 + (\omega_c\tau)^2\right]^2 + 4(\omega\tau)^2} \right\rangle \right.$$

$$\left. + i\omega \left\langle \frac{\tau^2\left[1 + (\omega\tau)^2 - (\omega_c\tau)^2\right]}{\left[1 - (\omega\tau)^2 + (\omega_c\tau)^2\right]^2 + 4(\omega\tau)^2} \right\rangle \right\} E_{ox} e^{-i\omega t}$$

Similarly, y - component current is

$$J_d = \frac{\sigma_o}{\langle \tau \rangle} \left\{ \omega_c \left\langle \frac{\tau^2 [1 - (\omega\tau)^2]}{[1 - (\omega\tau)^2 + (\omega_c\tau)^2]^2 + 4(\omega\tau)^2} \right\rangle \right.$$

$$\left. + i 2 \omega \omega_c \left\langle \frac{\tau^3}{[1 - (\omega\tau)^2 + (\omega_c\tau)^2]^2 + 4(\omega\tau)^2} \right\rangle \right\} E_{ox} e^{-i\omega t}$$

where $\quad \sigma_o = \frac{n e^2 \langle \tau \rangle}{m^*} \quad$, d.c. measurement conductivity

Let,

$$(\sigma_{xx})_r = \frac{\sigma_o}{\langle \tau \rangle} \left\langle \frac{\tau [1 + (\omega\tau)^2 + (\omega_c\tau)^2]}{[1 - (\omega\tau)^2 + (\omega_c\tau)^2]^2 + 4(\omega\tau)^2} \right\rangle$$

$$(\sigma_{xx})_i = \frac{\sigma_o}{\langle \tau \rangle} \omega \left\langle \frac{\tau^2 [1 + (\omega\tau)^2 - (\omega_c\tau)^2]}{[1 - (\omega\tau)^2 + (\omega_c\tau)^2]^2 + 4(\omega\tau)^2} \right\rangle$$

$$(\sigma_{xy})_r = \frac{\sigma_o}{\langle \tau \rangle} \omega_c \left\langle \frac{\tau^2 [1 - (\omega\tau)^2]}{[1 - (\omega\tau)^2 + (\omega_c\tau)^2]^2 + 4(\omega\tau)^2} \right\rangle$$

$$(\sigma_{xy})_i = \frac{\sigma_o}{\langle \tau \rangle} 2 \omega \omega_c \left\langle \frac{\tau^3}{[1 - (\omega\tau)^2 + (\omega_c\tau)^2]^2 + 4(\omega\tau)^2} \right\rangle$$

So

$$J_x = \left[(\sigma_{xx})_r + (\sigma_{xx})_i \right] E_{ox} e^{-i\omega t} \quad \cdots\cdots\cdots\cdots (1)$$

$$J_y = - \left[(\sigma_{xy})_r + (\sigma_{xy})_i \right] E_{ox} e^{-i\omega t}$$

E_x is induced by the field in the empty cavity, where the distribution of E field
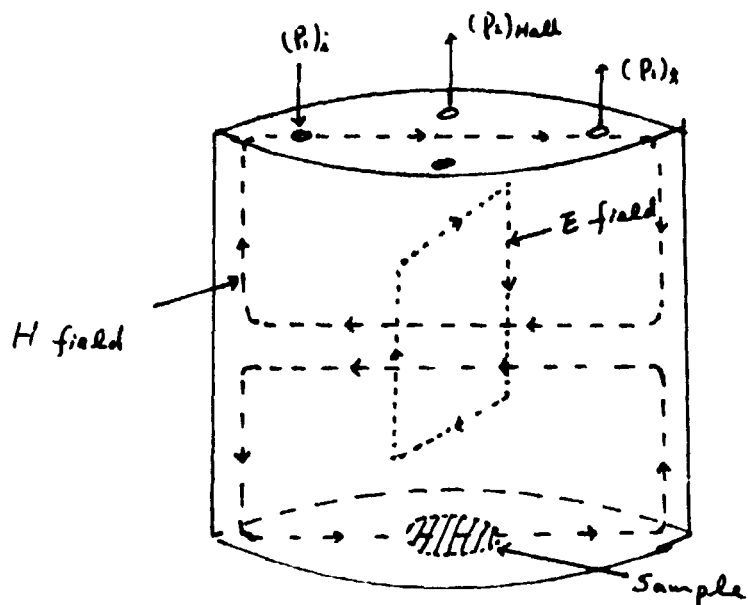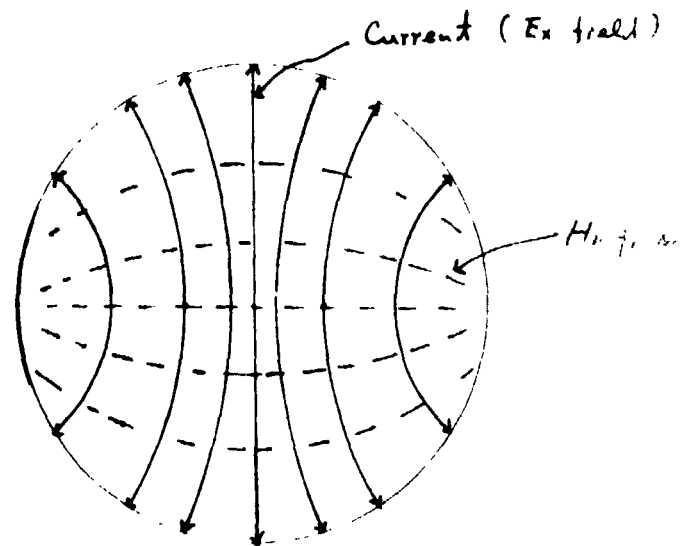
and H field are shown in figure (2)

Fig. (1)

The distribution of microwaves the TE_{112} cavity

H field pattern on the surface of TE_{112} cavity bottom

So, referring to Fig. (1), we can find $\bar{E}_x$ in medium by Maxwell's equation as following,

$$
\begin{cases}
J_x = (\overline{\sigma_{xx}})_r \, \bar{E}_x & \text{(assume: } \ell < \delta_o \text{ anomalous skin effect)} \\[2mm]
\nabla \cdot \bar{E}_x + \dfrac{1}{c}\dfrac{\partial \bar{H}_y}{\partial t} = 0 \\[2mm]
\nabla \times \bar{H}_y - \dfrac{(\mathcal{E}_{xx})_r}{c}\dfrac{\partial \bar{E}_x}{\partial t} - \dfrac{4\pi}{c}(\overline{\sigma_{xx}})_r \, \bar{E}_x = 0
\end{cases}
$$

and the boundary condition is

$$
\bar{H}_{\shortparallel} = (\bar{H}_y)_{z=0}
$$

where $\bar{H}_{\shortparallel}$ is the magnetic field of microwaves near the surface of the medium.

The solution is

$$H_y = H_{\shortparallel}\, e^{(-\beta + i\alpha)z}\, e^{-i\omega t}$$

$$E_x = -(A^2 + B^2)^{\frac{1}{2}}\, H_{\shortparallel}\, e^{(-\beta + i\alpha)z}\, e^{-i\omega t}\, e^{i\phi} \qquad \text{- - - - - - - - (2)}$$

where

$$\left.\begin{matrix} \beta \\ \alpha \end{matrix}\right\} = \sqrt{(\varepsilon_{xx})_r}\ \frac{\omega}{c}\left[\frac{\sqrt{1 + \left(\frac{4\pi(\sigma_{xx})_r}{\omega(\varepsilon_{xx})_r}\right)^2} \mp 1}{2}\right]^{\frac{1}{2}}$$

$$A = \frac{c}{4\pi(\sigma_{xx})_r}\ \frac{\beta + \left(\frac{\omega(\varepsilon_{xx})_r}{4\pi(\sigma_{xx})_r}\right)\alpha}{1 + \left(\frac{\omega(\varepsilon_{xx})_r}{4\pi(\sigma_{xx})_r}\right)^2},$$

$$B = \frac{c}{4\pi(\sigma_{xx})_r}\ \frac{\beta\left(\frac{\omega(\varepsilon_{xx})_r}{4\pi(\sigma_{xx})_r}\right) - \alpha}{1 + \left(\frac{\omega(\varepsilon_{xx})_r}{4\pi(\sigma_{xx})_r}\right)^2}$$

$$\phi = \tan^{-1}\frac{B}{A}$$

$$(\varepsilon_{xx})_r = \varepsilon_\infty - \frac{4\pi}{\omega}(\sigma_{xx})_i$$

Substituting (2) into (1) yields

$$J_x = -\left[(\sigma_{xx})_r + i(\sigma_{xx})_i\right](A^2 + B^2)^{\frac{1}{2}}\, H_{\shortparallel}\, e^{(-\beta + i\alpha)z}\, e^{-i\omega t}\, e^{i\phi}$$

Surface impedance:

$$Z_s = \frac{E_{x(z=0)}}{\int_0^\infty J_x \, dz}$$

$$= \frac{\left[\beta (\sigma_{xx})_r - \alpha (\sigma_{xx})_i\right] - i\left[\alpha (\sigma_{xx})_r + \beta (\sigma_{xx})_i\right]}{(\sigma_{xx})_r^2 + (\sigma_{xx})_i^2}$$

$$\approx \frac{\left[\beta (\sigma_{xx})_r - \alpha (\sigma_{xx})_i\right] - i\left[\alpha (\sigma_{xx})_r + \beta (\sigma_{xx})_i\right]}{(\sigma_{xx})_r^2}$$

Surface resistance:

$$R_s = R_e \, (Z_s)$$

$$= \frac{\beta (\sigma_{xx})_r - \alpha (\sigma_{xx})_i}{(\sigma_{xx})_r^2}$$

Hall field, $\quad E_y = R_H J_x B_z \qquad$ (if θ is small)

where $\quad R_H = \dfrac{1}{nec} \qquad$ (D. C. Hall coefficient)

Surface Hall coefficient:

$$Y_s = R_e \left[\frac{E_{y(z=0)}}{B_z \int_0^\infty J_x \, dx} \right]$$

$$= R_e \left[R_H (\beta - i\alpha) \right]$$

$$= \beta R_H$$

APPENDIX IX

RESISTIVITY OF GaAs FROM MICROWAVE REFLECTANCE

The basis for converting reflectance data to resistivity values is as follows:

$$K = \frac{\eta_a - \eta_1}{\eta_a + \eta_1} \tag{1}$$

where $\quad K$ = reflection coefficient defined by $|K| = \left(P_R/P_i\right)^{\frac{1}{2}}$

η_1 = impedance of air in the TE_{01} rectangular waveguide mode

η_a = surface impedance of GaAs

$$\eta_a = \frac{j\omega\mu}{\sigma + j\omega\epsilon} \tag{2}$$

Assuming $\sigma \gg \omega\epsilon$ (high conductivity case), Eq. (2) becomes

$$\eta_a \approx (\omega\mu\rho)^{\frac{1}{2}} \, e^{j\frac{\pi}{4}} \tag{3}$$

where $\quad \rho$ = resistivity $= \frac{1}{\sigma}$

Assuming also, that $\left(\dfrac{\sqrt{\dfrac{\omega\mu\rho}{2}}}{\eta_1}\right)^2 \ll 1$

then Eq. (1) can be solved for

$$\rho = \frac{2\eta_1^2}{\omega\mu} \left[\frac{-2\dfrac{P_R}{P_i} + \sqrt{5\dfrac{P_R}{P_i} - 1}}{4\dfrac{P_R}{P_i} - 1} \right]^2 \tag{4}$$

The fractional uncertainty in ρ is

$$\frac{d\rho}{\rho} = \left\{ \frac{5}{\sqrt{5\dfrac{P_R}{P_i} - 1}} - 4 - 8 \left[\frac{-2\dfrac{P_R}{P_i} + \sqrt{5\dfrac{P_R}{P_i} - 1}}{4\dfrac{P_R}{P_i} - 1} \right] \right\} \left\{ \frac{1}{-2\dfrac{P_R}{P_i} + \sqrt{5\dfrac{P_R}{P_i} - 1}} \right\} \frac{P_R}{P_i} \frac{dP_R}{P_R} \tag{5}$$

For a sample from boule G3-77 a typical value of surface resistivity was $0.50 \ \Omega - cm$ at room temperature and $d \ P_R/P_R$ was observed to be $\pm 0.5\%$. Therefore, Eq. 5 of this Appendix gives $d \rho/\rho$ of $\pm 5\%$ for the precision of each value of ρ calculated as the average within the skin depth and over the area of each resolution element.

PROPERTIES OF InSb

Property	Description	Comments	Reference
Melting Point	$525 \pm 0.5°C$ (ref. 1) $525° \pm 1°C$ (ref. 2)	A value of 523°C is frequently quoted in the literature.	1) T. S. Liu and E. A. Peretti, Trans. Amer. Soc. Metals 44, 539, (1952). 2) N. H. Nachtrieb and N. Clement, J. Phys. Chem., 62, 876, (1958).
Density	a) $5.7751 \pm .0003$ g/cm^3 at 300°K (ref. 3). b) 5.74 g/cm^3 for the solid at mp. c) 6.48 g/cm^3 for the liquid. d) density of liquid at 1000°C is 6.0 g/cm^3.		3) R. F. Potter, Phys. Rev., 103, 47 (1956). 4) K. F. Blume and J. B. Mullin, S.i. State Elect, 5, 211 (1962)
Crystal Structure	Zinc Blend Structure $a = 6.4760$ Å.		5) Same as ref. 1.
Point Group	$\overline{4}3\,m$		6) M. J. rger, Elementary Crystallography, John Wiley, N.Y. (1956).
Cleavage	The cleavage planes are {110}	InSb can be cleaved fairly readily.	7) H. Pfister, Z. Naturf, 10a, 79 (1955).
Phase Diagram	It was found that alloys within 0.5% of stoichiometric composition InSb were still two-phase.	X-ray measurement revealed no discernible change in lattice parameter.	8) Same as ref. 1.

Property	Description	Comments	Reference
Energy Gap	0.17 ev at 300°K 0.22 ev at 100°K 0.23 ev at 0°K	The band edges are at the center of Brillouin zone. Effective mass for electrons at the conduction band minimum usually lie between 0.013 m_0 and 0.015 m_0 (m_0 being the free electron mass). The corresponding gravity for heavy holes is 0.18 m_0.	9) Same as ref. 4.
Effective Mass	Lies between 0.013 m_0 and 0.015 m_0 (m_0 being the free electron mass)	There is evidence that light-hole effective mass is close to that for conduction band electrons.	10) Same as ref. 4.
Number of Intrinsic Carriers	2×10^{16} cm^{-3} at 300°K.		11) Same as ref. 4.
Electron and hole mobility in $cm^2/v - sec$	~ 7×10^4 – electrons ~ 7×10^2 – holes at 300°K ~ 6×10^5 – electrons 1×10^4 – holes at 77°K.		12) Same as ref. 4.
Coefficient of Linear Expansion $\alpha \times 10^6$ cm/deg^{-1}	6.50 at 80°K 5.04 at 300°K	Below 80°K it decreases, even becoming slightly negative, before tending to zero as 0°K is approached. Above 300°K it increases slightly.	13) Same as ref. 4.
Thermal Conductivity in cal/cm sec	.04 at 40°C .02 at 425°C	Depends upon specimen purity	14) A. D. Stuckes, Phys. Rev., 107, 427, (1957).

Property	Description	Comments	References
Specific heat at constant pressure c_p	0.04996 cal/gram degree at 298°K		15) Semiconductors and semimetals, Eds. Willardson and Beer, Vol 2, p 52, Academic Press, N.Y. (1966).
Etchants	1 HF 1 HNO$_3$	2 to 5 sec. (Polishing) Polish etch for ($\bar{1}\bar{1}\bar{1}$) and (110). No etching on (111) or (100)	16) Venables, J.D., et al J. Appl. Phys., 29, 1025 (1958).
	5 HF 5 HNO$_3$ 2 H$_2$O	20 secs. Etching (100) and ($\bar{1}\bar{1}$0)	17) Gatos, H.C., et. al. J. Electrochem. Soc. 107, 433 (1960).
	3 HF 5 HNO$_3$ 3 Acetic acid (CP-4A)	5 to 30 secs. Chemical polish. Also been used for etching (111).	18) Allen, J. W., Phil Mag. 2, 1475 (1957). 19) DeWald, J. F., J. Electrochem. Soc., 104, 244 (1957). 20) Bardsley, W., et.al. J. Electron. Contr., 3, 103 (1957).
	1 CP-4A 1 H$_2$O 1 Acetic acid	1 min. Etching (111) and planes from there out to (112)	21) Same as ref. 18.
	1 HF 1 30% H$_2$O$_2$ 1 H$_2$O	5 to 10 secs. etching (111)	22) Faust, J. W., et. al., J. Appl. Phys., 31, 331 (1960).
	0.4M solution of ferric ion in 6 N HCl	1 to 5 min. Etches InSb or GaAs at different temperatures.	23) Gatos, H. C., et.al., J. Electrochem Soc., 107, 427 (1960).

X-RAY METHODS FOR STUDYING CRYSTALLINE PERFECTION AND THEIR USEFULNESS IN THE SSL/UAH CRYSTAL CHARACTERIZATION PROGRAM

Introduction

Since the postulation of imperfections in crystals in 1922 by Darwin,[1] optical, x-ray, electron and neutron diffraction studies, etc. have shown that the atomic arrangement in real crystals is not ideal but subject to imperfections. The density and magnitude of these imperfections depend on several factors; for example, on the type of crystal, its purity, conditions of growth, treatment, etc. The SSL/UAH efforts in the area of crystal growth and crystal characterization are directed towards the investigation of the influence of reduced gravity on crystalline quality. Proper techniques for studying structural perfection in particular will have to be employed. Since x-ray techniques have been proven to be most compatible in studying structural perfection, I should like to outline briefly the techniques that are presently used. These techniques are, however, not used by very many researchers, a fact which is reflected in the very limited possibility of purchasing the required equipment.

CRYSTAL IMPERFECTIONS AND THEIR INFLUENCE ON X-RAY DIFFRACTION

The expression "crystal imperfection" can denote either:

A. point defects which include phonons, electrons and holes, excitons, vacancies, interstitial atoms, impurity atoms, or

B. mosaic structure, coherent and incoherent grain boundaries, and local strains and inclusions.

The diffraction effects which are the basis for studying these imperfections are:

1. peak broadening due to different orientations of the atomic planes

2. displacement of the diffraction peaks due to change in the lattice constants

3. increase in intensity of a reflection in the region corresponding to the zone of disturbance (due to extinction contrast)

4. reduction of anomalous transmission of x-rays

5. small angle x-ray scattering

6. change in the Kossel line pattern

7. change in x-ray diffuse scattering - anomalous scattering

The methods stemming from these aspects of x-ray diffraction are:

I. Methods of Studying Mosaic Structure

A. Methods Applying to Polychromatic Radiation

1. Laue Method:[2] This method is most widely used in solid state physics to determine crystallographic orientation. The shape and structure of interference spots can, however, be used to study the mosaic structure of the probed volume. Resolution depends on beam collimation.

2. Schulz Method:[3] White radiation emerging from a quasi-point source (≈ 30 μ diameter) is used. The beam is divergent and a large area of a crystal is probed under a continuously varying angle of incidence of the primary beam. The wavelength, for which the Bragg equation is satisfied, therefore, also varies continuously, and in the case of a perfect crystal, an almost continuous spectrum is obtained on the film. If the beam falls on to disoriented blocks, a break can be seen in the spectrum on the film. This brighter or darker area is due to overlapping of parts of the spectrum. Interpretation of the Schulz photographs is somewhat difficult; resolution is to about one minute of arc of lattice tilt.

3. Guinier and Tennevin Method:[4] The technique is a focusing Laue method; only one single Laue spot is observed. Misorientations in the order of 10 seconds of arc can be resolved. Effects due to internal strains cannot always be distinguished from effects caused by disorientations of mosaic blocks.

B. Methods Applying to Monochromatic Radiation

1. Berg-Barrett Method:[5] A line source aligned in a plane normal to the crystal surface under study is used. The crystal is set in a position satisfying the Bragg equation for a specific wavelength of a characteristic spectrum. In the case of an "ideal" crystal, only those beams are diffracted which are traveling strictly parallel to a specific direction of the incident beam. Since the beam is also divergent in the vertical direction, each point of the linear focal spot gives a vertical diffraction line. In consequence, a

representation of an area of the crystal is obtained on the film. Imperfect crystals will produce inhomogeneous reflections due to the different orientations of the mosaic blocks.

    2. <u>Barth Method:</u>[ ] This is a modification of the Berg method, macromosaic blocks of the order of 100 μ and tilt angles not larger than 1 minute of arc can be detected.

    C. <u>Spectrometric Methods</u>

    1. <u>Bragg Method</u>: The total intensity of an interference line of the characteristic radiation is studied. The total intensity of the line depends on the degree of crystal perfection.

    2. <u>Three-Crystal Spectrometer Method:</u>[ ] A relatively large, strictly monochromatic collimated beam is diffracted from the sample under investigation. The sample is mounted on the table of a Wild's goniometer. By rotating the crystal through a very small angle, the angle of incidence of the monochromatic primary beam is changed. For a specific angle of incidence, only a certain number of mosaic blocks can satisfy the Bragg equation. By changing the position of the crystal, a number of counts is recorded each time by a Geiger-Müller counter. This way, the mean angular distribution of the mosaic blocks may be measured. There are several modifications of this approach.

    3. <u>Lambot Method:</u>[ ] A divergent x-ray beam emerging from a linear source is reflected from a crystal monochromator and focused on the sample. The sample is placed at an angle to satisfy the Bragg law for the mean direction of the incident beam. For mosaic blocks disoriented by different angles, this condition is satisfied owing to the beam divergence within angular limits according to the beam divergence. Hence, an interference pattern is obtained on the film, each line being due to one of the blocks or microblocks of the same orientation. Resolution is to 25 μ for tilt angles of the order of 30 seconds.

    4. <u>Auleytner Method:</u>[ ] The spectrometer methods described above are not easy and are experimentally difficult. They require very expensive and high precision auxiliary equipment, such as high quality monochromators, spectrometers and electronic recording devices. With the Auleytner method, less sophisticated equipment is needed. A quasi-point source is used. The x-ray beam passes a narrow slit and the trace of the beam on the crystal coincides with the rotation axis of the crystal. The crystal oscillates

relative to a mean position, for which the Bragg condition is satisfied for a given spacing of the crystal planes under investigation, and for a given wavelength of the characteristic radiation. The diffraction pattern is recorded on a film. The movement of the film is coupled with the crystal oscillations. The angular speeds of both movements are constant and equal in magnitude and direction. The structure of a diffraction line reveals crystal imperfections down to mosaic block sizes of about 50 μ.

II. Methods of Studying Dislocation Structure

A. Oscillating Film Spectrometer: – (This method has been described in I.C.4) Precise analysis of the shape of the interference lines by comparing the lines obtained by a stationary film spectrometer will yield information on dislocation densities. The analysis is rather complicated and the method only useful to dislocation densities greater than 10^6 lines per cm^2.

B. Double Crystal Spectrometer: This technique is based on peak broadening due to different orientations of the atomic planes. Characteristic x-rays are reflected at the Bragg angle from a highly perfect reference crystal to the crystal to be studied. The reflecting planes of the crystal under investigation are usually parallel to those of the reference crystal. The sample is displaced through a small angle (rocking) while the reflections are observed. The integrated intensity diffracted by a crystal oriented near the Bragg angle and the half width of the Bragg peak both depend strongly on crystal perfection. The x-ray intensity versus $\Delta\theta$ – plot, the rocking curve, is used to express crystalline perfection by simply indicating the half width of the peak. The DCS is, however, restricted in its application to crystals with at least 10^4 dislocations per cm^2. At lower dislocation densities, there is no change of intensities and line profiles observable. The technique uses a point monochromatic x-ray source. Precision alignment and rocking of samples is required, temperature control and high vacuum should be implied

C. Borrmann Method:[13] The anomalous transmission of x-rays (Borrmann effect) is used with this topographical method. A crystal is placed in reflecting position in a collimated, monochromatic beam. If the crystal is of relatively high perfection, the transmitted and diffracted beams experience abnormally low absorption. A fine-grained photographic emulsion is placed in contact with the surface opposite to the surface where the beam is incident (both surfaces are plane parallel) and single dislocations show up after enlargement as dark shadow-lines.

D. Lang Method: [13] This technique is also suitable for detecting single disloca-
tions in the bulk of a crystal. A slit-collimated, monochromatic beam, preferably hard
radiation (AgK_α), from a point focus tube is used and the reflected beam that is trans-
mitted through the crystal is photographed. According to the absorption coefficients for
x-rays, specimen thickness has to be small enough for the sample to be transparent to the
radiation. With sample and film held stationary, a section topograph is obtained. Mount
ing the crystal and film on a carriage and moving back and forth during exposure with a
constant-velocity translation mechanism, large crystal slabs can be probed entirely. Both
survey of distribution of imperfections and registration of single dislocations are thus obtained

E. Barth-Method: This method is described in I.B.2. It can be used for mapping
of imperfections. The resolution is, however, less than with the Lang technique.

TECHNIQUES PROPOSED TO BE USED IN THE SSL/UAH CRYSTAL
CHARACTERIZATION PROGRAM

The brief outline of techniques to study crystal imperfections with x-rays presented
here covers only the major techniques that have been applied successfully. There are
modifications of these techniques and there are also more specialized techniques to look
at specific types of imperfections such as strain fields in crystals, etc.

For our purposes, techniques which enable characterization of relatively large
crystals over a wide spectrum of crystal perfection from virtually no dislocations to poly-
crystalline materials would be desirable. Since our time and manpower is rather restricted,
building up such facilities has to be done in such a way that only minor development and
construction of hardware is done by our own and we should rather rely on commercially
available equipment. Besides facilities to determine crystal orientation, one of the
techniques to study crystal perfection in terms of mosaic structure and one technique to
determine dislocation densities down to low levels should be made available.

Crystal orientation is generally determined by the Laue back reflection technique,
both polaroid and regular film camera should be obtained. A tungsten anticathode x-ray
tube with point focus is preferable; this equipment is available from Norelco, G.E. etc.

UAH has a Laue setup from Norelco in operation. We are, however, using the continuous spectrum of copper, which is not preferable due to the relatively strong intensities of the CuK_α and CuK_β lines in this continuum. Also, this radiation is relatively soft, which makes surface preparation more critical.

For studying mosaic structure of crystals, both the Schulz and Berg Barrett technique seem to be preferable. These setups are not available commercially. We have, however, experimented with both of these techniques at UAH, and they can be built up relatively simply by us. For the Schulz setup a quasi-point source for preferably hard, white radiation is required. The Berg method would require a monochromatic line source, which can also be purchased. Two universal goniometers for both sample and film mounting should be obtained.

Studies on dislocation densities can be done by a variety of techniques as outlined in the preceding paragraphs. The equipment for such studies, however, has to be rather sophisticated. After checking with a variety of x-ray supply companies, we have found the only setup commercially available is the Lang camera from G.E. Since this technique is versatile and is useful for both mapping of large crystal slabs and detection of single dislocations, this setup should be considered.

Mostly AgK_α radiation is used; an even harder radiation would be preferable since we are dealing with relatively heavy elements (Bi, InSb, InBi, Ge, etc.). The studies have to be done in transmission and slabs of these materials with thicknesses less than 1 mm have to be prepared without producing additional damage in both crystal surfaces and bulk. This will require proper cutting and surface preparation and the proper setups for each of the materials will have to be obtained. Catalogs and price lists have been obtained on these items and a rough estimate to set up the proposed arrangements is about 25K to 30K. Since basic equipment, including Laue cameras and various diffraction cameras, is already available at UAH, setting up similar facilities at UAH would amount to about 10K - 15K.

REFERENCES

1. C. G. Darwin, Phil. Mag. 43 (1922) 800.

2. T. Kovacs: Principles of x-ray Metallurgy, Plenum Press (1969).

3. L. G. Schulz, Trans. Am. Inst. Min. Metallurg. Engnrs. 200 (1954) 1082.

4. A. Guinier, J. Tennevin, Progr. Met. Phys. 2 (1950).

5. W. Berg, Naturwiss. 19 (1931) 391.

6. H. Barth, Z. Naturforschung 13a (1958) 680.

7. M. Renninger, Acta Cryst. 8 (1955) 597.

8. J. Backovsky, Czech. J. Phys. 6 (1956) 390.

9 Handbuch der Physik, XXXII (1957).

10. J. Auleytner, Fortscher. Miner. 38 (1960) 46.

11. L. G. Parrat, Phys. Rev. 41 (1932) 553.

12. G. Borrmann, W. Hartwig, H. Fruler, Z. Naturforschg. 13a (1958) 423.

13. A. R. Lang, J. Appl. Phys. 29 (1958) 59F.